Control of Gene Expression and Cytoskeleton in Migrating Neurons during Cerebral Cortex Development

by

Cansu Akkaya

A Dissertation Submitted to the
Graduate School of Sciences and Engineering
in Partial Fulfillment of the Requirements for
the Degree of

Doctor of Philosophy

in

Molecular Biology and Genetics

July 2020

Control of Gene Expression and Cytoskeleton in Migrating Neurons during Cerebral Cortex Development

Koç University

Graduate School of Sciences and Engineering

This is to certify that I have examined this copy of a doctoral dissertation by

Cansu Akkaya

and have found that it is complete and satisfactory in all respects,
and that any and all revisions required by the final
examining committee have been made.

Committee Members:

_____

Assoc. Prof. Nurhan Özlü (Advisor, Koç University)

_____

Assoc. Prof. Gülayşe İnce-Dunn (Co-Advisor, Helsinki University)

_____

Prof. Dr. Arzu Karabay Korkmaz (İstanbul Technical University)

_____

Asst. Prof. Elif Nur Fırat-Karalar (Koç University)

_____

Assoc. Prof. Tuğba Bağcı Önder (Koç University)

_____

Assoc. Prof. N. C. Tolga Emre (Boğaziçi University)

Date: July 13, 2020

ABSTRACT

The mammalian cerebral cortex is organized into six functional layers composed of excitatory glutamatergic neurons and inhibitory GABAergic interneurons. During development, excitatory neurons migrate from the proliferative ventricular zone towards to superficial marginal zone in an "inside-out" manner. Neurodevelopmental and psychiatric disorders are observed when radial neuronal migration is disrupted. In the first part of my thesis, I focused on the role of developmentally regulated *Kif2a* isoforms in neuronal function and cortical neuronal migration in mouse. KIF2A is a microtubule depolymerizing kinesin motor protein which has curial roles in axonal pruning and neural progenitor cell division. Moreover, alternative splicing of the *Kif2a* gene is dynamically regulated in neurons by specific RNA-binding proteins. However, our understanding of how individual alternative isoforms of KIF2A function to regulate mammalian cerebral cortex development is not known. I demonstrated that KIF2A is essential for dendritic arborization in primary cortical neurons and that all three alternatively spliced isoforms can fulfill this function. Intriguingly, only two of the *Kif2a* isoforms could support neuronal radial migration in the developing cortex. Finally, I identified the protein interacting partners of all KIF2A isoforms at a proteome-wide level by a proximity ligation based method (BioID) which revealed both previously known and new isoform-specific KIF2A interactors and how these interactions could potentially influence the function of individual isoforms. My results highlight the significance of alternative splicing and how it regulates isoform specific functions.

In the second part of my thesis, I focused on the regulation of gene expression in neuronal migration and found that the transcription factor Neurogenic Differentiation 2 (*Neurod2*) has a role at the terminal stage of neuronal radial migration by promoting neurons to localize to the uppermost region of the developing cortex. My data uncovered a new role for NEUROD2 as a modulator of the late stages of neuronal migration.

ÖZET

Memeli serebral korteksi, uyarıcı glutamaterjik nöronlar ve inhibitör GABAerjik internöronları içeren altı fonksiyonel katmandan oluşur. Gelişim boyunca, uyarıcı glutamaterjik nöronlar, proliferatif ventiküler bölgeden yüzeysel marjinal bölgeye doğru "içten dışa" bir şekilde göç ederler. Nöron göçü sırasındaki arizalar nörogelişimsel ve psikiyatrik hastalıklara neden olur. Tezimin birinci kısmında, fare korteksinde, gelişim boyunca kontrol edilen *Kif2a* izoformlarının nöron fonksiyonu ve kortikal nöron göçü üzerindeki görevlerini araştırdım. Mikrotübül depolimerazı KIF2A, aksonal budanma ve nöral öncül hücre bölünmesinde önemli rolleri olan bir kinesin motor proteinidir. Ayrıca, *Kif2a* geninin alternatif kırpılması nöronlarda RNA'ya bağlanan proteinler (RNABP) tarafından dinamik bir şekilde kontrol edilir. Fakat her bir KIF2A alternatif izomorfunun memeli serebral korteks gelişimini düzenlemede nasıl bir işlev gördüğü bilinmemektedir. Bu çalışmada, KIF2A'nın primer korteks nöronlarında dendrit budanması için gerekli olduğunu ve alternatif kırpılan KIF2A izoformlarının hepsinin bu görevi yerine getirebildiğini gösterdim. İlginç bir şekilde, sadece iki *Kif2a* izoformunun gelişen kortekstekı radyal nöron göçünü desteklediğini gösterdim. Son olarak, yakınlık etiketleme tabanlı bir yöntem (BioID) kullanarak tüm KIF2A izoformlarının protein etkileşim ortaklarını proteom çapında tanımladım ve bu etkileşimlerin potansiyel olarak her bir protein izoformunun işlevini nasıl etkileyebileceğini belirledim. Sonuçlarım, alternatif kırpılmanın önemini ve izoforma özgü fonksiyonu nasıl düzenlediğini anlamamıza ışık tutacaktır.

Tezimin ikinci kısımda, gen ifadesi kontrolünün nöron göçü üzerine olan etkisini inceledim. Transkripsiyon faktörü *Neurod2*'nin (Neurogenic Differentiation 2) nöronların ilkel kortikal bölgenin en üst kısmına lokalize olmasını teşvik ederek, nöron göçünün terminal evresinde rolü olduğunu gösterdim. Sonuçlarım NEUROD2'nin son evre nöron göçünde yeni bir rolünü ortaya çıkarmıştır.

ACKNOWLEDGEMENTS

First and foremost I would like to express my sincere gratitude to my advisor Dr. Gülayşe İnce-Dunn, for her continuous support, guidance, understanding, wisdom, patience and encouragements throughout my Ph.D. studies. She relocated to Helsinki in my second year of Ph.D. and supported me from there with online meetings whenever I asked for. Her guidance and limitless help gave me a great motivation for my research. I gained an immense knowledge, learned valuable techniques and experience from her. It has been a great pleasure and privilege to work with her and I feel very lucky that she was my advisor throughout my masters and Ph.D. I would also express my special thanks to my second advisor Dr. Nurhan Özlü for her guidance and sharing great knowledge. I am extremely grateful that she accepted me in her lab in my second year of Ph.D. She supported me through three years and I gained very insightful techniques and knowledge from her. Besides my advisors, I would like to thank my thesis monitoring committee members, Prof. Dr. Arzu Karabay Korkmaz and Dr. Elif Nur Fırat Karalar for their valuable guidance, comments and discussions throughout my research. I would like to thank Dr. Tuğba Bağcı Önder and Dr. N.C. Tolga Emre for accepting to be participate in my Ph.D. thesis defense jury. Moreover, I would like to thank all jury members for giving their valuable time and critical reading on my thesis. I would like to express my gratitude for Dr. Cory Dunn for giving valuable feedbacks on my manuscripts.

I would like to acknowledge the financial support of the Scientific and Technological Research Council of Turkey (TUBITAK) and also Koç University throughout during my doctoral education and research.

I gratefully acknowledge Koç University Animal Research Facility for providing timed pregnant mice. Especially, I would like to thank Dr. Ali Cihan Taşkın for his help and knowledge; also Ahmet Kocabay, Nilhan Coşkun, Mustafa Demir and Oğuzkan Yaralı for their worthful help with mice experiments. Moreover, I acknowledge the Proteomics Facility of Koç University and I would like to thank mass spectrometry specialist Büşra Aytül Akarlar for her noteworthy technical support in my mass spectrometry experiments. Finally, I would like to acknowledge the Molecular Imaging Core Facility of Koç University Research Center for Translational Medicine (KUTTAM-CMIC) funded by the Republic of Turkey Ministry of Development, especially Dr. Berna Morova for her assistance with confocal microscopy.

I would like to thank former members of molecular neurobiology laboratory, especially Gizem Güzelsoy and Sıla Rızalar for their endless help and suggestions during my Ph.D., for their valuable friendship, all the tea breaks, long phone calls across continents; we had lots of fun together both in and outside of the lab during these five years. I would also thank Dila Atak for her friendship and assistance with experiments. Moreover, I would like to thank members of the cell biology and proteomics laboratory, especially, Dr. Zeynep Cansu Üretmen Kagıalı, Dr. Nazlı Ezgi Özkan Küçük, Büşra Aytül Akarlar and Dr. Nazan Saner for their endless support and being there in both the good and the bad times.

I would like to thank my two best friends Günce Bayram Severoğlu and Mehmet Gazaloğlu. Their support throughout my Ph.D. was worth more than anything for me and they are the most thoughtful, incredible and joyful friends that I could ever imagine. Furthermore, I would like to thank my cousin Nuray Kara Kuş, and my friends Kıvanç Hedili, Şengül Fındıklar, Demet Ay, Fulya Keskin, Onur Gültek, Adil Çetinkaya, Berk Tuzcu and Emre Sivrioğlu for their support and incredible memories.

I would also like to thank members of KUDANS International Latin family and my dance coaches, I feel very lucky to be a part of this beautiful and prestigious family. Especially I would like to thank Murat Hoşgör who is my best friend in Koç University. I am very grateful for having such a wonderful friend in my life and I thank him for our bitter-sweet dance practices, our tea and lunch breaks, enjoyable competition memories and his great support with my every decision.

The greatest thank goes to my family, Kemal, Nükhet, Pınar and Kaya to whom this thesis is dedicated. I am deeply grateful to them for doubtlessly believing in me. They gave me lots of love, joy and support not only throughout my graduate life but also every step of my life. I would like to thank my parents Kemal Akkaya and Nükhet Akkaya to whom I owe my success, for their endless support, love and encouragements. I would like to thank my aunt Nimet Gül for cooking me delicious food and my brother-in-law Derya Saatçı for his support. I would like to thank the best sister in the world Pınar Akkaya Saatçı who gave me the most incredible gift of my life, my nephew Kaya Saatçı. She is always stand by me and will continue to her support no matter what. Last but not least, I would like to thank my lovely nephew Kaya Saatçı who I love the most in the world. He changed my life forever and he gave me a strength, energy, lots of joy and love; and I am very grateful for being aunt of such an incredible person.

To my lovely family Kemal, Nükhet, Pınar and Kaya....

TABLE OF CONTENTS

ABSTRACT iii
ÖZET iv
ACKNOWLEDGEMENTS v
TABLE OF CONTENTS ix
LIST OF TABLES xiii
LIST OF FIGURES xiv
NOMENCLATURE xvii
Chapter 1 1
INTRODUCTION 1
Chapter 2 5
ROLES OF DEVELOPMENTALLY REGULATED KIF2A ALTERNATIVE ISOFORMS IN CORTICAL NEURON MIGRATION AND DIFFERENTIATION 5
2.1 LITERATURE REVIEW 5
2.1.1 Alternative splicing (AS) and RNA binding proteins (RNABP) 5
2.1.2 RNA binding proteins: ELAVL Family 10
2.1.3 Control of nELAVL on *Kif2a* pre-mRNA alternative splicing 11
2.1.4 Kinesin superfamily 13
2.1.5 Kinesin superfamily protein 2A (KIF2A) 17
2.1.6 Isoforms of KIF2A 19
2.1.7 Mammalian cerebral neocortex 21
2.1.8 Overview of the “inside-out” formation of cortical layers 21
2.1.9 Types of neural progenitors located in the cerebral cortex 23
2.1.10 Neurons of the cerebral cortex: Glutamatergic excitatory neurons and GABAergic inhibitory interneurons 25

2.1.11 Neurogenesis and radial cortical neuronal migration 27
2.1.12 Four distinct phases of neuronal migration 30
2.1.13 Malformations of cortical development (MCD) and disease-causing *Kif2a* mutants 31
2.2 MATERIAL AND METHODS 33
2.2.1 Collection and lysate preparation from mouse cortex tissue at different developmental time points 33
2.2.2 Total RNA isolation of mice cortices at different developmental time points 33
2.2.3 cDNA synthesis (RT-PCR) 34
2.2.4 Real Time PCR (Q-PCR) 35
2.2.5 Cloning of Kif2a.1, Kif2a.2, Kif2a.3, Kif2a^{S317N} and Kif2a^{H321D} into pcDNA4A plasmid 35
2.2.6 Cloning of shRNA against *Kif2a* 37
2.2.7 Site-directed mutagenesis of shKif2a-resistant *Kif2a* isoforms 39
2.2.8 Coating of plates 41
2.2.9 Primary neuronal culture preparation 41
2.2.10 Transfection of E14.5 primary cortical culture with Lipofectamine® 2000 reagent 42
2.2.11 Transfection of HEK293T cells with Lipofectamine® 3000 reagent 43
2.2.12 Transfection of Neuro2A cells with Lipofectamine® 2000 reagent 44
2.2.13 *In utero* electroporation, immunofluorescence and image analysis 45
2.2.14 Use of animals 48
2.2.15 Cloning of *Kif2a.1, Kif2a.2, Kif2a.3* and *Kif2a^{H321D}* into pcDNA3.1(-) mycBirA (mycBirA*) plasmids 48
2.2.16 Transfection of Neuro2A cells with Polyethylenimine reagent 50
2.2.17 Biotin treatment of cultures 50
2.2.18 Affinity capture of biotinylated proteins and Proximity-dependent biotin identification (BioID) 51

2.2.19 Immunoassays and image analysis 56
2.2.20 Proximity Ligation Assay (PLA) 62
2.3 RESULTS 64
2.3.1 KIF2A and nELAVL protein expressions are developmentally controlled in the mouse cerebral cortex 64
2.3.2 *Kif2a* alternative mRNA isoform expression is developmentally controlled in mouse cerebral cortex 66
2.3.3 Alternatively spliced KIF2A isoforms have the same subcellular localization in Neuro2A cells 68
2.3.4 Endogenous KIF2A is successfully knocked down in primary cortical neurons .. 70
2.3.5 shRNA against KIF2A can suppress the expression of all three endogenous *Kif2a* isoforms, but not the shRNA resistant *Kif2a* cDNAs 72
2.3.6 KIF2A isoforms are interchangeable in their roles for dendritic arborization of primary mice cortical neurons 74
2.3.7 KIF2A's role in radial cortical neuronal migration is isoform-dependent 77
2.3.8 Proximity-labeling protein interactome analysis of alternatively spliced KIF2A isoforms uncover novel isoform-specific interactors 82
2.3.9 KIF2A disease mutations co-localize only with MTs in Neuro2A cells 96
2.3.10 KIF2A disease mutations have no effect on dendrite branching in mice cortical neurons 98
2.3.11 KIF2A disease mutation resulted in protein interactome rewiring 100
2.4 DISCUSSION 109
Chapter 3 122
TERMINAL NEURON LOCALIZATION TO THE UPPER CORTICAL PLATE IS CONTROLLED BY THE TRANSCRIPTION FACTOR NEUROD2 122
3.1 LITERATURE REVIEW 122
3.1.1 Overview of mammalian cortex development 122
3.1.2 Neurogenins and NeuroD proteins 123

3.1.3 Neurogenic Differentiation 2 (NEUROD2) 125
3.1.4 REELIN signaling pathway 127
3.2 MATERIAL AND METHODS 130
3.2.1 *In utero* electroporation, immunofluorescence and image analysis 130
3.3 RESULTS 131
3.3.1 NEUROD2 affects REELIN protein levels in marginal zone of developing cortex. 131
3.3.2 NEUROD2 regulates terminal stages of radial neuronal migration by controlling the neuronal soma placement to primitive cortical zone 135
3.4 DISCUSSION 137
BIBLIOGRAPHY 143
VITA 160
Appendix A: Proximal interaction partners of KIF2A isoforms (KIF2A.1, KIF2A.2 and KIF2A.3) and disease-causing KIF2A mutant ($KIF2A^{H321D}$) 161
Appendix B: Role of Protocadherin 7 (PCDH7) in radial neuronal migration 165
Appendix C: Primer List 170

LIST OF TABLES

Chapter 2

Table 2. 1: Primary Antibodies used in immunoblotting. 60
Table 2. 2: Secondary Antibodies used in immunoblotting. 60
Table 2. 3: Primary Antibodies used in immunofluorescence. 61
Table 2. 4: Secondary Antibodies used in immunofluorescence. 61

Appendix

Table A. 1: KIF2A isoform specific proximal protein interaction partners 161
Table A. 2: Common proximal protein interaction partners of KIF2A isoforms 162
Table A. 3: KIF2A.1 and KIF2A^{H321D} specific proximal protein interaction partners 163
Table A. 4: Common proximal protein interaction partners of KIF2A.1 and KIF2A^{H321D} 164

LIST OF FIGURES

Chapter 2

Figure 2. 1 Alternative splicing can result in a change in cellular function. 6
Figure 2. 2: Types of alternative splicing events. 7
Figure 2. 3: nELAVL proteins modulate *Kif2a* pre-mRNA AS in neurons. 12
Figure 2. 4: Kinesin-13 family members depolymerize MTs in an ATP-dependent manner. 16
Figure 2. 5: Schematic of KIF2A isoforms (KIF2A.1, KIF2A.2 and KIF2A.3). 20
Figure 2. 6: Neocortex is formed in "inside-out" manner in mammals. 22
Figure 2. 7: Neural progenitor types and their differentiation fates during development. .. 24
Figure 2. 8: Cortical neuronal migration occurs both radially and tangentially. 26
Figure 2. 9: Spatiotemporal development of mouse neocortex. 29
Figure 2. 10: Schematic of disease-causing KIF2A mutants ($KIF2A^{S317N}$ and $KIF2A^{H321D}$). 32
Figure 2. 11: *In utero* electroporation method is widely used protocol to investigate neuronal migration. 47
Figure 2. 12: Schematic representation of BioID method followed by LC-MS/MS analysis. 55
Figure 2. 13: Schematic of Sholl analysis. 59
Figure 2. 14: Proximity Ligation Assay (PLA) is used for *in situ* detection of protein-protein interactions. 63
Figure 2. 15: KIF2A and nELAVL protein expressions are developmentally controlled in mouse cortex. 65
Figure 2. 16: *Kif2a* isoform expressions are controlled across development at mRNA level in mouse cerebral cortex. 67
Figure 2. 17: All KIF2A isoforms have diffuse cytoplasmic and nuclear localization in Neuro2A cells. 69
Figure 2. 18: shRNA against KIF2A was cloned successfully. 70
Figure 2. 19: shKif2a knocks down expression of endogenous KIF2A in primary cortical neurons. 71
Figure 2. 20: *resKif2a* plasmids for all three isoforms were cloned with site-directed mutagenesis. 72

Figure 2. 21: shKif2a can suppress KIF2A isoforms expression but not the resKIF2 in comparison to control (NS) in HEK293T cells. 73
Figure 2. 22: All three KIF2A isoforms function in proper dendritic growth and branching. 76
Figure 2. 23: Different KIF2A isoforms are not interchangeable for regulating the radial migration of cortical neurons. 80
Figure 2. 24: Disorder protein segments of individual KIF2A isoforms were identified with IUPred2 and ANCHOR2 algorithms [124] 81
Figure 2. 25: Immunofluorescence staining confirms biotinylation of transfected cells. 84
Figure 2. 26: Immunoblotting confirms that external biotin supplementation caused protein biotinylation only in BirA* expressing Neuro2A cells. 85
Figure 2. 27: Immunoblotting with anti-biotin antibody validates the pull-down of biotinylated proteins with streptavidin. 86
Figure 2. 28: Protein interaction partners of KIF2A isoforms are identified by a proximity-labeling method. 89
Figure 2. 29: Interactome map reveals the unique and common interactors of all KIF2A isoforms. 90
Figure 2. 30: Gene ontology and interactome analysis for each of the KIF2A isoforms are constructed. 92
Figure 2. 31: KIF2A and RTN4 are partially co-localized in Neuro2A cells. 93
Figure 2. 32: KIF2A interacts with RTN4 (NOGO) in a spatial resolution in Neuro2A cells. 95
Figure 2. 33: *Kif2a* disease mutants co-localize predominantly to microtubules in Neuro2A cells. 97
Figure 2. 34: KIF2A disease mutants do not affect dendrite development. 99
Figure 2. 35: Immunofluorescence staining confirms the biotinylation of the transfected cells. 101
Figure 2. 36: Immunoblotting confirms only external biotin addition biotinylated the transfected Neuro2A cells. 102
Figure 2. 37: Immunoblotting with anti-biotin antibody validates the pull-down of biotinylated proteins with streptavidin. 103
Figure 2. 38: Protein interaction partners of KIF2A^{H321D} are identified by a proximity-labeling method. 105

Figure 2. 39: Interactome map reveals the unique and common interactors of all KIF2A.1 and KIF2A^{H321D} 106
Figure 2. 40: Gene ontology and interactome analysis with interactors of KIF2A.1 and KIF2A^{H321D} are constructed. 107
Figure 2. 41: Model of alternatively spliced KIF2A isoforms in cortical neuronal migration and dendrite arborization in mice. 111

Chapter 3

Figure 3. 1: Transcriptional regulation in progenitor maintenance, non-neuronal differentiation and neuronal differentiation. 124
Figure 3. 2: REELIN signaling pathway in neurons. 128
Figure 3. 3: REELIN protein levels are affected in MZ upon *Neurod2* suppression in the developing cortex. 134
Figure 3. 4: NEUROD2 controls the soma positioning of the neurons to the primitive cortical zone. 136

Appendix

Figure B. 1: PCDH7 protein expression is controlled developmentally at mouse cortex. 165
Figure B. 2: There are two isoforms of PCHD7 represented as PCDH7-b and PCDH7-c.167
Figure B. 3: Role of different PCDH7 isoforms in cortical radial migration. 169

NOMENCLATURE

ADP	Adenosine diphosphate
aIP	Apical intermediate progenitors
AP	Apical progenitor
APOER2	Apolipoprotein E receptor 2
APS	Ammonium persulfate
aRG	Apical radial glia
AS	Alternative splicing
Asn, N	Asparagine
Asp, D	Aspartic acid
ATP	Adenosine triphosphate
BDNF	Brain derived neurotrophic factor
BF	BME supplemented with Ultraglutamine, P/S and FBS
bHLH	Basic helix-loop-helix
BioID	Proximity-dependent biotin identification
bIP	Basal intermediate progenitors
BME	Basal medium eagle
BNBF	BF media containing N-2 and B-27
Bp	Basepair
BP	Basal progenitor
bRG	Basal radial glia
BSA	Bovine serum albumin
cAMP	cyclic adenosine monophosphate
Cdk5	Cyclin-dependent kinase 5
cDNA	Complementary deoxyribonucleic acid
ChIP-qPCR	ChIP followed by quantitative PCR

C-KIF	C-terminal motor domain kinesin
CNS	Central nervous system
CP	Cortical plate
CR	Cajal-Retzius
CREB	cAMP-response element binding protein
CrkL	Crk-like
Cys, C	Cysteine
Dab1	Disabled 1
DAPI	4’6-diamidino-2-phenylindole
DIV	Day *in vitro*
DMEM	Dulbecco’s modified eagle medium
DMSO	Dimethyl sulfoxide
DNA	Deoxyribonucleic acid
dNTP	Deoxynucleotide
DTT	Dithiothreitol
E	Embryonic day
E.coli	*Escherichia coli*
EDTA	Ethylenediaminetetraacetic acid
ELAV	Embryonic lethal abnormal vision
ELAVL	Embryonic lethal abnormal vision-like
EMEM	Minimum essential medium eagle
ER	Endoplasmic reticulum
EML1	Echinoderm microtubule-associated protein-like 1
FastAP	Fast alkaline phosphatase
FBS	Fetal bovine serum
FDR	False discovery rate

Flna	Filamin A
GABA	γ-aminobutyric acid
GFAP	Glial fibrillary acidic protein
GFP	Green fluorescent protein
Glu, E	Glutamic acid
GO	Gene ontology
GSK-3β	Glycogen synthase kinase-3β
GTP	Guanosine triphosphate
HBSS	Hank's balanced salt solution
HEPES	4-(2-Hydroxyethly)piperazine-1-ethanesulfonic acid
His, H	Histidine
HITS-CLIP	High-throughput sequencing of RNA isolated by crosslinking immunoprecipitation
HRP	Horseradish peroxidase
IgG	Immunoglobulin G
IPC	Intermediate progenitor cell
IZ	Intermediate zone
kDa	Kilodalton
KEGG	Kyoto encyclopedia of genes and genomes
KIF	Kinesin superfamily protein
KIF2A	Kinesin superfamily protein 2A
Kin-I	Kinesin-internal
L	Layer
LB	Luria broth
LC	Liquid chromatography
LGE	Lateral ganglionic eminence

LPA	Lysophosphatidic acid
Lys, K	Lysine
M1 and M2	Manders' coefficient 1 and 2
MCPH	Primary autosomal recessive microcephaly
MGE	Medial ganglionic eminence
M-KIF	Middle motor domain kinesin
mRNA	Messenger ribonucleic acid
MS	Mass spectrometry
MT	Microtubule
MZ	Marginal zone
NEC	Neuroepithelial cell
nELAVL	Neuronal embryonic lethal abnormal vision-like
NEUROD2	Neurogenic differentiation 2
N-KIF	N-terminal motor domain kinesin
NOGO-A	Neurite outgrowth inhibitor-A
NOVA	Neuro-oncological ventral antigen
NPC	Neural progenitor cell
n.s.	Non-significant
NS	Non-silencing
oSVZ	Outer subventricular zone
P	Postnatal day
PBS	Phosphate buffered saline
PCR	Polymerase chain reaction
PEI	Polyethylenimine
PFA	Paraformaldehyde
PIP3	Phosphatidylinositol 3,4,5-triphosphate

PIPKα	Phosphatidylinositol 4-phosphate 5-kinase alpha
PKB	Protein kinase B
PLA	Proximity ligation assay
PLL	Poly-L-Lysine
PP	Preplate
pre-mRNA	Precursor messenger ribonucleic acid
PCDH7	Protocadherin 7
P/S	Penicillin/Streptomycin
PSM	Peptide spectrum match
PTBP1	Polypyrimidine tract-binding protein 1
Q-PCR	Quantitative polymerase chain reaction
RBFOX	RNA-binding fox
RBM4	RNA-binding motif 4
resKIF2A	Resistant KIF2A
RG	Radial glia
RIPA	Radio immunoprecipitation assay buffer
RNA	Ribonucleic acid
RNABP	Ribonucleic acid binding protein
RNA-seq	RNA sequencing
RRM	Ribonucleic acid recognition motif
RTase	Reverse transcriptase
RTN4	Reticulon 4
RT-PCR	Reverse transcription-polymerase chain reaction
SAP	Subapical progenitors
SDS	Sodium dodecyl sulfate
SDS-PAGE	Sodium dodecyl sulfate polyacrylamide gel electrophoresis

S.E.M.	Standard error of mean
Ser, S	Serine
SFK	Src-family kinase
shKif2a	shRNA against KIF2A
shNeurod2	shRNA against NEUROD2
shRNA	Short hairpin ribonucleic acid
SOCE	Store-operated calcium entry
SP	Subplate
SRRM4	Serine/arginine repetitive matrix 4
STIM1	Stromal interaction molecule 1
SVZ	Subventricular zone
TBS-T	Tris buffered saline-Tween
TEMED	Tetramethylethyleneamine
TF	Transcription factor
Tyr, T	Tyrosine
UTR	Untranslated region
UV	Ultraviolet
Val, V	Valine
VLDR	Very low density lipoprotein receptor
VZ	Ventricular zone
WM	White matter
WT	Wild type

Chapter 1

INTRODUCTION

The mammalian brain has a very complex organization and it needs coordinated operations of migration, layering and timing of proliferation. Additionally it requires differentiation of discrete neuronal populations [1-3]. The neocortex is phylogenetically the most recent part of the human brain which forms the most superficial layer of the cerebral hemispheres and has a role in many high order cognitive, motor and sensory functions such as language learning, self-awareness, voluntary movement and communication [4, 5]. It is organized into six functional and horizontal layers and each layer includes excitatory projection neurons and inhibitory interneurons [5]. During development of the mammalian cerebral cortex, neural progenitor cells (NPCs) transform into radial glial cells (RG) and divide symmetrically in the ventricular zone (VZ). Then the division mode transitions into an asymmetric mode to produce early neurons which exit the cell cycle and migrate radially through the subventricular and intermediate zones (SVZ-IZ) until they reach their destined location at cortical plate (CP). Late-born neurons migrate and by-pass early-born neurons finally giving rise to six-layered cortex structure in an “inside-out” manner [5, 6]. When these developmental processes are disrupted, cortical development disorders such as pachygyria, microcephaly, polymicrogyria and lissencephaly are observed [2, 7-9].

During development of the nervous system, the control of the ordered production and differentiation of cell types are essential for the proper formation of the six-layered cortex. These processes are controlled tightly by gene expression mechanisms at both transcriptional and post-transcriptional levels [10, 11]. Post-transcriptionally, differential polyadenylation, mRNA transport and stability, splicing, translation and degradation of transcripts affect gene expression [10, 12]. Alternative splicing (AS) is one of the main molecular processes contributing to increased transcriptome and proteome diversity and also organismal complexity in metazoans [13-16]. AS is common in the nervous system [17, 18] and defects in AS often result in neurological disorders [19, 20]. AS is regulated dynamically throughout brain development, where it regulates crucial processes such as neuronal migration, synaptogenesis, axon guidance and cell-to-neuron transition, [14, 21, 22]. How AS regulates transcriptome and proteome diversification in a tissue-specific manner, and how each alternatively-spliced isoform functions to modulate the development of the nervous system is largely unknown. In the first part of my thesis, I focused on the distinguishable functions of three different isoforms of the Kinesin superfamily protein 2A (KIF2A) in development of the mouse cerebral cortex. KIF2A is a member of the Kinesin-13 family along with the other members KIF2B, KIF2C/MCAK and KIF24 and it is a microtubule (MT) depolymerizer which is enriched in both mitotic cells and developing neurons [9, 23-25]. In mitotic cells, it has many roles such as mitotic spindle assembly [26] and primary cilium disassembly [27, 28]. In differentiating neurons, it regulates axonal pruning [29, 30]. Alternative splicing of *Kif2a* pre-mRNA is modulated by neuron-specific RNA binding proteins (RNABP) [31], and during neural progenitor-to-neuron transition, its isoform abundance shifts dynamically [15]. However, our understanding of the functional roles of alternatively-spliced KIF2A isoforms is lacking. In this study, my results demonstrated that KIF2A is required for dendritic arborization in mouse primary cortical neurons and all three alternatively-spliced isoforms can fulfill this function. Moreover, I confirmed that KIF2A is

also required for radial neuronal migration and only two of these isoforms can support this process in the mouse developing cortex. I also identified differential functional roles for KIF2A protein isoforms by carrying out a proximity-ligation-based proteomic study. My results demonstrate that alternative splicing of KIF2A protein causes a change in its interacting protein partners and different KIF2A isoforms show differential effects on the migratory behavior of neurons during cerebral cortex development.

During development of the cerebral cortex, most superficial zone marginal zone (MZ) is composed of Cajal-Retzius (CR) cells. These cells secrete an extracellular glycoprotein REELIN which has a role in termination of neuronal migration [32]. Migrating neurons express intracellular adaptor protein DAB1 as well as REELIN receptors LRP8 (APOER2) and VLDLR. REELIN binding promotes receptor internalization and phosphorylation of DAB1 [32]. Activated REELIN signaling leads to anchorage of nascent primary dendrites to the extracellular matrix of the MZ as well as and migration termination and stabilization of the neuronal cytoskeleton [33-38]. In addition to the REELIN signaling pathway, combinatorial expression of particular transcription factors (TFs) also regulates cortical radial neuronal migration process [5]. Among these, Neurogenins and NeuroDs which are the members of a basic helix-loop-helix (bHLH) TF family have been shown to control particular steps of cortical radial migration as well as neuronal differentiation and cell fate specification [39-41]. However, how NEUROD2 modulates the expression of its downstream targets and how this modulation affects cortical migration was unknown. In the second part of my thesis, I investigated the role NEUROD2 in radial cortical migration [42]. *Neurod2* gene is highly expressed in embryonic cortex and in adulthood its expression remains at low levels in cortical excitatory neurons [43, 44]. Previously, genetic targets of NEUROD2 was characterized in the cerebral cortex at both embryonic day 14.5 (E14.5) and postnatal day 0 (P0) developmental time points by carrying out ChIP-Seq analysis by our group [43, 45]. Furthermore *Neurod2* expression was silenced in E14.5 primary cortical

neurons and RNA-Seq analysis was performed in order to identify those genes whose expression is regulated by NEUROD2. Our data identified several NEUROD2 targets such as *Reln, Lrp8* and *Dab1* which are known to function in the REELIN signaling pathway. Interestingly, in our ChIP-Seq analysis, we identified direct NEUROD2 binding within several introns of the *Reln* gene. We found that binding of NEUROD2 on conserved E-box domains in multiple introns of *Reln* suppresses *Reln* at the mRNA level. When we knocked down *Neurod2* in primary cortical neurons, we observed a strong upregulation of *Reln* mRNA levels. Interestingly, we also observed a slight, yet significant increase in protein levels. Finally, we observed a defect in terminal neuronal localization to the primitive cortical zone when we suppressed *Neurod2* expression by *in utero* shRNA electroporation in migrating neurons. Our data uncover a new role for NEUROD2 in neuronal migration at the terminal stage, and our analysis of genomic targets provides new genes which have potential roles in cortical lamination [42].

Chapter 2 covers my studies on the role of the developmentally regulated KIF2A alternative isoforms in cortical neuronal migration and differentiation. In Section 2.1, there is a detailed review of current literature about RNA binding proteins, alternative splicing, mouse cortex development and functional roles of the KIF2A protein. The materials and methods which are used in this study are explained in Section 2.2. The results of this project are represented in Section 2.3 and finally the discussion of the results is explained in Section 2.4.

Chapter 3 covers my studies on the role of NEUROD2 in radial neuronal migration. In Section 3.1, there is a review of transcription factor NEUROD2 and REELIN signaling pathway. The materials and methods which are used in this study are explained in Section 3.2. The results of this project are represented in Section 3.3 and finally the discussion of the results is explained in Section 3.4.

Chapter 2

ROLES OF DEVELOPMENTALLY REGULATED KIF2A ALTERNATIVE ISOFORMS IN CORTICAL NEURON MIGRATION AND DIFFERENTIATION

2.1 LITERATURE REVIEW

2.1.1 Alternative splicing (AS) and RNA binding proteins (RNABP)

Humans have approximately 20,000-25,000 genes and if only one protein is generated from each gene, it would create a limited proteome complexity. Alternative splicing (AS) of precursor mRNA (pre-mRNA) is one of the leading mechanism which increases both transcriptome and proteome complexity, hence organismal complexity and functional diversity in metazoans, by generating multiple mRNA isoforms from a single gene [16, 20, 46]. AS can generate cell type specific and functionally distinguishable protein isoforms [13] **(Figure 2.1)**.

High-throughput RNA sequencing (RNA-seq) analysis revealed that 90-95% of human multi-exon genes generate more than 100,000 different mRNA isoforms by AS and most of the isoform functions are completely unknown. AS creates complexity with regulated splicing mechanisms such as cassette exon, mutually exclusive cassettes, intron retention, alternative 5’ and 3’ splice sites, alternative promoter, and alternative polyadenylation

(Figure 2.2). In humans, the most frequent AS type is cassette exon usage (35.3%) followed by nearly even distribution of remaining events [16, 20].

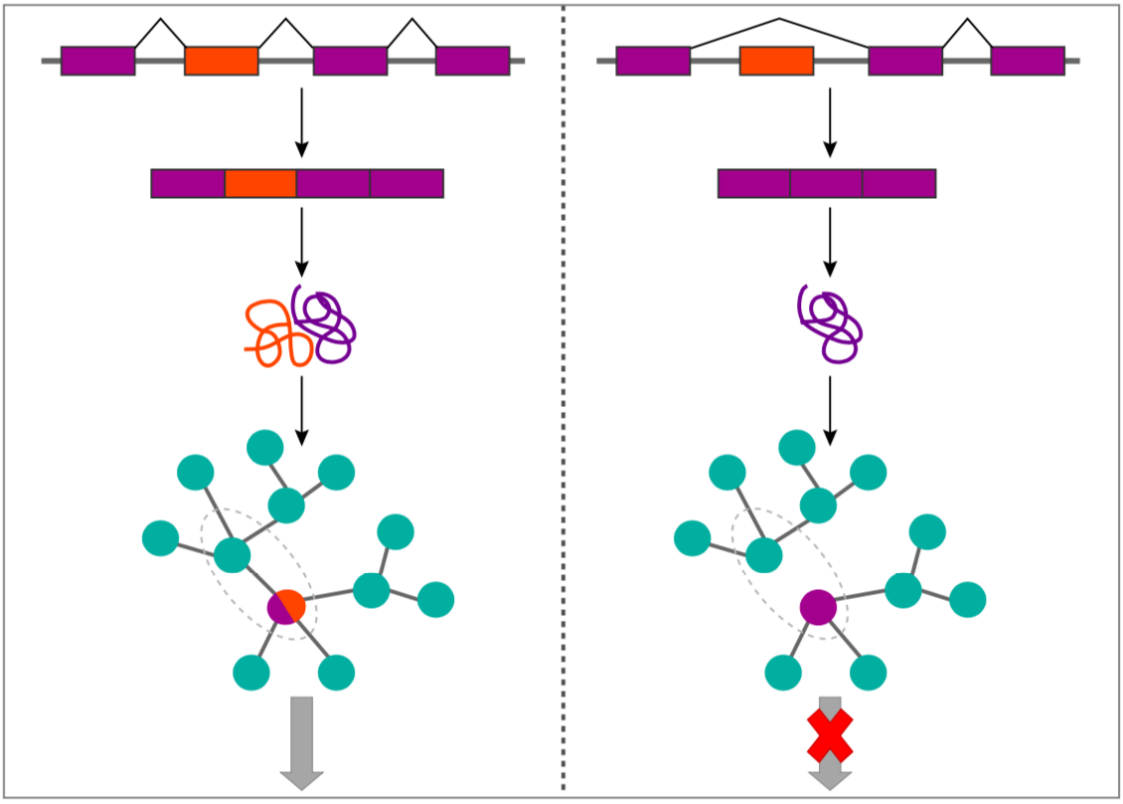

Figure 2. 1 Alternative splicing can result in a change in cellular function.

AS can generate functionally distinguishable isoforms which changes the protein interaction network hence affecting function (Adapted from [47, 48]).

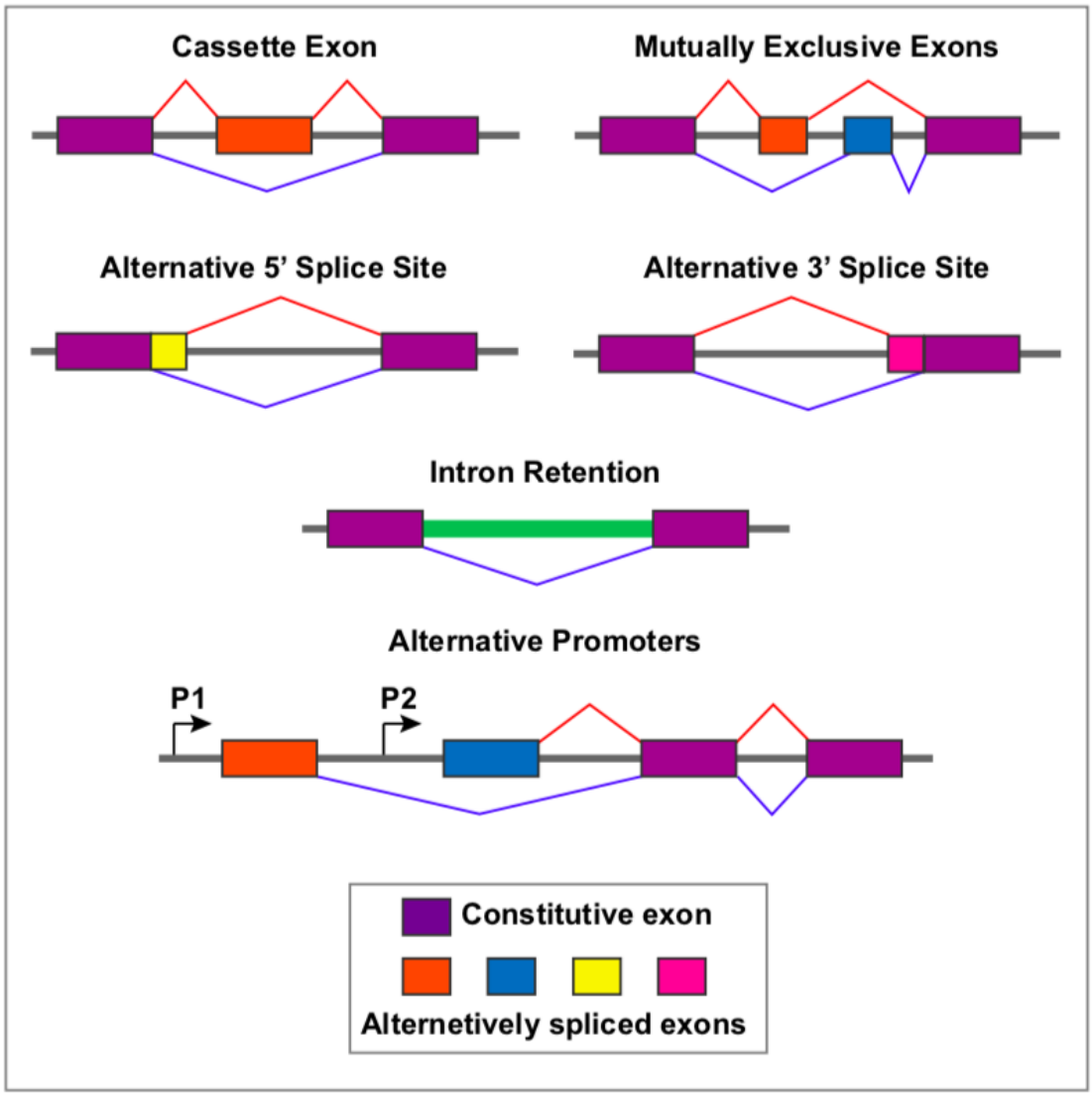

Figure 2. 2: Types of alternative splicing events.

There are six main types of AS events which are cassette exon, mutually exclusive exons, alternative 5' splice site, alternative 3' splice site, intron retention and alternative promoters (Adapted from [16, 49]).

Compared to other organs, genome-wide transcriptome profiling showed that AS occurs in mammalian brain at the highest frequency, contributing to the development of nervous system by playing roles in cell-fate decisions, neuronal migration, complex network formation, synaptogenesis, and axon guidance. For instance, during neuronal differentiation, AS regulates centriolar dynamics, metabolic pathways and signaling activity [14]. Furthermore, it affects neuronal development, function and cortical dynamics [13, 14, 16, 22]. RNA-seq analysis using purified neuronal progenitor cells (NPCs) and differentiating neurons showed that neurons are subject to AS during differentiation in mouse cerebral cortex [14, 15]. Moreover, diverse splicing patterns in radial glial (RG) cells, intermediate progenitor cells (IPCs) and neurons are revealed during cortical development using fetal neocortex and human cerebral organoids [14, 15, 50]. In particular, cytoskeletal genes which undergo AS encodes functionally interconnected protein interactomes implicated in neuronal migration and differentiation as well as NPC proliferation [15]. Moreover, genes that are involved in mouse cerebral cortex development such as *Macf1*, *Scrib*, *Ank2*, *Kif2a*, *Fln*a, *Syne2* and *Add1* are also alternately spliced [15]. It has been reported that impaired AS is often associated with neurological diseases due to damage in the neural development both in animal models and humans [13, 16, 19, 20, 51-53].

RNA binding proteins (RNABP) are at the center of post-transcriptional regulation and they have roles in regulating the abundance, form and stability of coding or non-coding RNA in eukaryotes which are very crucial for nervous system development [54, 55]. RNABPs have three RNA recognition motifs (RRM) and through these sites, they recognize and bind RNA and control post-transcriptional RNA processing [10, 56]. Various RNABPs such as embryonic lethal abnormal vision (ELAV), neuro-oncological ventral antigen (NOVA), RNA-binding motif 4 (RBM4), RNA-binding fox (RBFOX), polypyrimidine tract-binding protein 1 (PTBP1) and serine/arginine repetitive matrix4 (SRRM4) play roles in neuronal

development and maintenance in the brain by regulating AS of specific pre-mRNAs. Neuronal migration defects are observed if one of these splicing factors do not function properly [14, 57]. For instance, in the developing brain, RBM4 and PTBP1 control the expression pattern of Disabled-1 (DAB1) isoforms and defects in its AS affect REELIN-mediated cortical neuronal migration. Deficiency in RBM4 causes abnormalities in brain development [13, 58]. In addition, PTBP1 and RBFOX have a role in antagonist regulation of neuronal fate by modulating the selection of an alternative exon [14, 15]. PTBP1 regulates AS of *Filamin A (Flna)* by suppressing a premature stop codon-containing exon in NPCs, thus preserving apical progenitors. On the other hand, RBFOX modulates AS of *Ninein* by switching to a non-centrosomal form, thus enhancing NPC differentiation [14]. Finally, switching expressions of PTBP1 to PTBP2 occurs which is very important in stem cell-to-neuron transition during neurogenesis [14, 59, 60].

2.1.2 RNA binding proteins: ELAVL Family

As mentioned in **Section 2.1.1**, high amounts of RNABPs are expressed during development of nervous system and it has been known that they have critical roles in neuronal development [10, 31, 55]. Among these, highly conserved ELAVL (Elavl-like) proteins which share homology with the Drosophila ELAV/Hu (Embryonic Lethal and Abnormal Vision) display a neuronal-restricted expression pattern [10, 31, 55]. They are essential for neuronal differentiation process as well as synaptic plasticity [10]. In humans, ELAVL proteins were identified as autoantigens in paraneoplastic encephalomyelitis syndrome which is an autoimmune disorder of the nervous system linked to small cell lung carcinoma [10, 61, 62].. In this syndrome, several neurological deficiencies are observed due to an antibody-mediated autoimmune response that occurs via ectopic expression of Elavl antigens on by tumor cells. By unknown mechanisms in some patients these anti-ELAVL antibodies cross the blood brain barrier and attack ELAVL expressing neurons which then causes neuronal degeneration [10, 61, 62].

There are four members of ELAVL proteins (~40 kDa); ELAVL1 (HuA/HuR), ELAVL2 (HuB), ELAVL3 (HuC), and ELAVL4 (HuD). They contain three RRM motifs; two of them (RRM1 and RRM2) are located at the N-terminus and have roles in binding RNA targets, and one of them (RRM3) which binds to the poly(A) sequences is located at the C-terminus. These RRM domains are separated from each other with a hinge region which carries nuclear localization and export signals so that ELAVL proteins could shuttle between the cytoplasm and nucleus [10, 31, 63-65]. ELAVL1 is expressed ubiquitously and subcellularly localized to the nucleus. It has roles in regulation of mRNA stability, translation enhancement and repression, polyadenylation, DNA damage response, splicing, and negative regulation of apoptosis. ELAVL2, ELAVL3 and ELAVL4 have nervous system-specific

expression pattern thus, they are called as neuronal ELAVL (nELAVL). They play roles in positive regulation of mRNA stability, mRNA transport, translation enhancement, polyadenylation, splicing, neuronal maintenance, neuronal differentiation, learning and memory [10, 31, 55]. It has been shown that *Elavl4* knockout mice have cranial development nerve delay at embryonic day 10 (E10). At adult stage, these mice are infertile and also show defective motor abilities [66]. Furthermore, another study revealed that *Elavl3* null mice are viable and fertile but they demonstrate failure in cortical and cerebellar development [31].

2.1.3 Control of nELAVL on *Kif2a* pre-mRNA alternative splicing

High-throughput sequencing of RNA isolated by crosslinking immunoprecipitation (HITS-CLIP) method was used to find RNA binding sites of the nELAVL RNABPs [31]. nELAVL were found to bind preferentially to conserved U-rich sequences at exon-intron junctions and this binding regulated alternative exon inclusion. Furthermore, nELAVL proteins bind to 3'UTR to modulate mRNA levels [31]. Thirty-seven ELAVL3/4 dependent alternative exons are verified by qRT-PCR [31]. *Kinesin superfamily protein 2a* (*Kif2a*) which is microtubule (MT)-depolymerizing kinesin was identified as one of the top target pre-mRNAs [30, 67]. ELAVL3/4 bind to U-rich intronic sequences flanking the *Kif2a* alternative exon 18 and regulates its AS. Moreover, *Elavl3/4* deletion in mice causes a significant decrease in the ratio of exon 18 included to excluded *Kif2a* pre-mRNA **(Figure 2.3A)**. This result explains how nELAVL RNABPs binding regulate KIF2A isoform abundance by enhancing the formation of alternative exon 18-included isoform (KIF2A.1) which eventually repress the formation of isoform that lacks exon 18 (KIF2A.2) **(Figure 2.3B)**.

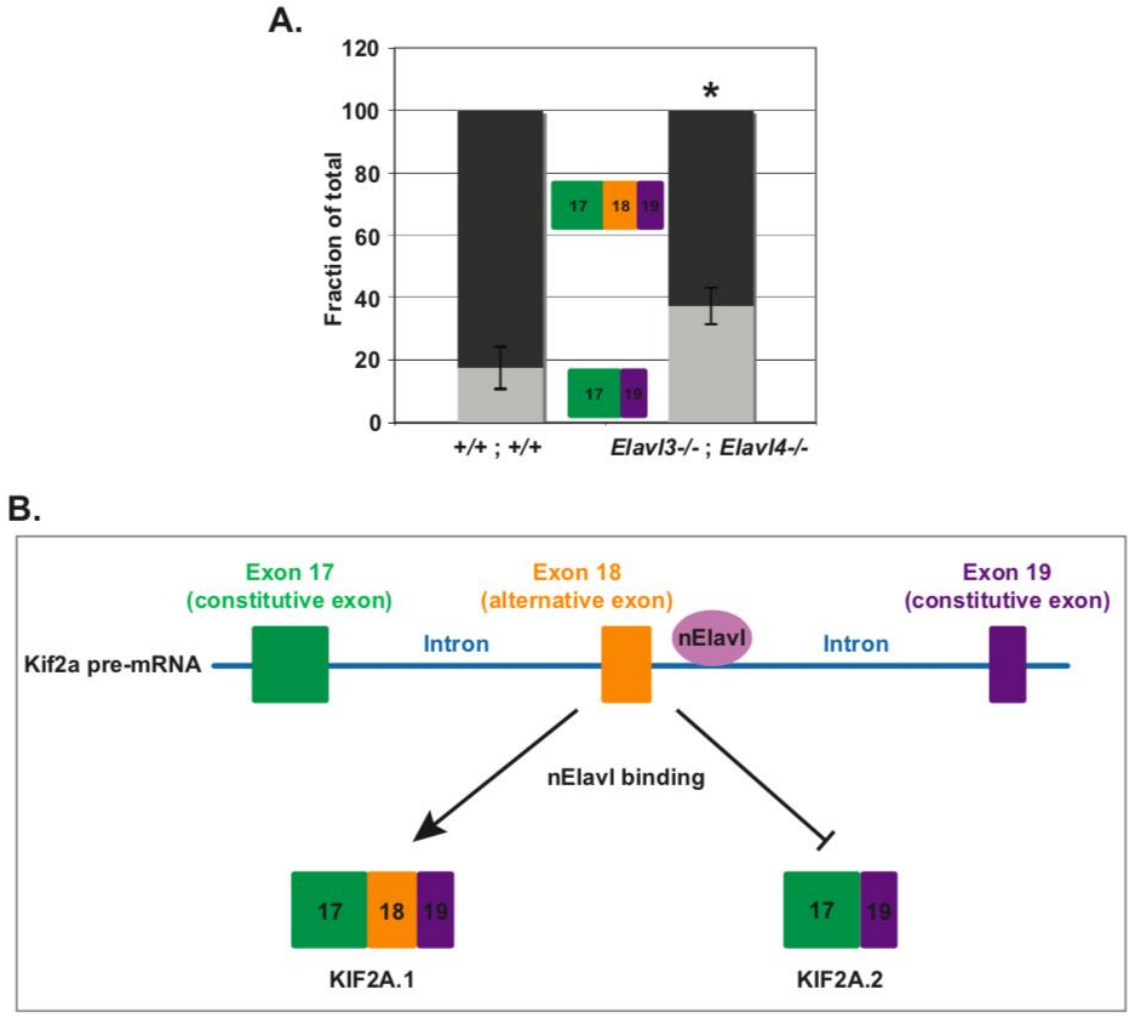

Figure 2. 3: nELAVL proteins modulate *Kif2a* pre-mRNA AS in neurons.

A. Deletion of *Elavl3/4* has an impact on the ratio of KIF2A.1 to KIF2A.2 [31]. **B**. nELAVL proteins bind to intronic region flanking to exon 18 and enhance the formation of KIF2A.1.

2.1.4 Kinesin superfamily

Microtubules (MTs) are one of the major polarized and dynamic components of the cytoskeleton which supports cell morphology, movement of flagella and cilia and cell polarity. They also have fundamental roles such as intracellular trafficking, cell cycle and cell motility [68, 69]. They are composed of α- and β- tubulin heterodimers which then form a cylindrical 13 protofilament structure [70]. Guanosine triphosphate (GTP) hydrolysis fuels dynamic instability of MTs [70, 71]. MTs also have cell type specific roles. For instance, in neurons which are highly polarized cells and have long processes, MTs have roles in axonal transport by organizing their plus ends through the axon tip. In mitotic cells, they form mitotic spindle to first align the chromosome in the equatorial plate and then segregate them toward the poles during mitosis. Moreover, they from 9+2 array to drive motility in flagella and cilia [69].

Molecular motor proteins generate cellular forces and control various types of intracellular movement [72, 73]. Polarized MTs function as a track for motor proteins including cytoplasmic dynein and kinesin superfamilies to transport their cargos unidirectionally inside the cell [23]. Kinesin motor proteins are involved in anterograde transport, whereas dynein motors transport cargos retrogradely [24]. In neurons, molecular motors play critical roles in different neuronal processes such as neuronal plasticity, survival, morphogenesis and function via transporting several types of cargos including neurotransmitter, synaptic vesicle precursors and mRNAs within the dendrites, synapses and axons [74].

Kinesin superfamily proteins (KIFs) are MT-dependent molecular motor proteins that are identified initially for their roles in axonal transport [74-77]. In intracellular trafficking, KIFs generally transport cargo towards the plus ends of MTs. However, some of the members move in the opposite direction and some regulate MT dynamics by stabilizing and depolymerizing the MTs [9, 77, 78]. They also have roles in crosslinking, aligning MTs into polarized bundles and modifying MT dynamics via interacting with MT tips [78]. Almost half of the KIFs are expressed in neurons and play a major role in the transport of several membranous organelles along axons and organization of the MTs and these activities make them central players in neuronal proliferation, neuronal migration, and post-migrational development [9]. For instance, KIF1A and KIF1Bb transport synaptic vesicle precursors; KIF5 has roles in transporting mitochondria, active zone vesicles, amyloid precursor protein-containing, TrkB and APOER2 vesicles; and finally KIF13B transports and phosphatidylinositol 3,4,5-triphosphate (PIP3) vesicles [74].

In mammals, there are 14 KIF classes containing 45 *Kif* genes in total [74, 79]. KIFs are classified according to position of their catalytic motor domain: C-terminal motor domain kinesins (C-KIFs), middle motor domain kinesins (M-KIFs) or kinesin-internal (Kin-I) and N-terminal motor domain kinesins (N-KIFs) [74, 80]. C-KIFs move toward the MT minus end whereas N-KIFs move towards the plus end of MTs. N- and C-KIFs, contain motor domain where they bind and move along the MTs by adenosine triphosphate (ATP) hydrolysis. They also contain tail region for cargo recognition and binding [74, 79].

Most KIF proteins are responsible for MT-based cargo trafficking. Unlike these conventional KIFs, Kinesin-8 and Kinesin-13 families depolymerize MTs by using an ATP-binding cycle. It has been shown that members of the Kinesin-13 family are essential for mitotic processes such as chromosome segregation, kinetochore-MT attachment and spindle dynamics [23, 68, 69, 80-82]. Amino-terminal extension also called as neck (60 amino acid stretch) enhances the recruitment of motor domain to MTs. Motor domain is located in the middle and it contains both KVD (Lysine (Lys), Valine (Val) and Aspartic acid (Asp)) amino acid sequence which is required for MT depolymerization and a KEC (Lysine (Lys), Glutamic acid (Glu) and Cysteine (Cys)) amino acid sequence which is the MT-binding motif. The carboxy-terminal tail also called the stalk of Kinesin-13 family members is required for dimerization which enhances depolymerization activity [27, 78].

As mentioned above Kinesin-13 family is a MT-depolymerizer. In solution Kinesin-13 proteins (KIF2A, KIF2B, KIF2C/MCAK and KIF24) are in their Mg-ATP-bound state. When they interact with the MT lattice, this stimulates Mg-ATP hydrolysis so that they can perform axial diffusion on the MT lattice in their ADP or ADP-Pi state. When they reach the MT end, ADP dissociation is induced which allows for ATP rebinding. ATP binding induces protofilament curling so that tubulin dimers can get released from the protofilament **(Figure 2.4)** [69, 78].

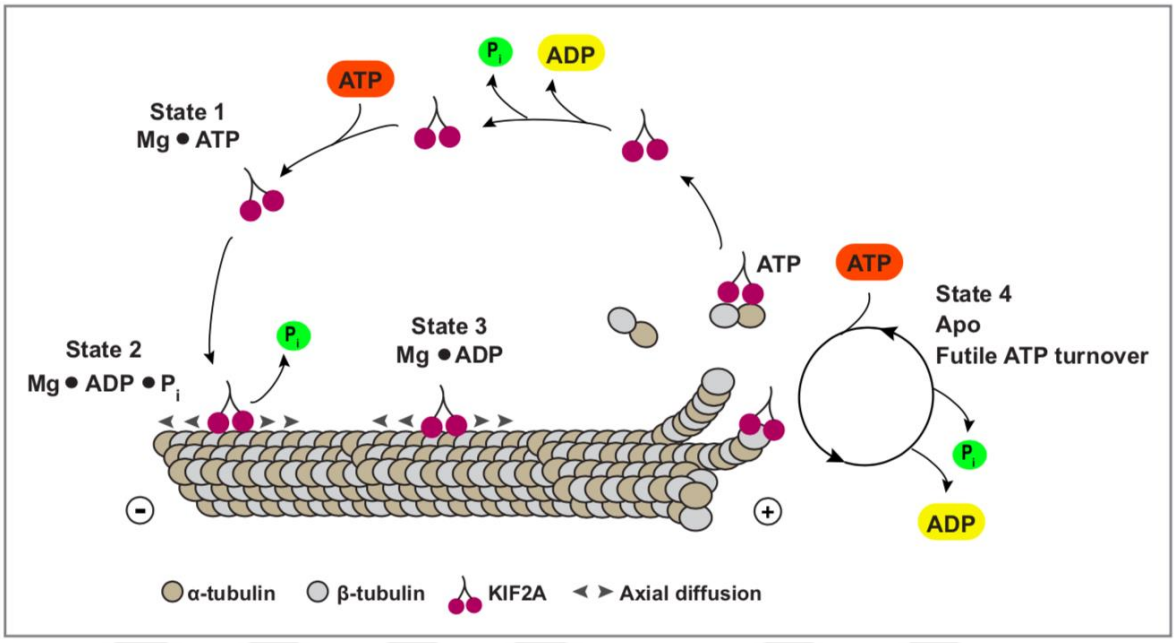

Figure 2. 4: Kinesin-13 family members depolymerize MTs in an ATP-dependent manner.

Members of the Kinesin-13 family (KIF2A, KIF2B, KIF2C/MCAK and KIF24) form dimers. This figure shows how KIF2A depolymerizes MTs. In solution, KIF2A is in its Mg-ATP state (State 1). Binding to MT lattice induces Mg-ATP hydrolysis (State 2) and inorganic phosphate is released from KIF2A. In this Mg-ADP bound state KIF2A moves along the MT lattice through its motor domain by axial diffusion (State 3). When KIF2A reaches the MT tip, inducing Mg-ADP release, it enters the Apo state (State 4) where Mg-ATP binds. In this state KIF2A-ATP stabilizes the curved formation of tubulin which leads to removal of the tubulin dimer from the MT tip (Adapted from [78]).

2.1.5 Kinesin superfamily protein 2A (KIF2A)

KIF2A is an ATP-dependent MT depolymerizer which is enriched in both mitotic cells and developing neurons [9, 23-25]. Subcellularly, KIF2A is localized to spindle MTs and poles in mitotic cells and to growth cones and axons in neurons [24, 26, 81, 83-85] and N-terminal is responsible for the localization of KIF2A to the spindle poles [86]. In mitosis, MT depolymerization activity of KIF2A is regulated positively by PLK1 (Polo-like kinase 1) and negatively by Aurora A kinase [81]. Moreover, phosphorylation of KIF2A by PLK1 regulates primary cilium disassembly by depolymerizing MTs at mother centriole in a growth-signal-dependent manner [27]. In addition to its roles in regulation of the mitotic process and primary cilium formation, KIF2A is involved in a number of different functions in the nervous system. KIF2A prunes axonal collateral branch formation by regulating MT dynamics and directly interacting with phosphatidylinositol 4-phosphate 5-kinase alpha (PIPKα) in growth cones [67, 87]. *Kif2a* knock-out neurons form abnormal axonal branching due to overextension of collateral branches and *Kif2a* knock-out mice die within a day after birth with their brains show multiple abnormalities such as lamination defects, ventricle enlargement, and lack of nerve nuclei [67]. KIF2A also induces axonal breakdown and pruning by depolymerizing MTs and *Kif2a* knock-out mouse shows skin hyperinnervation [30]. KIF2A also modulates neuronal morphology via regulating MT dynamics by two different sets of phosphorylation cascades that either accelerate (A-type) or brake (B-type) MT depolymerization. In A-type KIF2A phosphorylation, lysophosphatidic acid (LPA) binding stimulate ROCK2 kinase which phosphorylates KIF2A in a site-specific manner and phosphorylated KIF2A depolymerizes MTs and causes neurite outgrowth suppression. On the other hand, in B-type KIF2A phosphorylation, brain derived neurotrophic factor (BDNF) binding induces CDK5 and PAK1 kinases to phosphorylate KIF2A at different amino acid residues and this time MT depolymerizing activity of KIF2A is suppressed which enhances

the formation of neurites [80]. Moreover, *Cenpj* conditional knock out mice showed neurogenesis defects and abnormal long cilia formation and *Kif2a* expression in these mice rescued both of these phenotypes. These results indicate that KIF2A might be the downstream of Cenpj and cilia disassembly, neural progenitor cell (NPC) proliferation and cortical development processes are regulated by the centriole biogenesis protein Cenpj through KIF2A [88]. When KIF2A is depleted in embryonic mice cortices, neurogenesis is impaired by a significant accumulation of neurons in the ventricular zone-subventricular zone (VZ-SVZ) and intermediate zone (IZ) causing significantly less neuron migration towards the cortical plate (CP) [8, 88]. In NPCs, WDR62 interacts with CEP170 and this interaction leads localization of CEP170 to the basal body of the primary cilium where CEP170 recruits KIF2A for primary cilium disassembly via MT depolymerization. Primary autosomal recessive microcephaly (MCPH) is observed in cerebral organoids when this pathway is disrupted [28]. Furthermore, tamoxifen-inducible *Kif2a* conditional knock-out mice have epileptic hippocampus and dendro-axonal conversion in their dentate granule cells highlighting the importance of KIF2A in postnatal hippocampal wiring [29]. Finally, *Kif2a* is found to be one of the cytoskeleton-related gene that is been alternatively spliced during NPC-to-neuron transition [15].

2.1.6 Isoforms of KIF2A

It has been reported that nELAVL regulates AS of *Kif2a* pre-mRNA [31]. In mice *Kif2a* gene is composed of 20 coding exons and nELAVL binds to U-rich intronic sequences of the *Kif2a* pre-mRNA. This binding promotes the inclusion of exon 18 which encodes for a 37 amino acids rich in serine (Ser, S) residues. While cloning these two isoforms from the postnatal mouse cerebral cortex, our group identified a third isoform which contained exon 18, along with a truncated (by 20 amino acids) exon 5 as a result of alternative 5' splice site selection. Thus, we numbered these isoforms as *Kif2a.1* (exon 18+ and long exon 5), *Kif2a.2* (exon 18- and long exon 5) and *Kif2a.3* (exon 18+ and short exon 5) **(Figure 2.5).**

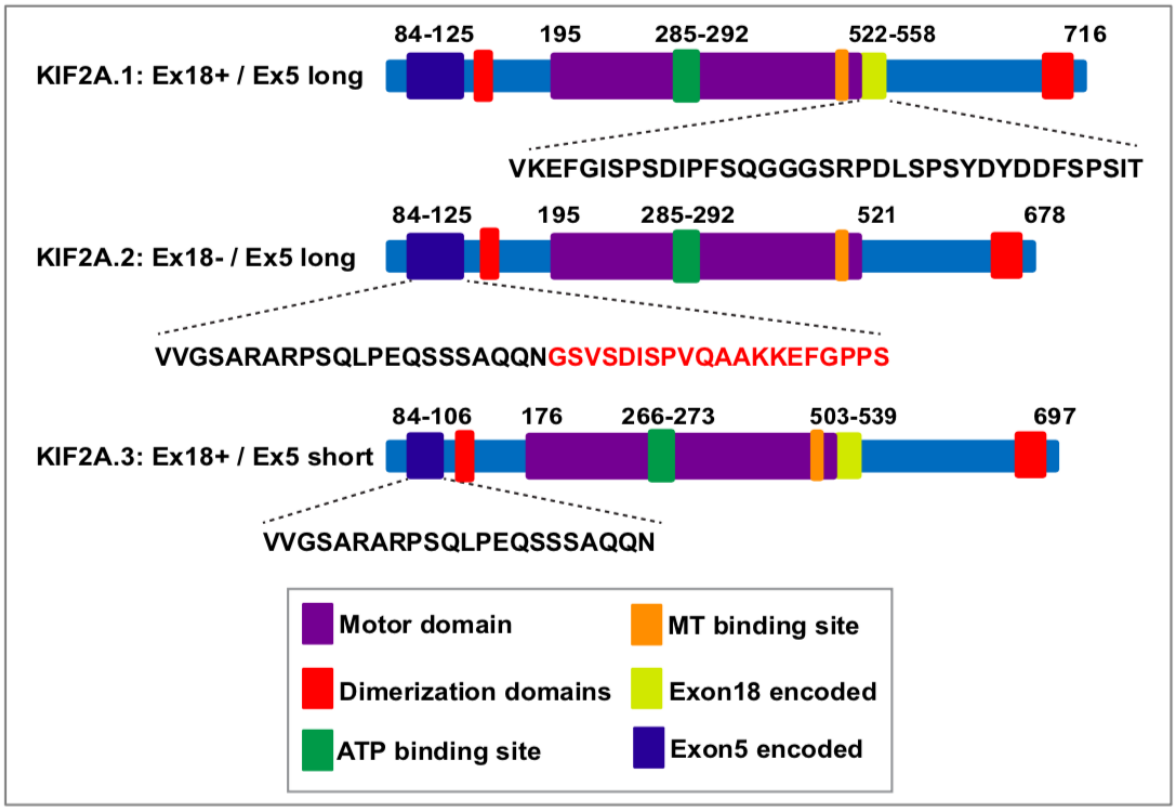

Figure 2. 5: Schematic of KIF2A isoforms (KIF2A.1, KIF2A.2 and KIF2A.3).

All three KIF2A isoforms have ATP binding site on their motor domains located at the middle. They also contain MT binding sites and dimerization domains. Amino acid sequences of Exon 18, Exon 5-long and Exon 5-short are indicated and the amino acid sequence absent in Exon 5 of KIF2A.3 is highlighted in red.

2.1.7 Mammalian cerebral neocortex

The cerebral neocortex is phylogenetically the newest part of the mammalian brain. It is involved in various higher functions such as motor, sensory, emotional, cognitive as well as sensory perception and consciousness. It is composed of six horizontal layers and develops in an "inside-out" manner [5, 15, 70]. Within each layer, neuronal identity and connectivity patterns tend to resemble each other. For instance, upper layer II-IV (LII-LIV) neurons mostly build ipsilateral or contralateral cortico-cortical connections, whereas deep layer V and VI (LV and LVI) neurons make connections with subcortical structures [4, 89].

2.1.8 Overview of the "inside-out" formation of cortical layers

Neuronal migration is a fundamental process which is essential for the development of the mammalian nervous system [90]. Cortical projection neurons are generated in the dorsal germinal zones of the telencephalon, the ventricular zone (VZ) and subventricular zone (SVZ). Newly born neurons then migrate radially through the intermediate zone (IZ) to reach their final destination in the cortical plate (CP). Starting at approximately embryonic day 10.5 (E10.5) in mice, the preplate (PP) which is a band of cells located at the superficial layer of cortical wall, is formed by the earliest generated cortical neurons. At around E11.5, the first cortical projection neurons are born and they migrate radially to form the nascent CP which subsequently gives rise to LII-LVI of the postnatal neocortex. Incoming CP neurons divide the PP into the marginal zone (MZ), which evolves into LI of postnatal cortex, and the deeper subplate (SP), which is located below LVI. These neurons are the first neurons to fulfill their morphological maturity and assemble synapses. As neurogenesis proceeds different subtypes of projection neurons are born consecutively and migrate to their destination in an "inside-out" manner **(Figure 2.6)**. Neurons that are born first settle in the deepest layers whereas, neurons that are generated later occupy more superficial layers and

as a result the six-layered cortex is formed. Thus, the birthdate of cortical projection neurons is closely connected with their laminar identity [5, 70].

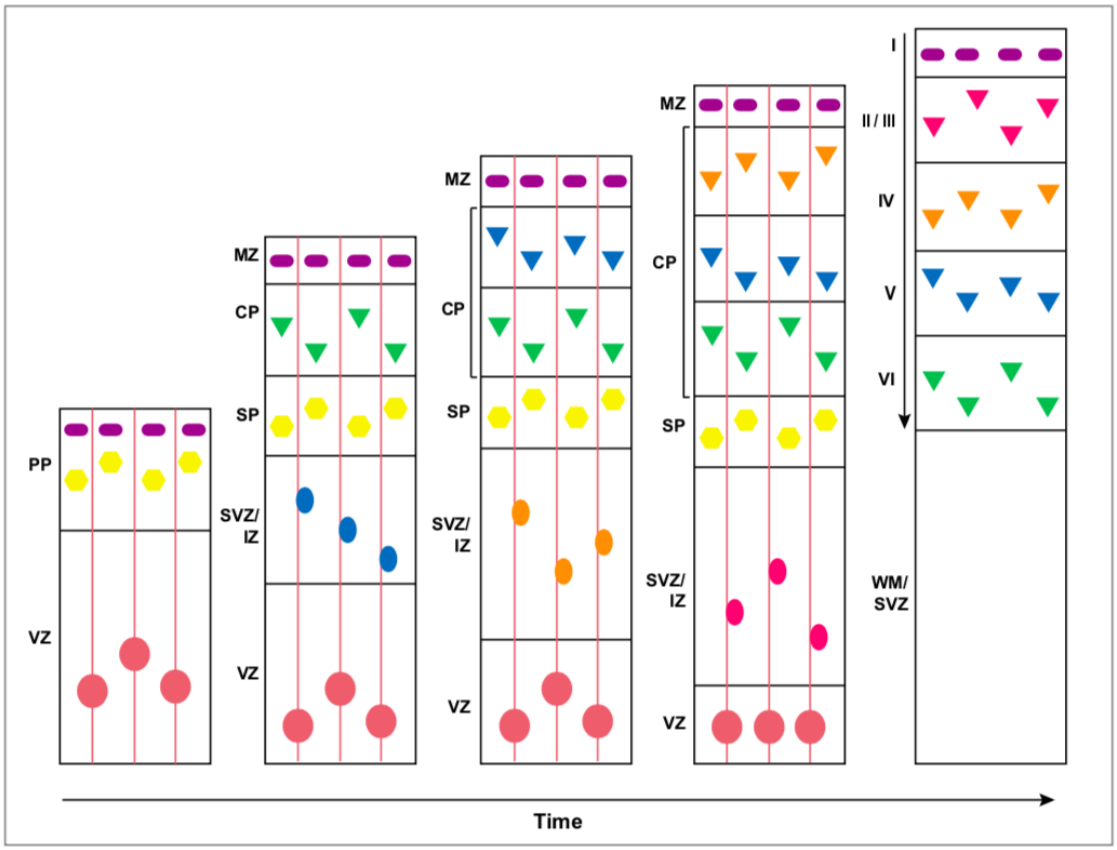

Figure 2. 6: Neocortex is formed in "inside-out" manner in mammals.

When first wave of post-mitotic neurons are born in the VZ, they migrate to the pial surface and form the PP. Second wave of neurons (green triangle) are born, migrate through SVZ/IZ, and separate PP into MZ (neurons are represented as purple ovals) and SP (neurons are represented as yellow hexagons). CP plate is expanded in an inside-out manner by neurons which are generated in a sequential manner (symbolized as different color triangles, blue, orange and pink by order of birthdate). Early-born neurons populate the deep layer whereas

late-born neurons pass the existing neurons to form more superficial layers. At later embryonic developmental stages, as the number of neural progenitor cells decrease, VZ progressively becomes smaller. During the postnatal stages to adulthood, SP disappears and the six-layer cortex (Layers I-VI) is formed. VZ, ventricular zone; PP, preplate; SP, subplate; SVZ/IZ, subventricular zone/intermediate zone; CP, cortical plate; MZ, marginal zone; WM, white matter (Adapted from [91]).

2.1.9 Types of neural progenitors located in the cerebral cortex

Neural progenitor cells have a key role in development of the mammalian cerebral cortex [92]. There are three classes of neural progenitor cells (NPC): apical progenitors (AP), basal progenitors (BP) and subapical progenitors (SAP). Apical progenitors which located in the VZ have three types which are apical intermediate progenitors (aIP), apical radial glia (aRG) and neuroepithelial cells (NEC). Basal progenitors are divided into two subtypes which are basal radial glia (bRG) and basal intermediate progenitors (bIP) **(Figure 2.7A)**. In early developmental stages, NECs undergo mitosis to expand their populations and this division eventually causes an expansion of the cortex both laterally and radially. During development (E9.5-E10.5 in mice), NECs transform into aRG cells and express specific marker proteins. aRG are bipolar cells and they have their somas located in the VZ. They have long basal radial processes attached to pial surface and a short apical process located at the VZ. Cortical neurogenesis starts with the transition of cell division mode of aRG from symmetric to asymmetric. This division leads to a self-renewal of mother cells since one of the daughter cell remains as aRG. The second daughter cell becomes either an aIP or a post-mitotic neuron. At the end of the neurogenic period the aRG cells change their division mode to gliogenesis to produce non-neuronal cells such as astrocytes and oligodendrocytes [4, 91] **(Figure 2.7B)**.

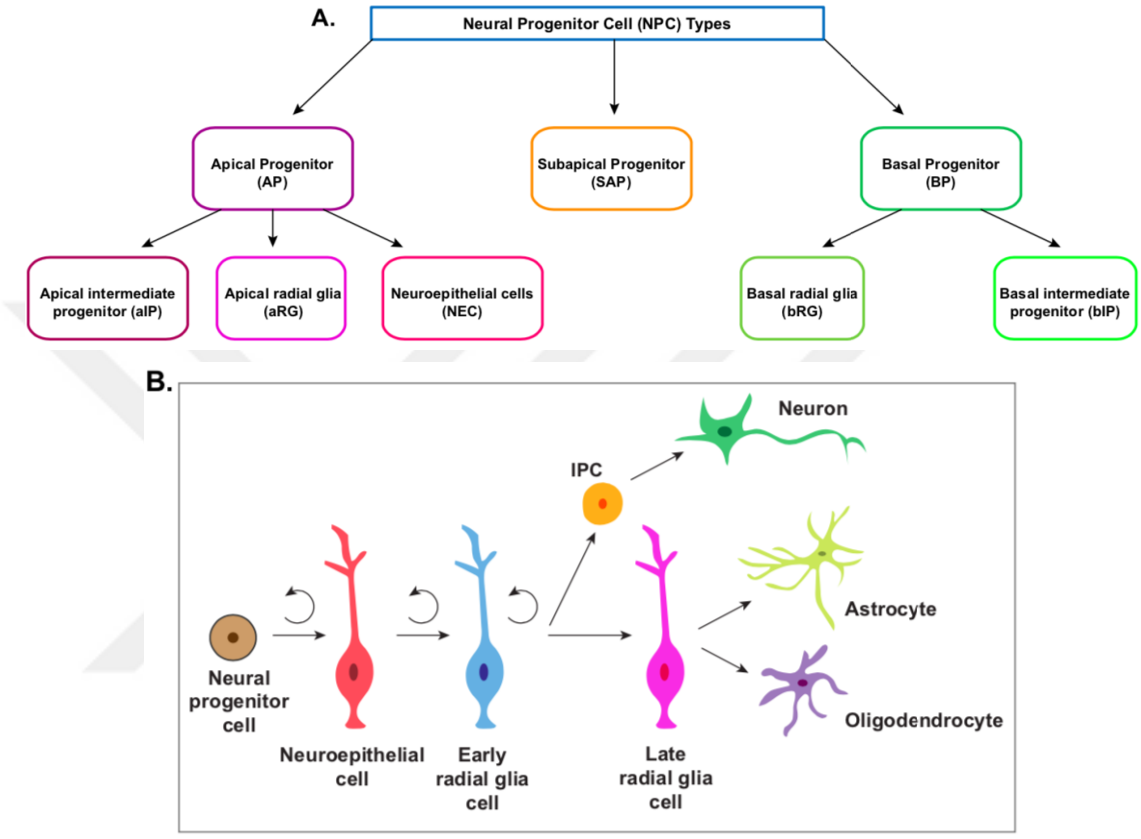

Figure 2. 7: Neural progenitor types and their differentiation fates during development. **A.** Table shows neural progenitor cell subtypes (Adapted from [4]). **B.** Neural progenitor cells (brown) are referred to as the stem cell of the nervous system. Neuroepithelial cells (red) are one of the earliest forms of neural progenitors which differentiate into elongated radial glia cells. Early radial glia cells (blue) divide asymmetrically to form another radial glia cell and an intermediate progenitor cell (orange). Intermediate progenitor cells (IPC) undergo limited number of divisions and form an immature neuron (green) which migrate radially to form cortical layers. After neurons are formed, early radial glia cells transform into late glia cells (pink) that differentiate into non-neuronal lineage such as oligodendrocytes (purple) and astrocytes (yellow) (Adapted from [93]).

2.1.10 Neurons of the cerebral cortex: Glutamatergic excitatory neurons and GABAergic inhibitory interneurons

During development, this six-layered mammalian neocortex is populated by two functionally and cytoarchitectonically distinct groups: glutamatergic excitatory projection (pyramidal) neurons and γ-aminobutyric acid (GABA)ergic inhibitory interneurons [6]. Glutamatergic excitatory projection neurons are generated in the dorsal germinal zone of telencephalon which is the VZ, whereas GABAergic inhibitory interneurons originate from the lateral and medial ganglionic eminences (LGE and MGE) which are the proliferative zones of the ventral telencephalon. Therefore, excitatory projection neurons migrate radially to reach their destination and inhibitory interneurons travel tangentially longer distances to reach the cortex [6, 90] **(Figure 2.8)**. Excitatory neurons and inhibitory interneurons originate following progenitor cell divisions during development and are spatially organized into six layers, which is essential for proper functioning of the neocortex. Excitatory neurons are comprise the vast majority (~70–80%) of cortical neurons and they have roles in generating excitatory output. Inhibitory interneurons produce a rich diversity of inhibitions which modulates the output of cortical circuits [91] .

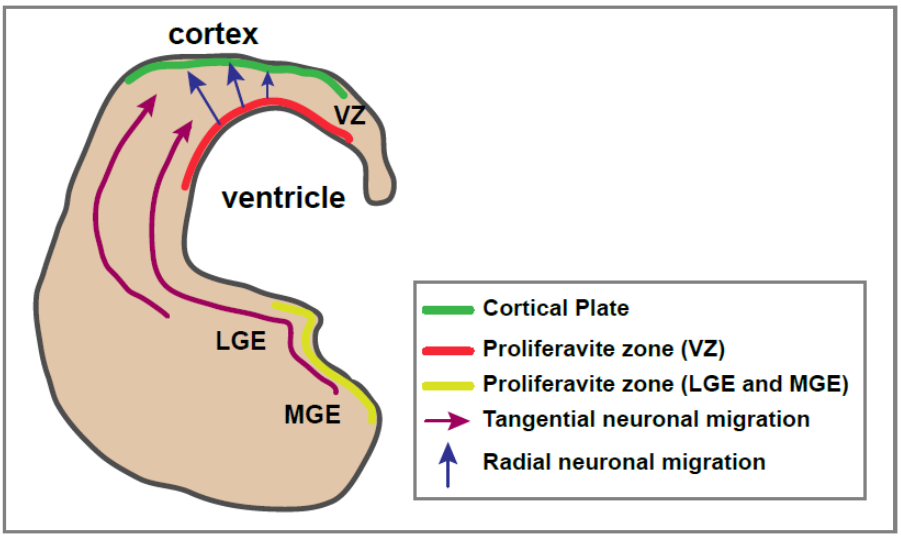

Figure 2. 8: Cortical neuronal migration occurs both radially and tangentially.

Schematic representation of coronal section of mouse developing anterior telencephalon at embryonic day 14 (E14). Excitatory neurons are born in ventricular zone (red line) migrate radially (blue arrows) through the cortical plate (green line). Inhibitory interneurons are generated in lateral and medial ganglionic eminences (yellow line) and migrate tangentially (purple arrows). VZ, ventricular zone; LGE, lateral ganglionic eminence; MGE, medial ganglionic eminence (Adapted from [90]).

2.1.11 Neurogenesis and radial cortical neuronal migration

Neurogenesis is the process by which NPCs form cortical projection neurons [5, 92, 94-96]. This process is initiated by aRG cells, followed by extensive radial neuronal migration, neuronal differentiation, development of dendrite and axons, synapse formation and organization of neuronal connectivity [6, 92, 96, 97]. aRG initiate waves of neurogenesis by giving rise to the projection neurons which migrate radially to their final locations. aRG cells have long basal processes connected to the pial surface and they enter mitosis in the VZ and divide either symmetrically to self-renew or asymmetrically to produce other type of progenitors such as IPCs. IPCs accumulate in the SVZ and they divide symmetrically to generate either two postmitotic neurons or a pair of progenitors which eventually generate a pair of neurons [15, 70, 91].

In mice, at the early stages of development, deep-layer excitatory neurons are born from aRGs and they migrate through the MZ using somal translocation. Neurons shift their mode of migration from basal to multipolar once the developing cortex becomes thicker and this migration continues until they reach IZ. After they reach the IZ, another transition in migratory mode occurs (multipolar to bipolar). Using the fibers of RG cells as a migratory scaffold, neurons migrate radially through the IZ and CP. This glia-guided locomotion proceeds towards the pia by passing the early-born neurons. Neurons switch to terminal translocation when they reach their destination beneath the MZ. As a result, six-layered cortex is formed in an inside-out and birth-date-dependent manner [90] **(Figure 2.9)**.

During development, neocortex expands both radially and laterally. Lateral (tangential) expansion starts with the symmetric division of neuroepithelial cells followed by symmetric division of aRG cells. Radial expansion is divided into two parts; expansion of ventricular zone and expansion of the cortical plate. aRG cells become more elongated and their growth causes the ventricular zone expansion. Radial expansion of cortical wall occurs due to asymmetric division of aRG cells, hence producing BPs. Self-renewing production of BPs eventually gives rise to an increase in neuron numbers which causes cortical layer thickening [92].

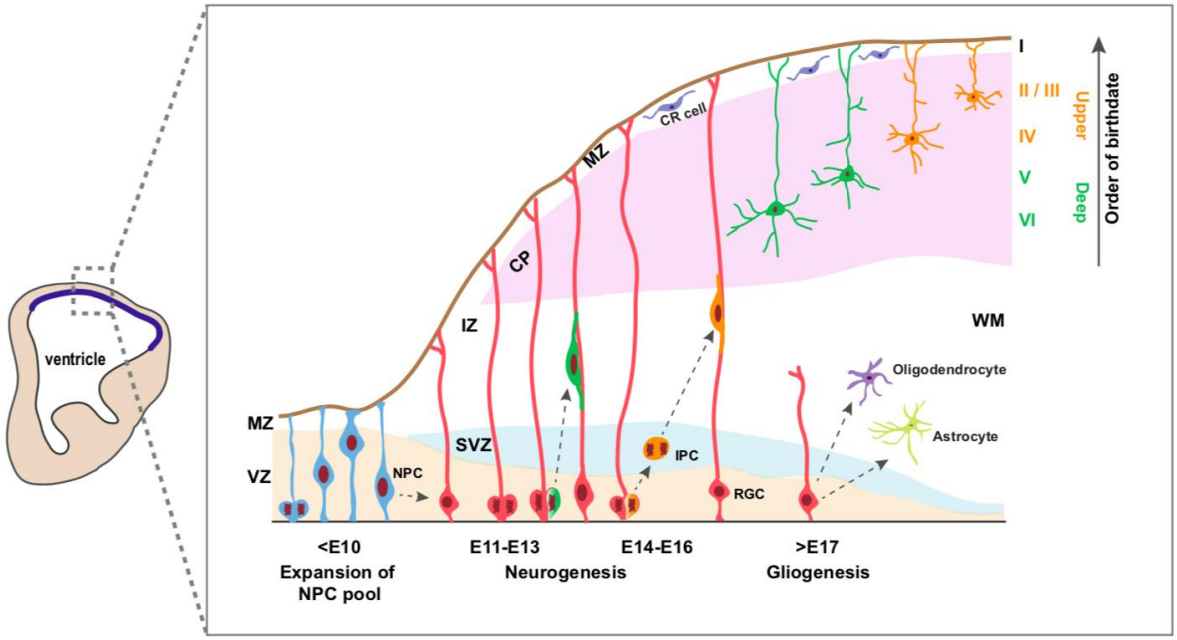

Figure 2. 9: Spatiotemporal development of mouse neocortex.

Left panel is the schematic of coronal section of mouse developing telencephalon at early developmental stages. VZ is represented as a blue line. The gray dashed line box area is enlarged in the right panel. Before the beginning of neurogenesis, NPCs (blue) located in the VZ divide symmetrically to increase their population. Starting at around embryonic day 11 (~E11), NPCs forms RGC (red) which has processes attached to pail surface and undergo asymmetrical division to form neurons. Newly born neurons (green and orange) use the RG cell processes to migrate radially to reach their destinations. During neurogenesis, sequential generation of different subtypes of projection neurons occurs in an inside first, outside last fashion; thus, early-born neurons (green) populate deep layers (Layers V and VI) whereas late-born neurons (orange) migrate and pass the early-born neurons, forming more superficial layers (Layers II-III and IV). Some daughter cells of RGCs become IPCs which divides in SVZ and then form upper layer neurons. At the end of neurogenesis at ~E17, gliogenesis

starts which is the process of formation of non-neuronal cells (astrocytes and oligodendrocytes) from RGCs. VZ, ventricular zone; MZ, marginal zone; SVZ, subventricular zone; IZ, intermediate zone; CP cortical plate; WM, white matter; NPC, neural progenitor cell; RGC, radial glia cell; IPC, intermediate progenitor cell; CR, Cajal-Retzius, E, embryonic day (Adapted from [5, 98]).

2.1.12 Four distinct phases of neuronal migration

Radial neuronal migration has four distinct phases: proliferation of neural progenitor cells, multipolar-to-bipolar cell transition, locomotion, and finally, terminal translocation. Phase one includes the generation of neurons from aRG cells in VZ and then radial migration to the SVZ in a multipolar shape. Phase two involves a pause in the SVZ-IZ to switch their mode from multipolar-to-bipolar by forming an extension of a thin axon and a thick leading process which is formed by a selected neurite. In third the phase, neurons extend a pia-directed leading process and start a RG-guided locomotion. In this step, nuclear translocation and forward movement of cell body are required. Nuclear translocation occurs by coupled movement of nucleus and centrosome and cytoskeletal coordination is required for this step. Endocytosis and neuronal adhesion are two processes which are implicated in forward movement of the cell body. In the final phase, when neurons reach their destinations, they terminate locomotion by detaching themselves from RG fibers which is called as the terminal translocation step and differentiate their dendrites and axons to reach their mature phase [99].

2.1.13 Malformations of cortical development (MCD) and disease-causing *Kif2a* mutants

The proper development of the complex architecture of the human cerebral cortex requires fine regulation of developmental steps such as proliferation of NPCs, neurogenesis followed by cortical neuronal migration, neuronal differentiation and finally establishment of connectivity [70]. Changes in one of these processes can cause neurodevelopmental disorders called as malformations of cortical development (MCD) which can lead to severe epilepsy, intellectual disability, dysmorphic features and psychomotor delay [2, 8]. Especially, several mutations in genes which regulate distinct aspects of neuronal migration can cause severe brain malformations including periventricular and cortical band heterotopias, as pachygyria, microcephaly, polymicrogyria and lissencephaly highlighting the significance of the cortical neuronal migration process [2, 5, 7, 9].

It has been shown that cytoskeletal elements are one of the most crucial components for cortex development, and several intracellular and extracellular signals that modulate these cytoskeletal elements control the formation of six-layered cortex and neuronal migration [90]. Mutations in both MT-homeostasis proteins such as DCX and LIS1, tubulin genes including α-tubulin TUBA1A, β-tubulin TUBB2B, TUBB3 and TUBB and γ-tubulin TUBG1, and MT-related motor proteins DYNC1H1, KIF5C and KIF2A are identified and predominant in MCD patients [2, 8, 70, 100].

Furthermore, several *de novo* missense mutations (c.950G>A, p.Ser317Asn; c.959C>T, p.Thr320Ile; c.961C>G, p.His321Asp and c.962A>C, p.His321Pro) in the motor domain of KIF2A were identified in patients with MCD such as pachygyria, microcephaly and lissencephaly [2, 8, 9, 101]. Motor domain mutations especially around the nucleotide binding pocket, suggests impaired ATP binding and/or hydrolysis in these mutants which leads to the disruption of MT depolymerizing activity. Among these mutations, Ser317 and His321 mutations show the highest rate of incidence [9] **(Figure 2.10)** and these two mutants affect neuronal positioning, and cell cycle of neuronal progenitors [8]. Conditional knock-in mice which have the His321 mutation show neuroanatomical anomalies, epilepsy and microcephaly as well as having an increased rate of apoptosis and an abnormal transition from multipolar to bipolar state [102].

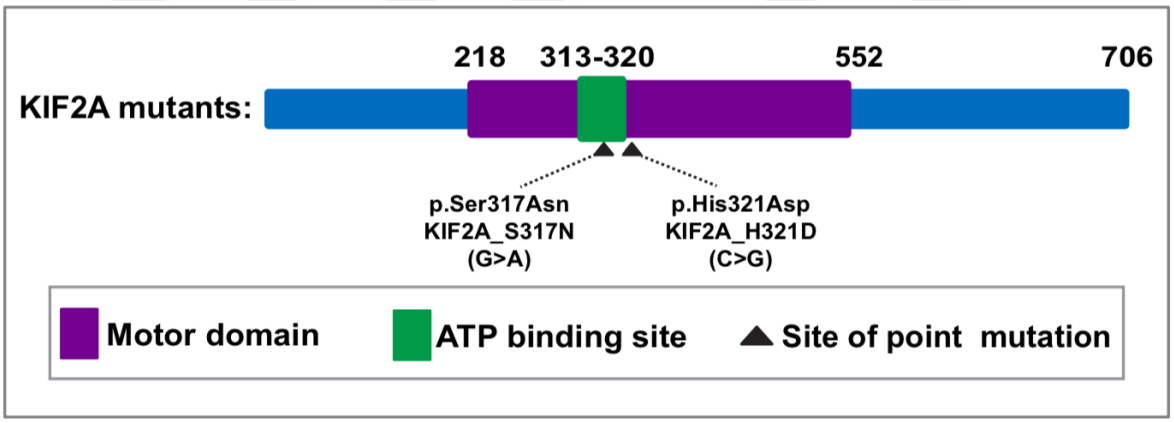

Figure 2. 10: Schematic of disease-causing KIF2A mutants (KIF2A^{S317N} and KIF2A^{H321D}).

Both *Kif2a*^{S317N} and *Kif2a*^{H321D} dominant negative point mutations are located on the KIF2A motor domain and lead to MCD in humans (Adapted from [2]).

2.2 MATERIAL AND METHODS

2.2.1 Collection and lysate preparation from mouse cortex tissue at different developmental time points

Brains from mice at different time points (embryonic day 14, 16, 17, 18, postnatal day 0, 7, 14, 21, 28 and adult) were collected and their cortices were dissected in ice-cold 1X in PBS. Cortices were homogenized in ice-cold RIPA buffer (0.05 M Tris-HCl pH 7.5, 1% Na-DOC, 0.15 M NaCl, 1% Triton X-100, and 0.1% SDS) supplemented with protease inhibitor (Roche, Cat. #11836170001) with Dounce homogenizer. Lysed cortices were transferred into 1.5 ml centrifuge tubes and were centrifuged at 14000 rpm for 10 minutes at 4^{o}C. Supernatant was transferred into clean 1.5 ml centrifuge tubes and stored at -20^{o}C for western blotting.

2.2.2 Total RNA isolation of mice cortices at different developmental time points

Three sets of cortices of mice at different developmental time points (embryonic day 14, 16, 18, postnatal day 0, 7, 14, 21, 28 and adult) were dissected 1X cold PBS for total RNA isolation. 1 ml of Qiazol (QIAGEN, Cat. #79306) was added per 0.1 g of tissue and tissue was triturated by pipetting and incubated at room temperature for 5 minutes. For per 1ml of homogenate, 200 µl of chloroform was added and tubes were shaken well for 15 seconds and homogenates were incubated at room temperature for 3 minutes. Then, homogenates were centrifuged at 14000 xg at 4^{o}C for 15 minutes. Upper (aqueous) phase was taken and transferred into clean 1.5 ml centrifuge tubes. For per 1ml of homogenate, 500 µl of isopropanol was added and vortexed well and incubated at room temperature for 10 minutes. Centrifugation was performed at 14000 xg at 4^{o}C for 10 minutes. Supernatant was discarded. Visible RNA pellets were washed with 1ml of RNase free 75% ethanol and

centrifuged at 10000 xg minutes at 4ºC for 5 minutes. Supernatant was discarded and pellet was left under tissue culture hood for drying. 50 µl of nuclease free ddH_2O was used to dissolve RNA pellet and concentration was measured with NanoDrop2000©. 250 ng RNA samples were prepared using nuclease free ddH_2O for RT-PCR analysis.

2.2.3 cDNA synthesis (RT-PCR)

Cortices from mice at different time points (embryonic day 14, 16, 18, postnatal day 0, 7, 14, 21, 28 and adult) were dissected in ice-cold 1X HBSS for RNA isolation. RNA was isolated which was explained in **Section 2.2.2.** From 250 ng total RNA, cDNA was synthesized using Transcriptor High-Fidelity cDNA Synthesis Kit (Roche, Cat. #05091284001) according to manufacturer's protocol. Briefly, 60 µM random hexamer primer was mixed with 500 ng/µl of total RNA and the mixture was denatured at 65ºC for 10 minutes. 1X Transcriptor High Fidelity Reverse Transcriptase Reaction buffer, 5 mM DTT, 1mM deoxynucleotide mix, 20 Unit RNase inhibitor and 10 Unit Transcriptor High Fidelity Reverse Transcriptase (RTase) was added into tube (Incubation conditions: 29ºC-10 minutes, 48ºC-60 minutes and 85ºC-5 minutes; cover temperature: 50ºC). No RTase containing tube was used as negative control.

2.2.4 Real Time PCR (Q-PCR)

Quantitative Real Time PCR (Q-PCR) was performed using Luminaris HiGreen qPCR Master Mix (Thermo scientific, Cat. #K0991) with a CFX Connect Real-Time PCR detection System (Bio-Rad). Briefly, 0.3 µM forward primer, 0.3 µM reverse primer **(Appendix C)** , 1X Master Mix, and 2500 pg template cDNA was mixed (Q-PCR conditions: Initial denaturation 5ºC-10 minutes, denaturation 95ºC-10 seconds, annealing 61ºC-20 seconds and extension 72ºC-20 seconds; denaturation-annealing-extension for 40 cycles; melting curve, 65ºC-5 seconds and 95ºC-5 seconds). *Kif2a* mRNA levels were normalized to *Gapdh* mRNA using the $2^{-\Delta\Delta CT}$ method.

2.2.5 Cloning of Kif2a.1, Kif2a.2, Kif2a.3, Kif2a^{S317N} and Kif2a^{H321D} into pcDNA4A plasmid

Kif2a.1, Kif2a.2, Kif2a.3, Kif2a^{S317N} and *Kif2a^{H321D}* inserts were subcloned from pEGFPC1 vector into pcDNA4A plasmid. Inserts were amplified from *Kif2a.1, Kif2a.2, Kif2a.3, Kif2a^{S317N}* and *Kif2a^{H321D}* in pEGFPC1 vector with PCR which was set up in 30 µl reaction mixture containing 1X Phusion HF reaction buffer (Bio Labs, Cat. #B0518S), 0. 5 µM forward primer and 0.5 µM reverse primer **(Appendix C)**, 300 µM dNTP's, 1 Unit Phusion Hot Start Flex DNA Polymerase (New England Biolabs, Cat. #M0530L) and 150 ng pEGFPC1-Kif2a.1, pEGFPC1-Kif2a.2, pEGFPC1-Kif2a.3, pEGFPC1-Kif2a^{S317N} or pEGFPC1-Kif2a^{H321D} as DNA template (PCR conditions: Denaturing 98ºC-15 seconds, annealing 55ºC-30 seconds and extension 72ºC-1.5 minutes; 40 cycles). PCR products were run on 1% agarose gel and plasmid DNA was purified using EZ-10 Spin Column PCR Products purification kit (Bio Basic Canada Inc., Cat. #BS364). Both purified PCR products and pcDNA4A plasmid were digested with *EcoR*I and *BamH*I restriction endonucleases which have recognition sites embedded in designed forward and reverse primer pairs,

respectively, as well as in pcDNA4A vector. Restriction enzyme digestion was set up in 20 µl reaction mixture containing 1X Cut Smart Buffer (New England Biolabs, Cat. #B7204S), 5 Unit *EcoR*I-HF (New England Biolabs, Cat. #R3101L), 5 Unit *BamH*I-HF (New England Biolabs, Cat. #R3136S), 0.5 µl of pcDNA4A plasmid DNA and 10 µl of purified PCR product (Double digest conditions: 37ºC-overnight). Next day, to prevent plasmid DNA self-ligation, dephosphorylation was performed with 1 µl of FastAP (Alkaline phosphatase) (Thermo Scientific, Cat. #EF0651) at 37ºC for 1 hour followed by purification of digestion products with EZ-10 Spin Column PCR Products purification kit (Bio Basic Canada Inc., Cat. #BS364). Ligation of pcDNA4A vector with PCR products was carried out in a 10 µl reaction mixture containing, 1X T4 Ligase Buffer (Thermo Scientific, Cat. #B69), 5 Unit T4 ligase (Thermo Scientific, Cat. # EL0011), 50 ng pcDNA4A and 20 ng PCR products (Ligation conditions: Room temperature-2 hours). Ligation product was used to transform into chemically competent DH5α *Escherichia coli (E.coli)* cells according to standard transformation protocol. Briefly, 1 µl of ligation product was incubated with 50 µl of *E.coli* DH5α on ice for 10 minutes and then heat shock was applied by incubation at 42ºC for 1 minute. 500 µl of Luria broth (LB) medium was added onto cells and cells were incubated at 37ºC for 1 hour with 300 rpm shaking. Cells were plated on LB-ampicillin plate since pcDNA4A vector has ampicillin resistant gene with spread plate technique. Plates were incubated at 37ºC, overnight. Next day, miniprep cultures were prepared by single colony selection with incubation at 37ºC, overnight with shaking. Plasmid DNAs were purified by GeneJET Plasmid Miniprep Kit (Thermo Scientific, Cat. #K0503) according to manufacturer's protocol. Diagnostic digestion was carried out in 20 µl reaction mixture containing 1X Cut Smart Buffer (New England Biolabs, Cat. #B7204S), 5 Unit *EcoR*I-HF (New England Biolabs, Cat. #R3101L), 5 Unit *BamH*I-HF (New England Biolabs, Cat. #R3136S) and 1µl of DNA (Double digest condition: 37ºC-2 hours). Samples were run on

1% agarose gel for confirmation of the correct size insert of the selected colonies. Concentrations were measured by using NanoDrop2000© (Thermo Scientific) and 5 µl of miniprep DNA were sent to direct sequencing to Macrogen Company, The Netherlands for validation. After confirmation, maxi-prep cultures were incubated at 37°C, overnight with constant shaking. *Kif2a.1, Kif2a.2, Kif2a.3, Kif2a*^{S317N} and *Kif2a*^{H321D} plasmid DNAs were purified separately with PureLink™ HiPure Plasmid Maxiprep Kit (Invitrogen, Cat. #K210006).

- Cloning of pEGFPC1-Kif2a isoforms was performed by Gökhan Güner using primers that have *Hind*III (forward primer) and *Eco*RI (reverse primer) endonuclease recognition sites. Primer sequences were written in **Appendix C**.

- pEGFPC1-Kif2a^{S317N} and pEGFPC1-Kif2a^{H321D} constructs were cloned by site-directed mutagenesis using pEGGFPC1-Kif2a.1 as backbone vector [103]. Primer sequences were written in **Appendix C**.

2.2.6 Cloning of shRNA against *Kif2a*

Cloning of Non-silencing (NS) and shKif2a short hairpin RNAs (shRNA) into pSUPER-neo-EGFP (www.oligoengine.com) were carried out using the manual. Briefly, pSUPER-neo-EGFP vector digestion was set up in 20 µl reaction mixture containing 1X Buffer, 1 µl of *Bgl*II, 1 µl of *Hind*III and 3 µl of pSUPER-neo-EGFP vector (Digestion condition: 37°C-3 hours, 72°C-20 minutes). 2 hours and 10 minutes after starting the digestion, oligo annealing procedure was started. Oligo annealing was set up in 50 µl reaction mixture containing 3 µg shRNA_F and 3 µg shRNA_R for shKif2a **(Appendix C)**, 46.8 µl of oligo annealing buffer (100 mM NaCl, 50mM HEPES pH 7.4) (Oligo annealing condition: 94°C, 80°C, 75°C, 70°C, 65°C, 60°C, 55°C, 50°C, 45°C, 40°C-4 minutes each temperature,

37ºC-20 minutes). Next, digested pSUPER-neo-EGFP and oligo (shRNA) constructs were ligated. Ligation was set up 10 µl reaction mixture containing 1 µl of digested pSUPER-neo-EGFP, 2 µl of oligo (shRNA), 1X T4 Ligase Buffer (Thermo Scientific, Cat. #B69), 5 Unit T4 ligase (Thermo Scientific, Cat. # EL0011) (Ligation condition: Room temperature-3 hours). 1 µl of ligation product was transformed into chemically competent DH5α *E.coli* cells with heat shock followed by plating of cells on LB-ampicillin plates with spread plate technique. Approximately 12 single colonies were picked and miniprep cultures were incubated at 37ºC overnight with constant shaking. Plasmid DNA's were purified by GeneJET Plasmid Miniprep Kit (Thermo Scientific, Cat. #K0503) according to manufacturer's protocol. Diagnostic digestion was set up in 20 µl reaction mixture containing 1µl of DNA, 1X Buffer (Thermo Scientific, Cat. #BR5), 10 Unit *Bgl*II (Thermo Scientific, Cat. #ER0082), 5 Unit *Hind*III (Thermo Scientific, Cat. #ER0501) (Double digest conditions: 37ºC-1 hour). Samples were run on 1% agarose gel for insert confirmation. Concentrations were measured by using NanoDrop2000© (Thermo Scientific) and 5 µl of miniprep DNA were sent to direct sequencing to Macrogen Company, The Netherlands for validation. After confirmation, maxi-prep cultures were incubated at 37ºC overnight with constant shaking and NS and shKif2a plasmid DNAs were purified with The EndoFree Plasmid Maxi Kit (QIAGEN, Cat. #12362).

For *in utero* electroporation experiments, the EGFP cassette was exchanged with an mCherry cDNA by subcloning into the *Age*I and *Not*I sites of pSUPER-neo. First of all, both pSUPER-mcherry and pSUPER-neo-EFGP_Kif2a were digested with *Age*I (*BshT*I) and *Not*I restriction endonucleases. 20 µl reaction mixture containing 1X Buffer O (Thermo Scientific, Cat. #B05), 3 Unit *Age*I (*BshT*I) (Thermo Scientific, Cat. #ER1461), 3 Unit *Not*I (Thermo Scientific, Cat. #ER0591) and 100 ng DNA (Double digest conditions: 37ºC-2 hour). Digestion products were run on 1% agarose gel and the correct bands (mcherry band for

pSUPER-mcherry, shKif2a backbone band for pSUPER-neo-EGFP_shKif2a) were excised under UV light. Plasmid DNA was extracted from excised agarose gel using EZ-10 Spin column DNA Gel Extraction Kit (Bio Basic Canada Inc., Cat. #BS353). Ligation of shKif2a with mcherry was performed in 10 µl reaction mixture containing, 1X T4 Ligase Buffer (Thermo Scientific, Cat. #B69), 5 Unit T4 ligase (Thermo Scientific, Cat. # EL0011), 7.5 ng mcherry insert and 40 ng shKif2a (Ligation conditions: Room temperature-2 hours). Ligation product was used to transform into chemically competent DH5α *E.coli* cells according to heat shock based transformation protocol onto LB-ampicillin plates. Next day, miniprep cultures were prepared by single colony selection and cultures were incubated at 37^{o}C, overnight with shaking. Plasmid DNA's were purified by GeneJET Plasmid Miniprep Kit (Thermo Scientific, Cat. #K0503) according to manufacturer's protocol. Diagnostic digestion was carried out in 1X Buffer O (Thermo Scientific, Cat. #B05), 5 Unit *Age*I (*BshT*I) (Thermo Scientific, Cat. #ER1461), 5 Unit *Not*I (Thermo Scientific, Cat. #ER0591) and 1 µl of DNA (Double digest conditions: 37^{o}C-2 hour). Samples were run on 1% agarose gel for confirmation of the correct size insert of the selected colonies. Maxi-prep cultures were incubated at 37^{o}C overnight with constant shaking and plasmid DNA was purified with The EndoFree Plasmid Maxi Kit (QIAGEN, Cat. #12362).

- Non-silencing (NS) shRNA cloning was performed by Gökhan Güner. Primer sequences for NS cloning was written in **Appendix C**.

2.2.7 Site-directed mutagenesis of shKif2a-resistant *Kif2a* isoforms

Three silent mutations (A1521T, C1524G and T1527C) were introduced into three Kif2a isoforms (*Kif2a.1, Kif2a.2* and *Kif2a.3*) by site directed mutagenesis in pcDNA4A backbone vector within the shKif2a target sequence **(ggaatggcatcctgtgaaa)** [85] to create shKif2a-resistant cDNA (resKIF2A.1, resKIF2A.2 and resKIF2A.3). PCR reaction mixture

contained 1X Phusion HF reaction buffer (New England BioLabs, Cat. #B0518S), 3% DMSO, 0.5 µM forward primer and 0.5 µM reverse primers **(Appendix C)**, 200 µM dNTP's, 10 ng pcDNA4A-Kif2a.1, pcDNA4A-Kif2a.2 and pcDNA4A-Kif2a.3 as DNA template and 1 Unit Phusion Hot Start Flex DNA Polymerase (New England BioLabs, Cat. #M0535L). (PCR conditions: Denaturing 98^{o}C-45 seconds, annealing 60^{o}C-2 minutes and extension 72^{o}C-7 minutes; 25 cycles). EZ-10 Spin Column PCR Products purification kit (Bio Basic Canada Inc., Cat. #BS364) was used to purify PCR products and DNA concentrations were measured by NanoDrop2000© (Thermo Scientific). Phosphorylation at 5' end of PCR products was carried out by preparing 50 µl mixture containing 1X Polynucleotide Kinase Buffer A (Fermentas, Cat. #00048086), 1 mM ATP (New England BioLabs, Cat. #P0756S), 10 Unit Polynucleotide Kinase (Thermo Scientific, Cat. #EK0032), and 50 ng purified PCR product (Phosphorylation condition: 37^{o}C-60 minutes). Deactivation of PNK enzyme was carried out by incubation at 65^{o}C for 25 minutes. Ligation reaction was performed in 20 µl reaction mixture containing 1X T4 Ligation Buffer (Thermo Scientific, Cat. #B69), 5 µl of phosphorylation reaction product and 2.5 Unit T4 DNA Ligase (Thermo Scientific, Cat. # EL0011) and 5 µl of DNA to circularize the products (Ligation condition: Room temperature-2 hours). 1 µl of ligation products were transformed into *E. coli* DH5α cells by heat shock method with spread plate technique using LB-ampicillin plates. Miniprep cultures were stared by picking single colonies and incubated 37^{o}C overnight. Next day, miniprep was performed by GeneJET Plasmid Miniprep Kit (Thermo Scientific, Cat. #K0503) to purify plasmid DNA. After measuring the concentrations using NanoDrop2000©, 5 µl of miniprep DNA were sent for direct sequencing for validation and then plasmid DNA were purified with The EndoFree Plasmid Maxi Kit (QIAGEN, Cat. #12362).

2.2.8 Coating of plates

One well of 24 well plate with coverslip (sterilized with 70% Ethanol) was coated with 500 µl of coating solution (0.1 mg mouse laminin (Millipore, Cat. #CC905), 1mg Poly-L-Lysine Hydrobromide (Sigma Life Sciences, Cat. #P9155), in 30 ml of 1X PBS) overnight in tissue culture incubator (37^{o}C, 5%CO_2). Next day, plates were washed with 1 ml of sterile ddH_2O, three times and they either used immediately or stored at 4^{o}C for 3 weeks.

2.2.9 Primary neuronal culture preparation

CD1 pregnant mice at embryonic day 14.5 (E14.5) were sacrificed with cervical dislocation. Embryos' brains were removed and their cortices were dissected in ice-cold 1X HBSS containing 10 mM HEPES. Cortices were transferred into enzyme solution (20 U/ml papain, 6.4 mg L-cysteine) prepared in dissociation media (30 mM K_2SO_4, 20 mM glucose, 5.8 mM $MgCl_2$, 82 mM Na_2SO_4, 1 mM HEPES pH 7.4, 0.2 mM NaOH, 0.001% phenol red in ddH_2O) with sterile glass pipette. Cortices were digested in enzyme solution at 37^{o}C for 10 minutes. To terminate the digestion, tissue was transferred and incubated with first into light inhibitor (10 mg trypsin inhibitor and 10 mg BSA in dissociation media, 100 mM NaOH for pH adjustment) at 37^{o}C for 1 minute and then into heavy inhibitor (100 mg trypsin inhibitor and 100 mg BSA in dissociation media, 100 mM NaOH for pH adjustment) for 1 minute at 37^{o}C. Tissue was washed with Basal Media Eagle (BME) (Lonza, Cat. #BE12-105F) supplemented with 0.5% Ultraglutamine (Lonza, Cat. #BE17-605E/U1), 1% Penicillin/Streptomycin (P/S) (Pan Biotech, Cat. #P06-07100) and 5% Fetal Bovine Serum (FBS) (Pan Biotech, Cat. #P30-1902) (BF) twice at room temperature. Tissue was triturated in BF three to five times and incubated until the large clumps settled down. Cell suspension filtered into a new 50 ml falcon without disturbing the clumps. 300.000 cells were counted with cytometer and plated onto each well of pre-coated 24-well plate in 500 µl BF volume.

After 2 hours incubation at 37ºC, medium was aspirated and 500 µl of fresh BF media containing N-2 (Gibco Life Technologies, Cat. #17502-048) and B-27 (Gibco Life Technologies, Cat. #12587-010) (BNBF) was added per well.

- All solutions were sterilized by filtering with 0.22 µm filter.

2.2.10 Transfection of E14.5 primary cortical culture with Lipofectamine® 2000 reagent

Plasmids were transfected into E14.5 primary cortical neurons at 2 day *in vitro* (DIV) using Lipofectamine® 2000 reagent (Invitrogen, Cat. #11668019) according to manufacturer's protocol. Briefly, media (conditioned media) were collected into falcon and saved at 37ºC and 500 of Opti-MEM®I was added onto cells and plate was returned to tissue culture incubator. 2 µl of Lipofectamine® 2000 reagent was mixed with 250 µl of Opti-MEM®I and 1.5 µg of DNA (0.5 µg NS or shKif2a and 1 µg pcDNA4A or one of three reKIF2A isoforms) was mixed with 250 µl of Opti-MEM®I for one of 24-well plate that contained sterile coverslip. Tubes were incubated for 10 minutes at room temperature and Lipofectamine® 2000-Opti-MEM®I and DNA-Opti-MEM®I were mixed with each other after incubation. Reaction mixture was incubated at room temperature for 20 minutes and 500 µl of the mixture was added onto one well of 24-well plate dropwise. Plate was placed back into tissue culture hood and incubated for 2 hours. After incubation medium was changed with 500 µl of 50% conditioned medium and 50% fresh BNBF.

2.2.11 Transfection of HEK293T cells with Lipofectamine® 3000 reagent

HEK293T cells were maintained 6 well plate containing DMEM supplemented with 10% FBS (Pan Biotech, Cat. #P30-1902), 1% P/S (Pan Biotech, Cat. #P06-07100) and 0.5% L-Glutamine (Pan Biotech, Cat. #P04-80050). After cells reached 70% confluency, plasmids were transfected using Lipofectamine™ 3000 reagent (Invitrogen, Cat. #L3000015) according to manufacturer's protocol. Briefly, medium was changed with DMEM containing 10% FBS and 0.5% L-Glutamine. Two 1.5 ml centrifuge tubes were prepared; first one contained 125 µl of Opti-MEM®I and 3.6 µl of Lipofectamine™ 3000 reagent, second one contained 125 µl of Opti-MEM®I and 3.6 µl of P3000™ reagent and 4.5 µg total DNA (1.5 µg of NS or shKif2a and 3 µg of pcDNA4A or one of three pcDNA4A-Kif2a or one of three resKIF2A isoforms). Tubes were incubated at room temperature for 5 minutes. After incubation, tubes were mixed and incubated at room temperature for 20 minutes. 250 µl of reaction mixture was added onto cells dropwise and plate was put in tissue culture incubator for 4 hours. Medium was aspirated and complete DMEM was put onto cells.

2.2.12 Transfection of Neuro2A cells with Lipofectamine® 2000 reagent

Neuro2A cell line (ATCC®CCL-131™) was maintained 24 well plate containing EMEM (Lonza, Cat. #BE12-125F) supplemented with 10% FBS (Pan Biotech, Cat. #P30-1902), 1% P/S (Pan Biotech, Cat. #P06-07100) and 0.5% L-Glutamine (Pan Biotech, Cat. #P04-80050) (complete EMEM). After cells reached 70% confluency, plasmids were transfected using Lipofectamine® 2000 reagent (Invitrogen, Cat. #11668019) according to manufacturer's protocol. Briefly, two 1.5 ml centrifuge tubes were prepared; first one contained 50 µl of Opti-MEM®I and 2 µl of Lipofectamine® 2000 reagent, second one contained 50 µl of Opti-MEM®I and 2 µg total DNA (pEGFPC1, pEGFPC1_Kif2a.1, pEGFPC1_Kif2a.2, pEGFPC1_Kif2a.3, pEGFPC1_Kif2a^{S317N}, pEGFPC1_Kif2a^{H321D}). Tubes were incubated at room temperature for 5 minutes. After incubation, tubes were mixed and incubated at room temperature for 20 minutes. 100 µl of reaction mixture was added onto cells which were seeded on 24-well plate with coverslips (sterilized with UV) dropwise and plate was put in tissue culture incubator.

2.2.13 *In utero* electroporation, immunofluorescence and image analysis

In utero electroporation protocol was explained schematically in **Figure 2.11A**. At 14.5, CD1 pregnant mice were anesthetized with isoflurane (isoflurane machine, Harvard Apparatus). In order to reduce the pain after surgery, both painkiller (Bavet-Meloxicam, 7 µl/g body weight; prepared in physiological serum solution with 1:9 ratio) and Anestol Pomad (Sandoz, Novartis) were applied subcutaneously and onto skin. Pregnant mice were put on heating pad in order to stabilize the body temperature of mice to 37^{o}C throughout the operation. Limbs of the mice were taped and eye lotion was applied to prevent eye damage. Electric shaver (Dingling) was used to remove the hair on the belly and sterile parafilm was placed on the belly both to determine the area and prevent contact of the embryos to the skin. Laparotomy was performed and embryos were taken out with ring forceps without giving harm to any of the internal organs, uterine horns and blood vessels. Pre-warmed Ringer's solution (155 mM NaCl, 10 mM D-glucose, 5 mM HEPES, 4.5 mM KCl, 2 mM CaCl2, and 1 mM MgCl2, pH 7.4) was used to keep both the uterus and embryos wet and warm during the operation. 1 µl of DNA solution was injected into the lateral ventricle of each embryo using pulled glass capillaries (Drummond® PCR micropipettes, Cat. #5-000-1001-X10, pulled as 60 µm diameter) connected with an aspirator tube assemblies for calibrated micro capillary pipettes (Sigma, Cat #A5177-5EA). DNA solution was composed of 333 ng/µl NS (control) or shKif2a plasmids mixed with 333 ng/µl resKIF2A.1, resKIF2A.2 or resKIF2A.3 along with 333 ng/µl pCAGGS-IRES-tdTomato for visualizing the transfected neurons and 0.1% Fast Green FCF for monitoring the injection. Plasmid DNA was electroporated into the NPCs localized in VZ with 5 mm Tweezertrodes (BTX® Harvard Apparatus) by 0.5 pulses at 30 V for 400 ms intervals with an electroporater (BTX® Harvard Apparatus, Cat. #ECM830). Embryos were placed back into abdominal cavity and with ring forceps and body cavity was filled with pre-warmed Ringer's solution. Periton was sutured and staples were

applied to the skin. Embryos were allowed to continue their normal development for three days (E17.5). Pregnant mice was sacrificed using CO_2 and electroporated brains were harvested in 1X cold PBS. Brains were fixed with 4% Paraformaldehyde (PFA) (Merck, Cat. #K33810405 442; dissolved in ddH_2O with heating and stirring, adjusted pH to 7.2) in PBS at 4^oC, overnight. Next day, brains were transferred into 30% sucrose in PBS solution and incubated at 4^oC until brains were sunk onto the bottom of the 1.5 ml centrifuge tubes. Brains were embedded into cryostat embedding medium (Bio-Optica, Cat. #05 9801) using Peel-a-way disposable embedding molds (Polysciences, Cat. #18646A-1) at -20^oC. Coronal sections were taken as 50 µm thickness onto Polysine coated slides (Thermo Scientific, Cat. #J2800AMNZ) using cryostat (Leica Biosystems, Cat. #CM1950). Sections were dried onto 37^oC heat block for one hour and at 4^oC for another one hour. A general frame containing the sections was drawn with a liquid blocker pen (Thermo Scientific, Cat. #008877) to prevent solution leakage. Tissues were rehydrated with 1X cold PBS and then only DAPI (1:500) staining was applied onto brain sections. Sections were mounted with mounting media (Thermo Scientific, Cat. #TA-060-UG). LEICA DMI8 SP8 CS/DLS microscope was used to capture optical z-series through 50 µm images and LasX Life Science software was used to generate maximum intensity projections. Ten bins grid for the cell counting was positioned on images that were opened in Adobe Photoshop CC (Adobe Systems) and then number of the transfected cells were counted with cell counter tool of ImageJ (NIH) **(Figure 2.11B)**. For further analysis, data were transferred to Excel (Microsoft Office). Number of transfected cells in different bins were summed to represent the zones of the cortex (Bin 1-5: cortical plate, bin 6-9: subventricular-intermediate zones and bin 10: ventricular zone). Finally, graphs were plotted using GraphPad Prism 5 software.

- Dila Atak assisted the *in utero* electroporation experiments.

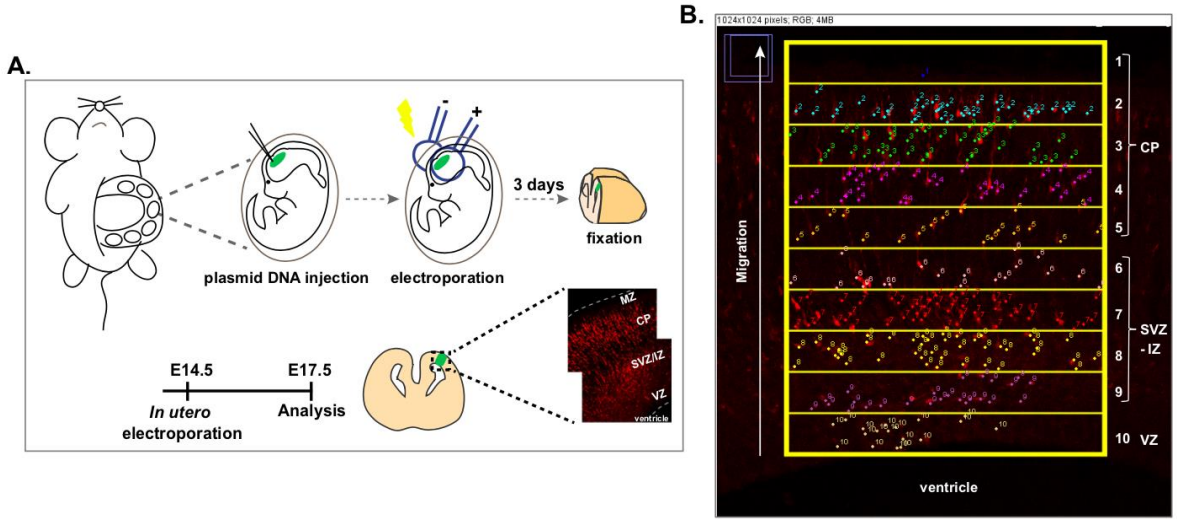

Figure 2. 11: *In utero* electroporation method is widely used protocol to investigate neuronal migration.

A. Schematic outline of *in utero* electroporation protocol. Plasmid DNA is injected into embryo's lateral ventricle and transfected into radial glia cells at E14.5. Electroporated brains are collected and fixed at E17.5 and migration process is analyzed with immunofluorescence and microscopy (Adapted from [104, 105]). **B.** Representation of *in utero* electroporation image analysis. Migration direction is indicated with white arrow. Yellow rectangles represent the bins (1-10) and numbers in different colors indicates the transfected neurons in each bin. VZ, ventricular zone; SVZ-IZ, subventricular zone-intermediate zone; CP, cortical plate.

2.2.14 Use of animals

All animal experiments were carried out in accordance with the guidelines for the care and use of laboratory animals of Koç University and the Ministries of Food, Agriculture and Live Stock, Forestry and Water Management of Turkey. All mice were housed, maintained and bred at the Koç University Animal Facility. Ethics approval with license no. 2014–9 was obtained from Koç University Institutional Animal Care and Use Committee.

2.2.15 Cloning of *Kif2a.1, Kif2a.2, Kif2a.3* and *Kif2a*^{H321D} into pcDNA3.1(-) mycBirA (mycBirA*) plasmids

Kif2a.1, Kif2a.2, Kif2a.3 and *Kif2a*^{H321D} inserts were subcloned from pEGFPC1 vector into pcDNA3.1(-)mycBirA (mycBirA*, N terminal) vector which was a kind gift from Dr. Elif Nur Fırat Karalar, Koç University, Istanbul. *Kif2a.1, Kif2a.2, Kif2a.3* and *Kif2a*^{H321D} inserts were amplified from *Kif2a.1, Kif2a.2, Kif2a.3* and *Kif2a*^{H321D} in pEGFP-C1 vector, respectively with PCR method. PCR was carried out in 30 µl reaction mixture containing 1X Phusion HF reaction buffer (Bio Labs, Cat. #B0518S), 0. 5 µM forward primer and 0.5 µM reverse primers **(Appendix C)**, 300 µM dNTP's, 1 Unit Phusion Hot Start Flex DNA Polymerase (New England Biolabs, Cat. #M0530L) and 150 ng pEGFPC1-Kif2a.1, pEGFPC1-Kif2a.2, pEGFPC1-Kif2a.3 or pEGFPC1-Kif2a^{H321D} as DNA template (PCR conditions: Denaturing 98^{o}C-15 seconds, annealing 59^{o}C-30 seconds and extension 72^{o}C-1.5 minutes; 30 cycles). PCR products were run on 1% agarose gel and under UV light the correct band was excised. Plasmid DNA was extracted from excised agarose gel using EZ-10 Spin column DNA Gel Extraction Kit (Bio Basic Canada Inc., Cat. #BS353). Gel purified PCR products and mycBirA* plasmid were digested with *Xho*I and *EcoR*I restriction endonucleases which have recognition sites embedded in designed forward and reverse primer pairs, respectively. Restriction enzyme digestion was carried out in 20 µl reaction

mixture containing 2X Tango Buffer, 5 Unit *Xho*I (Thermo Scientific, Cat. #ER0691), 5 Unit *EcoR*I (Thermo Scientific, Cat. #ER0271), 0.5 µl of mycBirA* plasmid DNA and 10 µl of gel purified PCR product (Double digest conditions: 37ºC-overnight). Next day, to prevent self-ligation of the plasmid DNA, dephosphorylation was carried out with 1 µl of FastAP (Alkaline phosphatase) (Thermo Scientific, Cat. #EF0651) at 37ºC for 1 hour and then digestion products were purified with EZ-10 Spin Column PCR Products purification kit (Bio Basic Canada Inc., Cat. #BS364). Ligation of mycBirA* vector with PCR products was performed in a 10 µl reaction mixture containing, 1X T4 Ligase Buffer (Thermo Scientific, Cat. #B69), 5 Unit T4 ligase (Thermo Scientific, Cat. # EL0011), 50 ng pcDNA3.1(-)mycBirA vector and 20 ng PCR products (*Kif2a.1*, *Kif2a.2*, *Kif2a.3* and *Kif2a*^{H321D}) (Ligation conditions: Room temperature-2 hours). Ligation product was used to transform into chemically competent DH5α *E.coli* cells according to heat shock based transformation protocol and LB-ampicillin plates were used for spreading the cells on the plate. Next day, miniprep cultures were prepared by single colony selection and cultures were incubated at 37ºC, overnight with shaking. Plasmid DNA's were purified by GeneJET Plasmid Miniprep Kit (Thermo Scientific, Cat. #K0503) according to manufacturer's protocol. Diagnostic digestion was set up in 20 µl reaction mixture containing 1X NEB 3 Buffer (New England Biolabs, Cat. #B7003S), 10 Unit *EcoR*I (New England Biolabs, Cat. #R0101S), 5 Unit *Xho*I (New England Biolabs, Cat. #R0146S) and 1µl of DNA (Double digest condition: 37ºC-2 hours). Samples were run on agarose gel for confirmation of the correct size insert of the selected colonies. Concentrations were measured by using NanoDrop2000© (Thermo Scientific) and 5 µl of miniprep DNA were sent to direct sequencing to Macrogen Company, The Netherlands for validation. After confirmation, maxi-prep cultures were incubated at 37ºC overnight with constant shaking. *Kif2a.1*, *Kif2a.2*, *Kif2a.3* and *Kif2a*^{H321D} plasmid

DNA's were purified separately with PureLink™ HiPure Plasmid Maxiprep Kit (Invitrogen, Cat. #K210006).

2.2.16 Transfection of Neuro2A cells with Polyethylenimine reagent

Neuro2A cell line was maintained in EMEM (Lonza, Cat. #BE12-125F) supplemented with 10% FBS (Pan Biotech, Cat. #P30-1902), 1% P/S (Pan Biotech, Cat. #P06-07100) and 0.5% L-Glutamine (Pan Biotech, Cat. #P04-80050) (complete EMEM). When the confluency of the cells reached to 70%, transfection was performed using 1mg/ml Polyethylenimine (PEI) dissolved in sterile ddH_2O (Polysciences Inc., Cat. #23966). Cells were washed with 1X PBS and warm (37ºC) EMEM medium (500 µl for 24 well-plate, 2 ml for 6 well plate and 12 ml for 15 cm plate) containing 10% FBS and 0.5% L-Glutamine was added on cells and plates were put back into tissue culture incubator. 1.5 µg DNA and 4.5 µl of PEI were added into 40 µl of Opti-MEM®I (Gibco, Cat. #31985-047) for 24 well plate, 3 µg DNA and 9 µl of PEI were added into 200 µl of Opti-MEM®I for 6 well plate and 60 µg DNA and 180 µl of PEI were added into 3 ml of Opti-MEM®I for 15 cm plate. Tubes were vortexed for 30 seconds and incubated at room temperature for 40 minutes. Transfection mixture was added on cells dropwise and plates were replaced into tissue culture incubator for 6 hours. After 6 hours, medium was changed with complete EMEM (500 µl for 24 well plate, 2 ml for 6 well plate and 15 ml for 15 cm plate).

2.2.17 Biotin treatment of cultures

One day after transfection, media of the cells were changed with fresh media containing 0.05 mM D-biotin (Life Technologies, Cat. #B1595) (0.5 mM stock was prepared by dissolving 2.4 mg D-biotin in 20 ml serum-free EMEM with 1%P/S and 0.5% L-Glutamine). Plates were replaced into the tissue culture incubator overnight.

2.2.18 Affinity capture of biotinylated proteins and Proximity-dependent biotin identification (BioID)

One day after biotinylation cells were washed with 1X cold PBS. Cells were collected with 1 X cold PBS (1 ml for 6 well plate and 5 ml for 15 cm plate) with cell scraper. Cells were centrifuged at 1000 rpm, 4^{o}C for 5 minutes and supernatant was discarded. Cells were frozen in liquid nitrogen and stored at -80^{o}C until next use. Cells were lysed in 150 µl of Lysis Buffer (10 mM Tris-HCl pH7.6, 150 mM NaCl, 2% NP40, 1 mM EDTA and 0.5% SDS) supplemented with 10 mM iodoacetamide and protease inhibitor (Roche, Cat. #11836170001) for both 6 well plate and 15 cm plate. Cells were burst by passing through an insulin syringe 7-8 times. Cells were incubated on ice for 15 minutes with vortexing few times and centrifuged at 7500 rpm, 4^{o}C for 15 minutes. Supernatant was collected (for 6 well plate 30 µl of supernatant was transferred into separate 1.5 ml centrifuge tube and labelled as "input"). BCA Protein Assay Kit (Thermo Scientific, Cat. #23225) was used to measure protein concentration. Pierce® Streptavidin Plus UltraLink® Resin (Thermo Scientific, Cat. #53117) were transferred into clean 1.5 ml centrifuge tubes (50 µl of beads for 6 well plate and 175 µl of beads for 15 cm plate) and beads were spin down at 10000 xg for 2 minutes. Supernatant was discarded and beads were washed with first 1X PBS and then Lysis Buffer twice for 2 minutes on rotator. For each wash step, beads were centrifuged at 10000 xg for 2 minutes and supernatant was discarded. Equal amount of protein from each condition was mixed with equal volume of pre-washed Streptavidin beads and incubated at 4^{o}C overnight on a tube rotator. Next day, beads were centrifuged at 1000 rpm for 5 minutes and supernatant was discarded (50 µl of supernatant was taken as "unbound" for 6 well plate). Then beads were washed with 500 µl of Wash buffer 1 (2% SDS), 500 µl of Wash Buffer 2 (50 mM HEPES pH 7.5, 50 mM NaCl, 1% Triton X-100, 2% Na-DOC, and 1 mM EDTA), 500 µl of Wash Buffer 3 (1% Triton X-100, 0.5% NP-40, 0.5% Na-DOC, 500 mM NaCl, 10 mM Tris-

HCl pH 8.1, and 1 mM EDTA,) and 500 µl of Wash Buffer 4 (50 mM NaCl and 50 mM Tris-HCl pH 7.4) and each wash was performed for 10 minutes, twice using tube rotator. Beads were centrifuged at 14000 rpm for 5 minutes to precipitate the beads between washes and supernatant was discarded after each centrifugation.

For affinity capture experiment followed by western blot, proteins were eluted with 50 µl of elution buffer (500 nM D-biotin in 2X Laemmli Buffer with 0.1 M DTT) at 98ºC, for 10 minutes with 1000 rpm shaking. Beads were centrifuged at 1000 rpm for 5 minutes and supernatant were transferred into clean 1.5 ml centrifuge tubes and labelled as "pull-down" and stored at -20ºC. Samples were boiled at 85ºC for 5 minutes prior to gel loading.

For identification of biotinylated proteins by mass spectrometry **(Figure 2.12)**, on bead-digest for streptavidin captured biotinylated proteins was performed thus sample loss would be eliminated. After this step, "proteomics clean" centrifuge tubes, pipettes, pipette tips and instruments were used. Beads were washed with 500 µl of 8 M urea solution (in 0.1 M Tris-HCl pH 8.5) for 10 minutes twice on tube rotator. Samples were reduced by treatment with 250 µl of 100 mM DTT in urea solution at 56ºC for 30 minutes at 1000 rpm shaking. And then washed with 500 µl of urea solution at room temperature for 10 minutes on tube rotator. 250 µl of 0.05 M iodoacetamide (in 8 M urea) was added onto beads and incubated at room temperature for 20 minutes under dark on tube rotator for alkylation of cysteine residues. Next, beads were washed with 450 µl of urea solution at room temperature for 10 minutes on tube rotator, twice and then 500 µl of 50 mM ammonium bicarbonate (NH_4HCO_3) (dissolved in HPLC grade water) at room temperature for 15 minutes on tube rotator, twice. After each step up to this stage, centrifugation was performed at 1000 rpm for 5 minutes in order to discard supernatant. Trypsin (MS Grade Trypsin Protease, Pierce) was diluted in 1 mM HCl and added onto beads and then 50 mM ammonium bicarbonate was added until

total volume was reached to 300 µl. For 300 µg of protein digestion, 2 µg of trypsin (MS Grade Trypsin Protease, Pierce) was added onto beads at 37ºC for 16 hours with 1000 rpm shaking. Next day, beads were centrifuged at 1000 rpm for 5 minutes and supernatant (peptides) were transferred into clean 1.5 ml centrifuge tubes. 500 µl of ammonium bicarbonate was added onto beads and incubated for 5 minutes on tube rotator. Beads were centrifuged at 1000 rpm for 5 minutes and supernatant was collected and pooled with the tube that contained peptide solution. In order to terminate trypsin digestion, peptides were treated with 10% acetic acid peptides until solution's pH was reached to 2-3 (pH was controlled with turnsole paper) were dried using Speed-Vacuum system. Peptides were eluted by Stage Tip method using C18 stage tips [106]. Briefly, stage tips were prepared by putting three C18 columns into each clean 200 µl pipette tips and top part of the tips were cut and stage tips were placed into a holder and then 2 ml clean centrifuge tubes. Stage tips were conditioned first with 60 µl of Methanol (spin at 2500 rpm for 10 minutes, discard the flow-through) and then 60 µl of Stage Buffer A (0.5% Formic Acid in 5% Acetonitrile) twice (spin at 2500 rpm for 10 minutes, discard the flow-through). Peptides were re-dissolved in 60 µl of Stage Buffer A and then samples were sonicated at 4ºC for 2 minutes. Samples were added onto the stage tips (spin at 2500 rpm for 10 minutes, discard the flow-through). Peptides were washed with 60 µl of Stage Buffer A, twice (spin at 2500 rpm for 10 minutes, discard the flow-through). Tips were placed into clean 1.5 ml centrifuge tubes and peptides were eluted with 60 µl of Stage Buffer B (0.1% Formic Acid in 70% Acetonitrile). Samples were centrifuged at 3000 rpm for 15 minutes and tips were discarded. Elutes was dried using Speed-Vacuum system and stored at -20ºC until the mass spectrometry analysis. Samples were analyzed using a Thermo Scientific Q-Exactive LC-MS/MS mass spectrometer. The data sets were analyzed as two technical replicates against the *Mus musculus* Swissprot/Uniprot database [107]. For analysis, fold change ratios and FDR values for each

KIF2A isoform (KIF2A.1, KIF2A.2 and KIF2A.3) and KIF2A^{H321D} mutant were calculated using spectral counts of protiens with the qspec-param programme of qprot_v1.3.5. Proteins found in less than two biological replicates were removed and PSM values of proteins with the same gene name were merged via summation. Proteins were filtered with a 0.05 cut-off for Z-statistics and FDR values followed by elimination of proteins with less than 1.5-fold change. Further analysis was performed with Excel (Microsoft Office). Interactome map and heat map were created using Cytoscape (version 3.7.2) and Prism 8, respectively. For cluster analysis, String database v11.0 [108] by Cytoscape StringApp [109] with 0.4 confidence was used to analyze significant protein hits. Affinity propagation clustering of the network was carried out with Cytoscape (version 3.7.2) and its plugin clustermaker [110]. g:Profiler was used to carry out GO and KEGG enrichment analysis of the network [111].

- Mass spectrometry (LC-MS/MS) was performed by Büşra Aytül Akarlar.
- Gene ontology analysis and interactome mapping were carried out by Altuğ Kamacıoğlu.

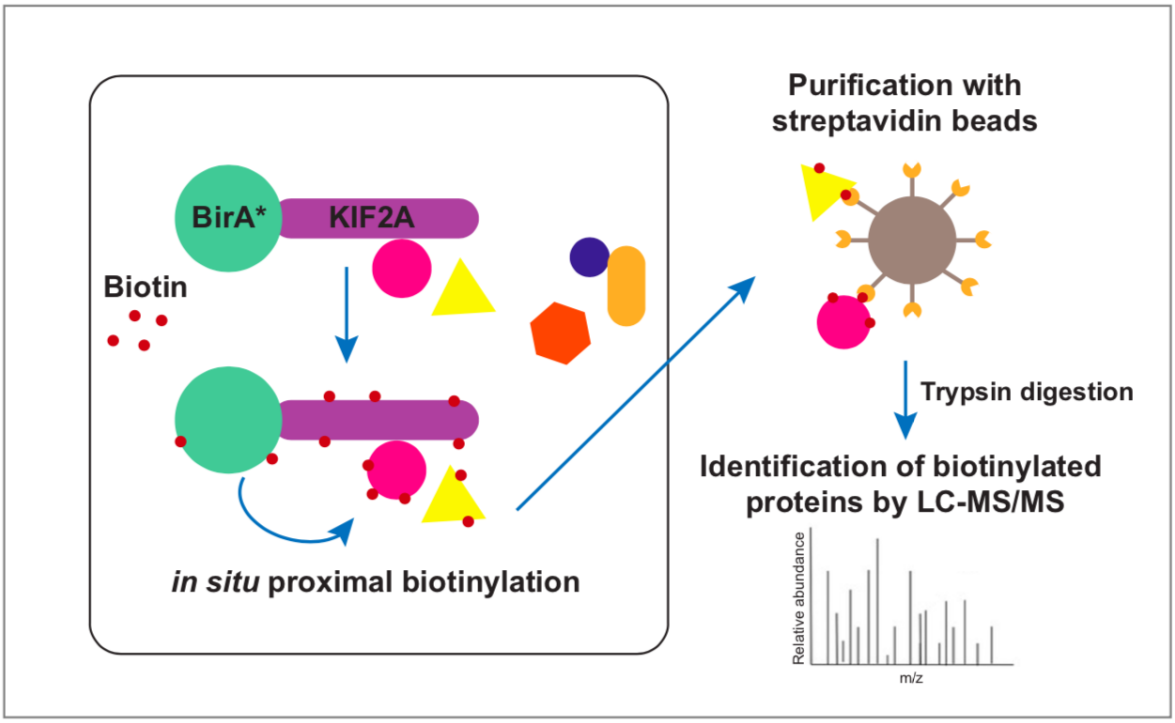

Figure 2. 12: Schematic representation of BioID method followed by LC-MS/MS analysis.

(Adapted from [112]).

2.2.19 Immunoassays and image analysis

For immunoblotting (or western blotting), protein lysates were collected 2 days after transfection either in in ice-cold RIPA buffer (0.15 M NaCl, 0.05 M Tris-HCl, pH 7.5, 1% Na-DOC, 1% Triton X-100, 0.1% SDS) supplemented with protease inhibitor (Roche, Cat. #11836170001) or Lysis Buffer Lysis Buffer (10 mM Tris-HCl pH7.6, 150 mM NaCl, 2% NP40, 1 mM EDTA and 0.5% SDS) supplemented with protease inhibitor (Roche, Cat. #11836170001) and 10 mM iodoacetamide. For immunoblotting of mice cortical lysates, cortices at different developmental time points (E14, E17, E18, P0, P7, P14, P21, P28 and adult) were collected in 1X cold PBS and tissues were homogenized in ice-cold RIPA buffer supplemented with protease inhibitor (Roche, Cat. #11836170001) with a Dounce homogenizer. 1 tablet of protease inhibitor was added for 10 ml of all of the lysis buffers. Samples were centrifuged at 14000 rpm, 4^{o}C for 20 minutes and supernatant was collected into clean 1.5 ml centrifuge tube. Protein concentration was measured with BCA Protein Assay Kit (Thermo Scientific, Cat. #23225). 7.5 µg – 10 µg protein samples were mixed with 2X Laemmli sample buffer (20% glycerol, 0.02% (w/v) bromophenol blue, 4% (w/v) SDS, 120 mM Tris-Cl (pH 6.8)) containig 100 mM dithiothreitol (DTT) with the ratio of (v/v). Samples were heated at 95^{o}C for 5 minutes and loaded into wells. GangNam-Stain Prestained Protein Ladder (INtRON Biotechnology, Cat. #24052) was used as a ladder to determine the molecular weight of protein samples. A 5% stacking SDS-PAGE gel (650 µl of 30% Acrylamide-Bisacrylamide (29:1), 1.25 ml of 4X Tris-Cl/SDS pH 6.8, 25 µl of 10% APS, 5 µl of TEMED) was added on top of either 7.5% separating SDS-PAGE gel (3.75 ml of 30% Acrylamide-Bisacrylamide (29:1), 3.75 ml of 4X Tris-Cl/SDS pH 8.8, 50 µl of 10% APS, 15 µl of TEMED).

Samples were run at 80 V for 30 minutes and 100 V for 1.5 hours in 1 L of 1X SDS Running Buffer pH 8.3 (10X; 187.6 g Glycine, 30 g Tris Base, 1% SDS in 1L total volume). Proteins were transferred to nitrocellulose membrane (GVS, Cat. #1215471) with wet-transfer method (7.25 g Glycine, 1.45 g Tris Base, 150 ml Methanol in 1L total volume) at 40 V (or 55 mA) overnight in cold room (at 4^{o}C). Next day, membrane was incubated in blocking buffer (5% Nonfat Dried Milk Powder (AppliChem, Cat. #A0830) in 1X TBS-T (0.05% Tween, 10 mM Tris-HCl, 150 mM NaCl,)) for 45 minutes and thein with primary antibody diluted in 2% Bovine Serum Albumin (BSA) (SantaCruz Biotechnology Inc., Cat. #sc-2323A) in 1X TBS-T either at room temperature for 2 hours or at 4^{o}C overnight. Membrane was rinsed with 1X TBS-T for 5 minutes, three times and incubated with secondary antibody diluted in blocking buffer at room temperature for 1 hour. Then, membrane was washed with 1X TBS-T again for 5 minutes 3 times. Proteins were visualized with the Pierce ECL Western Blotting Substrate (Thermo Scientific, Cat. #32106) in dark room. Primary and secondary antibodies with dilution ratios that used in immunoblotting were indicated in **Table 2.1** and **Table 2.2**, respectively. For cortex lysate analysis (immunoblotting with α-Elavl, α-Kif2a and α-β-actin antibodies), band intensities were measured with ImageJ software [113, 114] and then protein levels (KIF2A and nElavl) were normalized to β-actin.

For immunofluorescence staining, both media containing Neuro2A cells and E14.5 primary cortical neurons were fixed with 4% PFA under hood at room temperature for 20 minutes. Cells were washed with 1X cold PBS for one minute three times. Coverslips were placed facing upwards onto a staining chamber covered with parafilm. Blocking solution (3% BSA, 0.3% TritonX-100 in 1X PBS) was added onto each coverslip and incubated at room temperature for 45 minutes. Then, cells were incubated with primary antibody diluted in blocking solution either at room temperature for 2 hours or at 4^{o}C overnight. Cells were

washed with 1X cold PBS for 5 minutes 3 times and then incubated with secondary antibody diluted in blocking solution at room temperature for 1 hour under dark. Coverslips were washed with 1X cold PBS for 5 minutes under dark and then incubated with DAPI (diluted 1:500 in 1X PBS) for 10 minutes under dark. After DAPI incubation, cells were washed with 1X cold PBS for 5 minutes followed by mounting of coverslips with mounting media (Thermo Scientific, Cat. #TA-060-UG). Images of E14.5 primary cortical neurons were captured using Nikon Eclipse 90i confocal microscope and NIS-Elements AR software and Neuro2A cells were imaged using LEICA DMI8 SP8 CS/DLS confocal microscope and LasX Life Science software. Primary and secondary antibodies with dilution ratios that used in immunofluorescence were indicated in **Table 2.3** and **Table 2.4**, respectively. Dendrite arborization quantification was carried out using Sholl analysis with ImageJ software's Sholl analysis plug-in [113, 114] **(Figure 2.13)**. Co-localization quantification was carried out using ImageJ software's JACoP plugin that calculates the Manders' Coefficients M1 and M2. Both M1 and M2 values provide direct metric of the quantity of interest independent of signal proportionality [115-117].

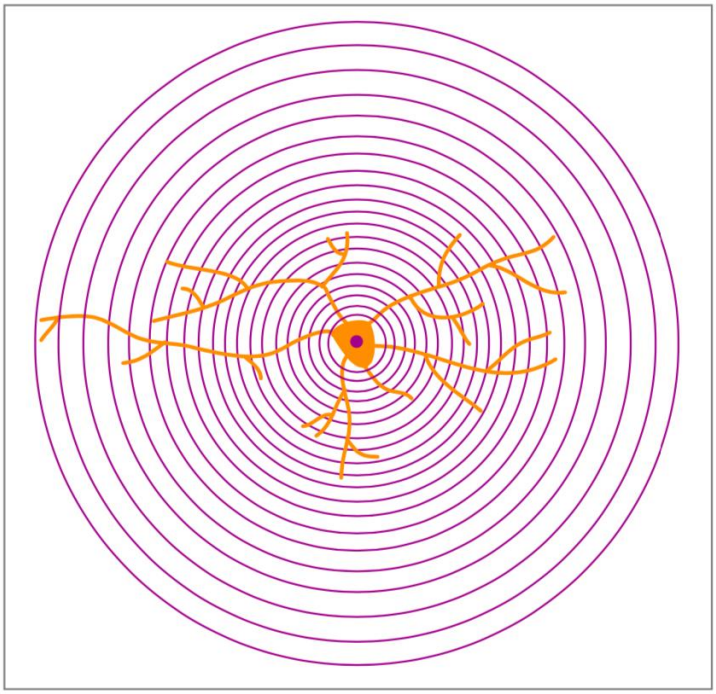

Figure 2. 13: Schematic of Sholl analysis.

Orange drawing is the neuron with axon and dendrites. Purple circles represents the concentric circles used for Sholl analysis.

Table 2. 1: Primary Antibodies used in immunoblotting.

Antibody	Host	Company	Catalogue Number	Dilution
β-actin	Mouse	Abcam	ab6276	1:5000
hnRNP C1+C2	Mouse	Abcam	ab10294	1:2000
myc	Mouse	Santa Cruz	sc-40	1:1000
Radford (for nElavl)	Human	*	-	1:10000
Biotin	Rabbit	**	-	1:20000
Histone H3	Rabbit	Cell Signaling	9715S	1:2500
Kif2a	Rabbit	Abcam	ab37005	1:5000
* Human anti-sera was a kind gift of Dr. Robert Darnell, Rockefeller University ** Biotin antibody was a kind gift of Dr. Timothy J Mitchison, Harvard Medical School				

Table 2. 2: Secondary Antibodies used in immunoblotting.

Antibody	Host	Company	Catalogue Number	Dilution
Anti-Mouse IgG HRP-linked	Mouse	Cell Signaling	7076S	1:2500
Goat Anti-Human IgG (H+L) HRP-linked	Human	Thermo Scientific	31412	1:5000
Anti-Rabbit IgG HRP-linked	Rabbit	Cell Signaling	7074S	1:2500

Table 2. 3: Primary Antibodies used in immunofluorescence.

Antibody	Host	Company	Catalogue Number	Dilution
GFP	Chick	Aves Labs	GFP-1020	1:800
Alpha tubulin	Mouse	Cell Signaling	3873S	1:1000
myc	Mouse	Santa Cruz	sc-40	1:1000
Nogo C-4	Mouse	Santa Cruz	sc-271878	1:500
βIII Tubulin (Tuj1)	Mouse 2b	Abcam	ab7751	1:500
Kif2a	Rabbit	Abcam	ab37005	1:5000

Table 2. 4: Secondary Antibodies used in immunofluorescence.

Antibody	Host	Company	Catalogue Number	Dilution
Goat Anti-Chick IgG (H+L) Alexa Fluor®488	Chick	Life Technologies	A11039	1:1000
Donkey Anti-Mouse IgG (H+L) Alexa Fluor®488	Mouse	Invitrogen	A21202	1:1000
Streptavidin Alexa Fluor®488 conjugate	-	Life Technologies	S32354	1:5000
Donkey Anti-Mouse IgG (H+L) Alexa Fluor®594	Mouse	Invitrogen	A21203	1:1000
Donkey Anti-Rabbit IgG (H+L) Alexa Fluor®594	Rabbit	Invitrogen	A21207	1:1000

2.2.20 Proximity Ligation Assay (PLA)

Proximity Ligation Assay was carried out using Duolink® In Situ Red Starter Kit Mouse/Rabbit (Sigma-Aldrich, Cat. #DUO92101) according to manufacturer's protocol **(Figure 2.14A and B)**. Briefly, Neuro2A cells were plated on 24 well plate with UV-sterilized coverslips and fixed with 3.2% PFA at room temperature for 15 minutes. Coverslips were placed onto a dark humidity chamber which was covered with parafilm. Coverslips were blocked with Duolink® Blocking Solution at 37ºC for 30 minutes and incubated with primary antibody pairs or only one primary antibody as control, diluted in Duolink® antibody diluent at 4ºC overnight. Next day, coverslips were washed with Wash Buffer A at room temperature for 5 minutes, twice and then incubated with Duolink® Plus and Minus PLA probes in antibody diluent for 1 hour at 37ºC. Coverslips were washed with Wash Buffer A at room temperature for 5 minutes, twice and ligation was carried out with ligase diluted in Duolink® Ligation buffer for 30 minutes at 37ºC. Cells were washed again with Wash Buffer A at room temperature for 5 minutes, twice. Amplification was carried out using polymerase diluted in Duolink® Amplification buffer for 100 minutes at 37ºC. Coverslips were washed with Wash Buffer B at room temperature for 10 minutes, twice followed by washing with 0.01X Wash Buffer B at room temperature for 1 minute. Coverslips were mounted with mounting medium containing DAPI and nail polish was applied to seal the coverslips on the slides. Microscopy images were captured with LEICA DMI8 SP8 CS/DLS microscope using red channel (λex 594 nm; λem 624 nm) to observe PLA dots and DAPI channel to observe nuclei. Maximum intensity option of the LasX Life Science software was used to project optical z-series images into a flattened plane. Analysis was carried out with ImageJ (NIH) software [118]. Antibodies and dilutions used were as follows: KIF2A (Abcam, Cat. #ab37005, 1:5000); RTN4 (Nogo C-4, Santa Cruz Biotechnology, Cat. #sc-271878, 1:500).

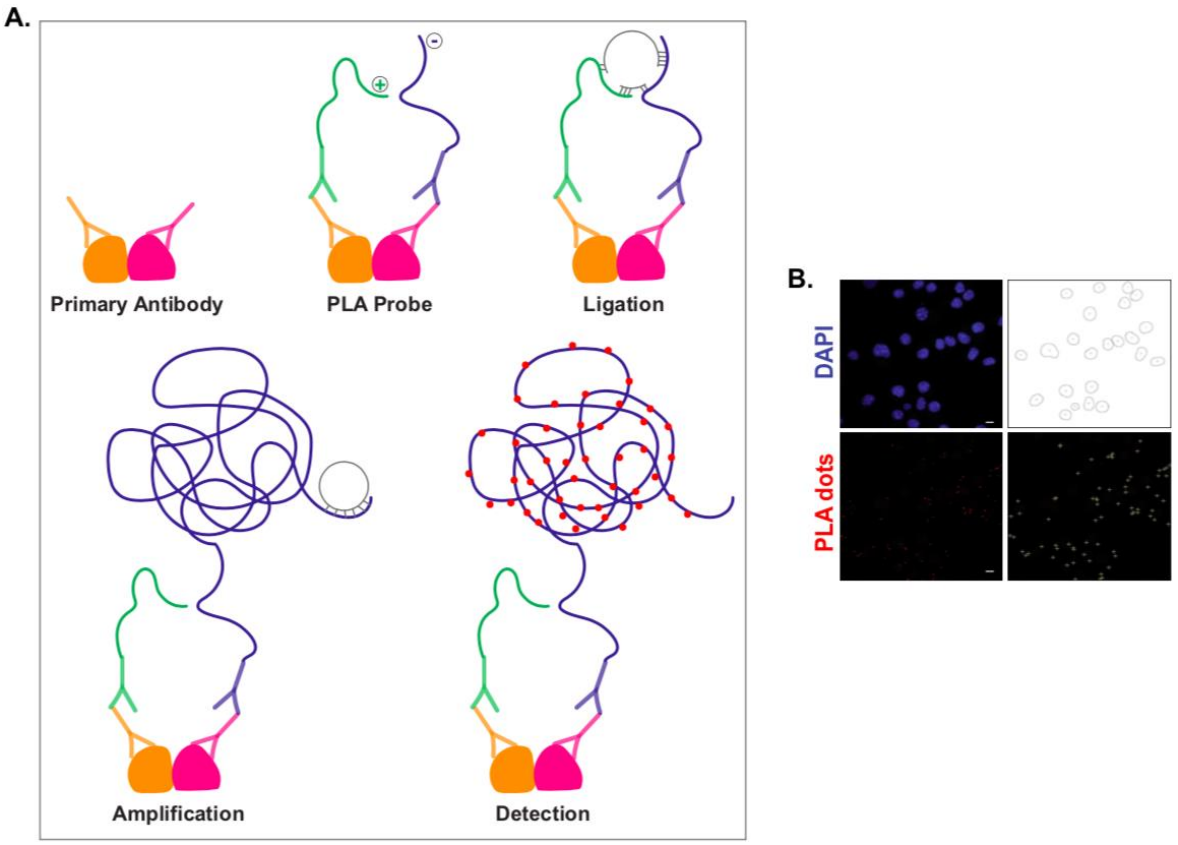

Figure 2. 14: Proximity Ligation Assay (PLA) is used for *in situ* detection of protein-protein interactions.

A. Schematic outline of PLA. Two protein of interests are recognized by two primary antibodies. PLA probe (oligonucleotide) couples secondary antibodies bind to primary antibodies. PLA probes are ligated when they are in close proximity. DNA polymerase amplify the circular DNA. PLA signals are formed with the fluorochrome-coupled detection oligos and detected by microscopy as separate red signals which show protein-protein interaction (Adapted from [119]). **B.** Quantification of total number of PLA dots and nuclei using ImageJ software [118].

2.3 RESULTS

2.3.1 KIF2A and nELAVL protein expressions are developmentally controlled in the mouse cerebral cortex

It has been shown that *Kif2a* mRNA is one of the top target whose AS is regulated by nELAVL RNABPs [31]**.** *Kif2a* gene has 20 exons and alternative splicing of *Kif2a* pre-mRNA enhances the inclusion of exon 18 which encodes for a 37 serine-rich amino acid sequence (KIF2A.1). The other isoform (KIF2A.2) is devoid of exon 18. We also identified a third isoform (KIF2A.3) which also contains all 20 exons, but also has a shorter exon 5 (by 20 amino acids). Initially, I focused on the developmental expression patterns of both KIF2A and nELAVL to observe whether these patterns were correlated with each other. Since there is no antibody for individual KIF2A isoforms (and generating antibodies which are isoform specific is very challenging), I quantified the total KIF2A protein amount that includes all three isoforms. For this purpose, I collected mice cortices at different developmental time points from both embryonic and postnatal days, and performed immunoblotting from their lysates to see overall protein abundance. I observed that the protein expression pattern of nELAVL and KIF2A generally correlate with each other, where the protein abundance is higher in embryonic days and then downregulated postnatally **(Figure 2.15A and B)**. These results suggested that nELAVL RNABPs might control the stability of *Kif2a* mRNA together with its AS.

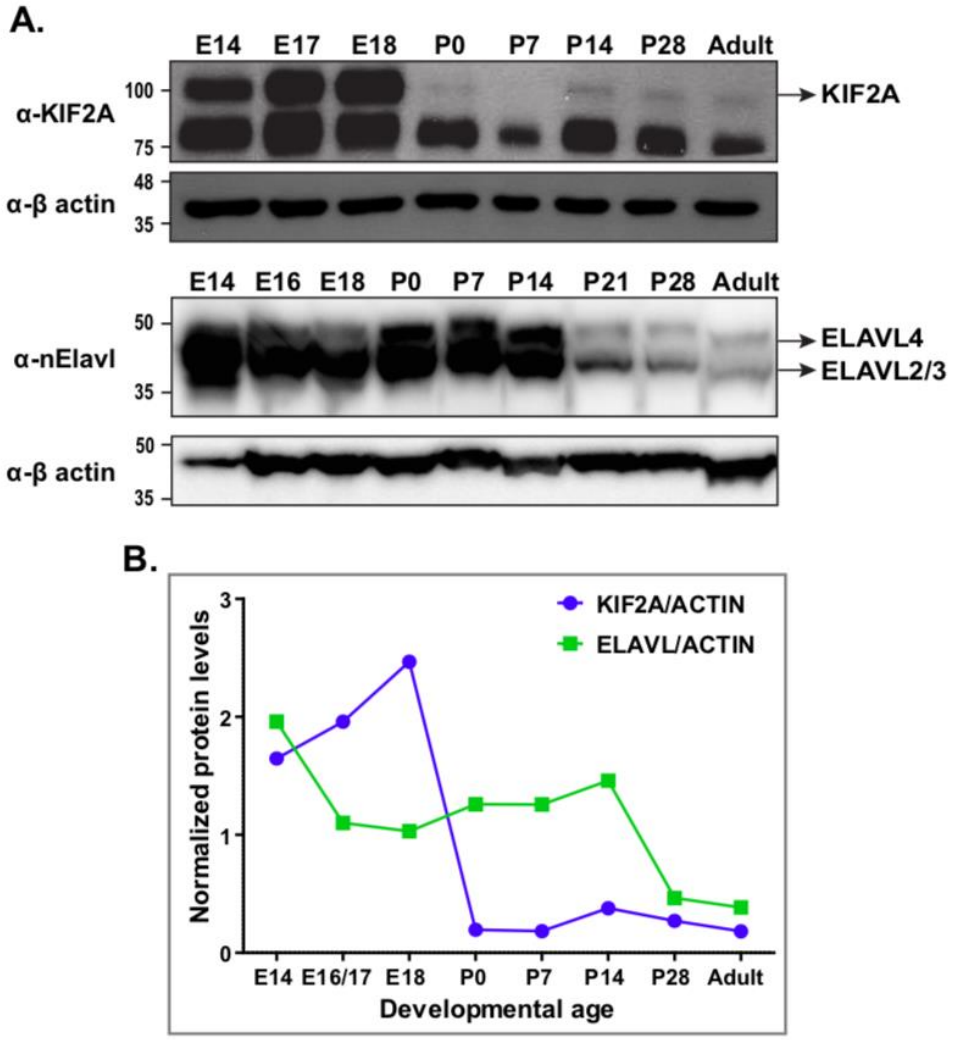

Figure 2. 15: KIF2A and nELAVL protein expressions are developmentally controlled in mouse cortex.

A. Immunoblotting analysis of total KIF2A (top panel) and nELAVL (bottom panel) protein levels during different developmental ages in mouse cerebral cortex. **B.** Quantification of immunoblot represented in **(A)**. Protein levels of both nELAVL and KIF2A are normalized to the loading control β-actin.

2.3.2 *Kif2a* alternative mRNA isoform expression is developmentally controlled in mouse cerebral cortex

After testing the protein expression abundance, I next examined the expression pattern of three *Kif2a* isoforms at the mRNA level at different developmental time points in the mouse cerebral cortex. Toward this aim, I performed quantitative RT-PCR (RT-qPCR) by isolating total RNA from mice cortices at different developmental times, synthesized cDNA by reverse transcription and then identified the mRNA level abundance by real time PCR. My RT-qPCR results showed that in all developmental stages, *Kif2a.1* and *Kif2a.2* isoforms are predominantly expressed with high expression levels during embryogenesis and lower expression in postnatal and adult stages. The third isoform *Kif2a.3* is the minor isoform throughout development and its expression reaches a peak during late embryogenesis (~E18) and then once again during the second postnatal week (P14) **(Figure 2.16)**. Together with the KIF2A protein expression pattern, these observations suggest that there is an overall trend where the KIF2A isoform expressions are high during embryonic stages of developing mouse cortex which is the time period when both NPC proliferation and neuronal migration take place.

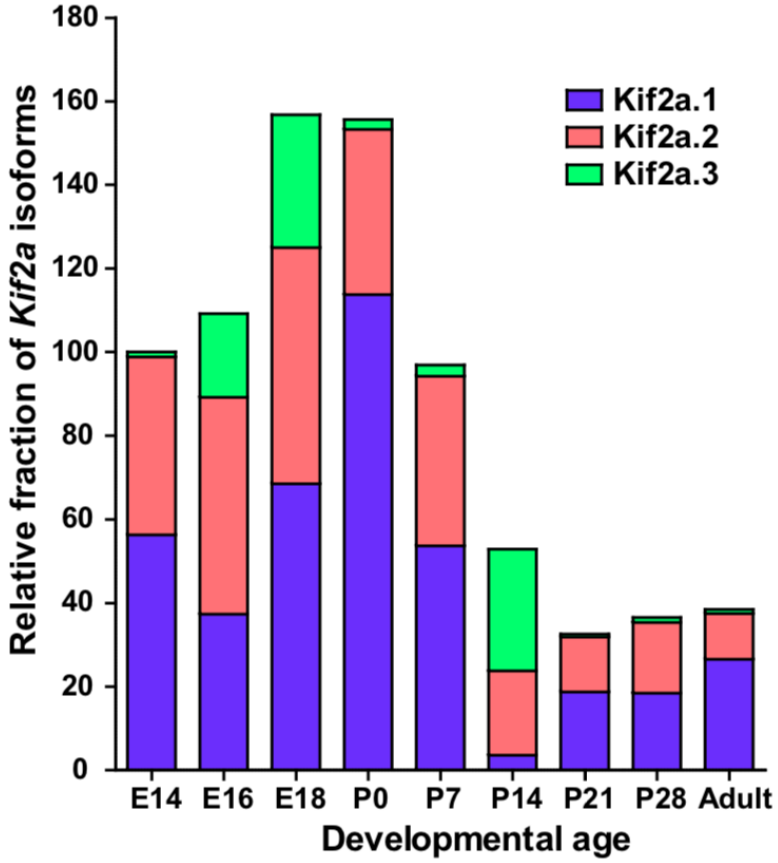

Figure 2. 16: *Kif2a* isoform expressions are controlled across development at mRNA level in mouse cerebral cortex.

Relative fraction of all three *Kif2a* isoforms expression were quantified after normalization to first *Gapdh* and then to E14 levels by qRT-PCR analysis. Data represents 3 biological x 2 technical replicates.

2.3.3 Alternatively spliced KIF2A isoforms have the same subcellular localization in Neuro2A cells

To further understand the mechanism underlying the functional roles of AS of KIF2A, I first focused on whether AS has an effect on KIF2A isoforms subcellular localization. Toward this aim, I performed immunofluorescence analysis by expressing all three KIF2A-EGFP fusion protein isoforms in both Nuero2A cells and embryonic day 18.5 (E18.5) primary cortical neurons. My analysis showed that all three KIF2A isoforms are diffusely localized to the cytoplasm and nucleus in both primary cortical neurons [103] and Neuro2A cells **(Figure 2.17)**. Hence, my results suggest that AS of KIF2A does not change its subcellular localization in both primary cortical neurons [103] and Neuro2A cells.

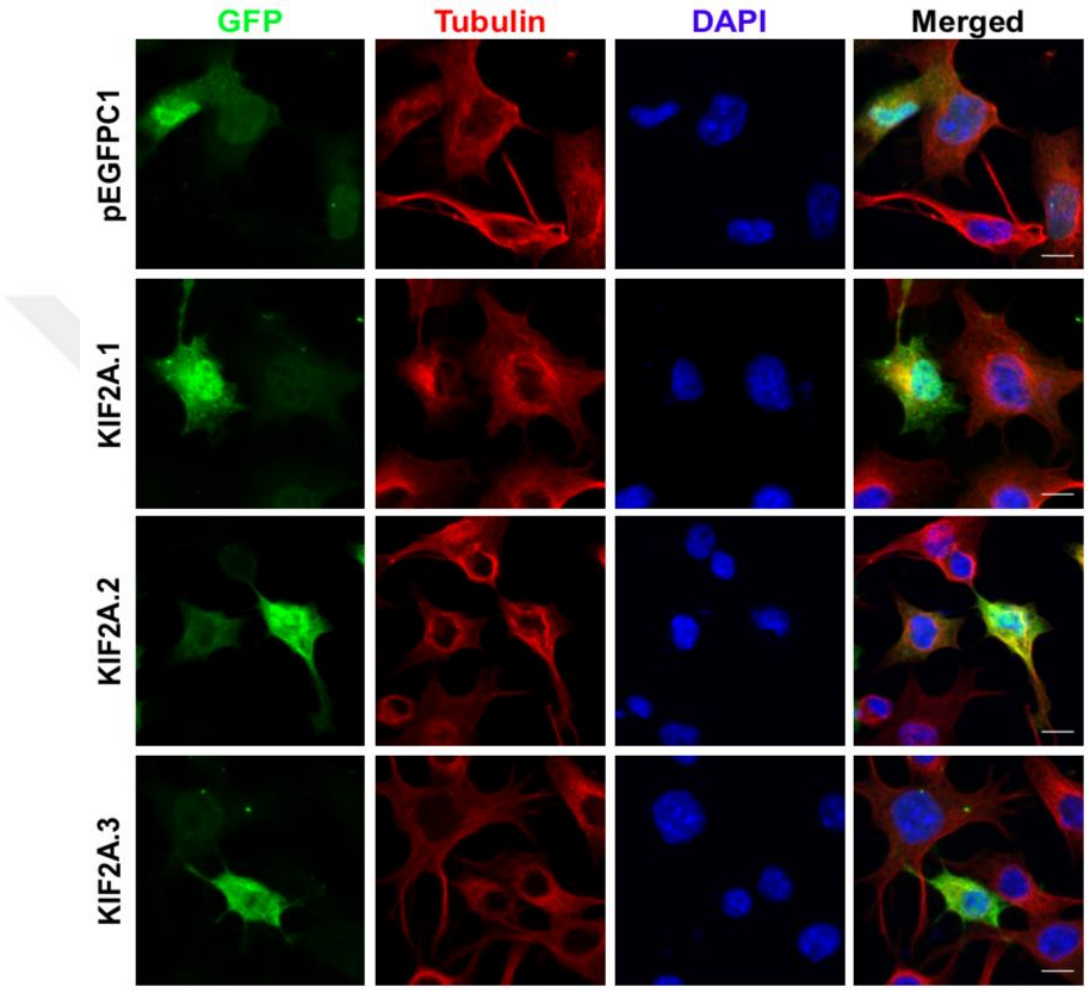

Figure 2. 17: All KIF2A isoforms have diffuse cytoplasmic and nuclear localization in Neuro2A cells.

Neuro2A cells transfected with pEGFPC1-tagged KIF2A isoforms (KIF2A.1, KIF2A.2 and KIF2A.3) 2 days after plating, fixed with 4% paraformaldehyde (PFA) 2 days after transfection and immunostained with anti-GFP (green) antibody to detect transfected pEGFPC1-tagged KIF2A isoforms. Microtubules (MTs) were visualized with anti-αTubulin (red) and DAPI (blue) was used to stain the nucleus. Scale bar, 10 μm.

2.3.4 Endogenous KIF2A is successfully knocked down in primary cortical neurons

To further understand the mechanism underlying the effect of *Kif2a* AS on neuronal differentiation and migration, I first cloned shRNA targeting a sequence common to all three *Kif2a* isoforms into the mammalian shRNA expression vector pSuper_GFP (shKif2a) **(Figure 2.18)**.

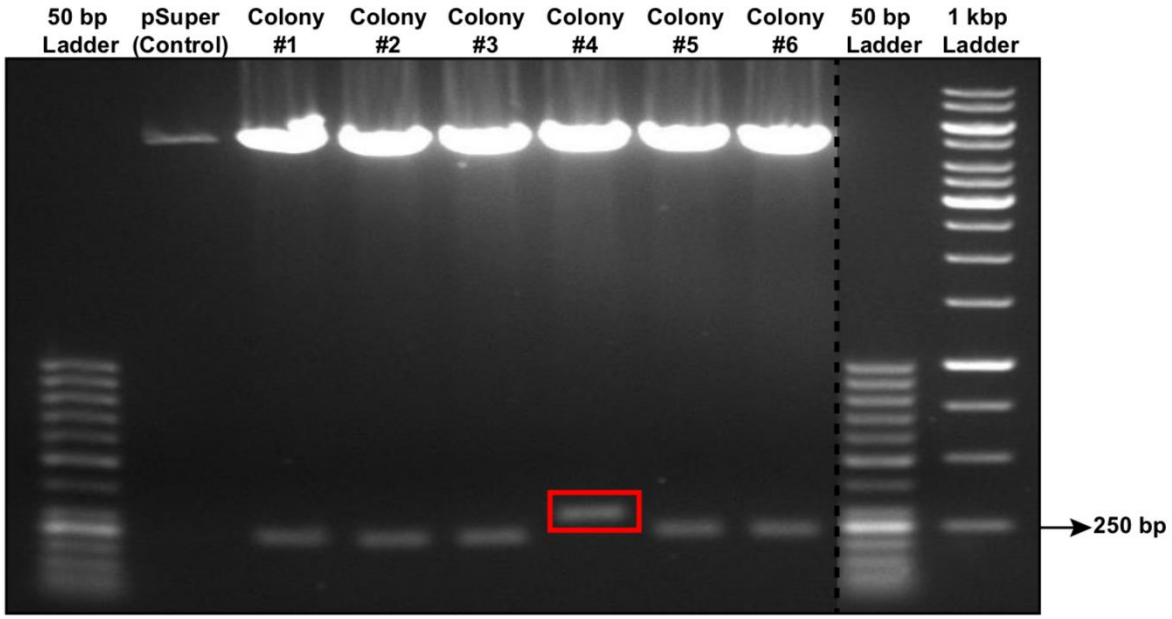

Figure 2. 18: shRNA against KIF2A was cloned successfully.

Agarose electrophoresis result showing diagnostic digestion of cloned pSuper_shKif2a-GFP (shKif2a). Correct construct is highlighted in red box.

Next, I cultured E14.5 primary cortical neurons and transfected them with shKif2a to achieve knockdown or with non-silencing (NS) shRNA as a control. My immunofluorescence images showed that control (NS) transfected neurons have the same endogenous KIF2A expression compared to non-transfected neurons whereas the shKif2a transfected neurons have decreased KIF2A expression compared to NS-transfected neurons **(Figure 2.19)**.

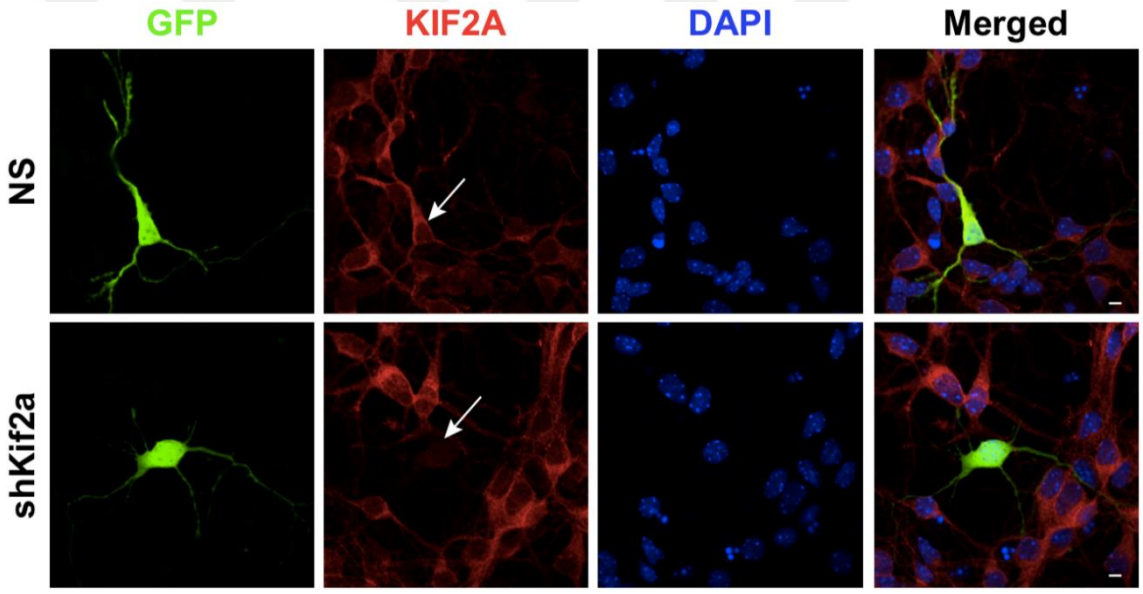

Figure 2. 19: shKif2a knocks down expression of endogenous KIF2A in primary cortical neurons.

Primary cortical neurons from E14.5 embryos were transfected with either non-silencing shRNA (NS) or shRNA against KIF2A (shKif2a) at 2 day *in vitro* (DIV), fixed at 4 DIV with 4% PFA and immunofluorescently stained against GFP (green) and KIF2A (red) proteins. DNA was observed with DAPI staining. Transfected cells were identified based on their co-expression of GFP from NS or shRNA expressing plasmid. Transfected neurons are indicated with white arrows. Scale bar, 10 μm.

2.3.5 shRNA against KIF2A can suppress the expression of all three endogenous *Kif2a* isoforms, but not the shRNA resistant *Kif2a* cDNAs

To re-introduce individual KIF2A isoforms in *Kif2a* silenced cells, I cloned shRNA resistant constructs into pcDNA4A (pc4A) vector by creating three silent mutations on the shRNA target site by site directed mutagenesis **(Figure 2.20)**.

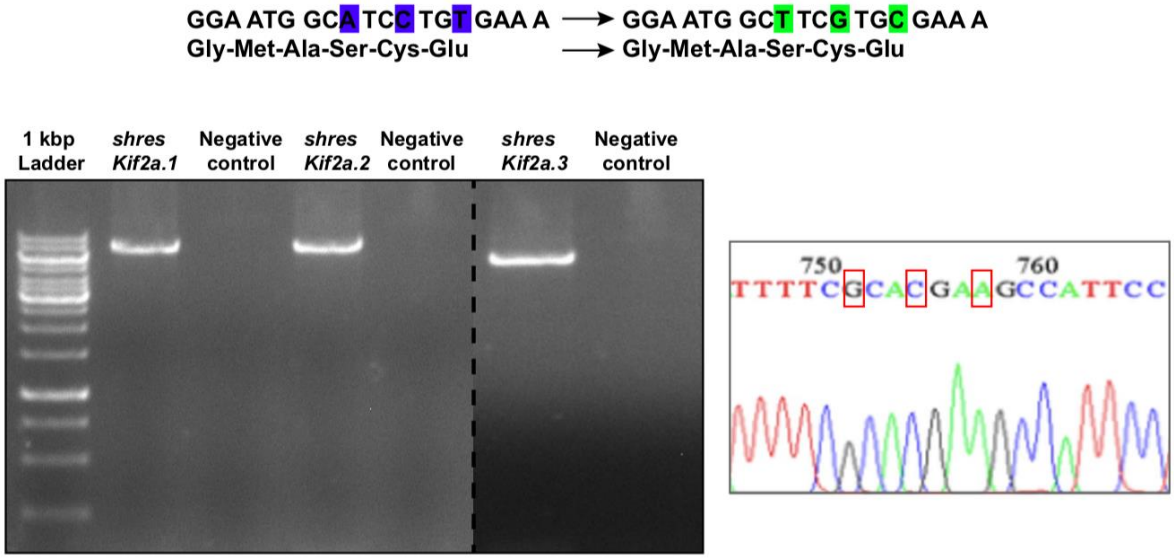

Figure 2. 20: *resKif2a* plasmids for all three isoforms were cloned with site-directed mutagenesis.

Top panel: Target sequence for shKif2a. Nucleotides in blue boxes are the chosen nucleotides for creating shRNA-resistant mutation and mutated nucleotides are shown in green boxes. Introduced mutations did not change the amino acid sequence. **Bottom left panel:** Agarose gel result of site-directed mutagenesis PCR for three *resKif2a* isoforms. **Bottom right panel:** Point mutations were verified by direct sequencing. Site of mutations are shown in red boxes.

To confirm whether these resKIF2A constructs can rescue KIF2A expression in KIF2A-knockdown cells, I first co-transfected NS or shKif2a with individual KIF2A isoforms in HEK293T cells and I observed all three KIF2A isoform expression in NS-KIF2A isoform co-transfected cells **(Figure 2.21 lanes 2, 3 and 4)**. I observed significantly reduced expression of three KIF2A isoforms in shKif2a-KIF2A isoform co-transfected cells **(Figure 2.21 lanes 5, 6 and 7)**. Moreover, when I co-transfected the HEK293T cells with shKif2a and individual resKIF2A isoforms, I observed that resKIF2A expression for each isoform (resKIF2A.1, resKIF2A.2 and resKIF2A.3) was not affected by shKif2a **(Figure 2.21 lanes 8, 9 and 10)**.

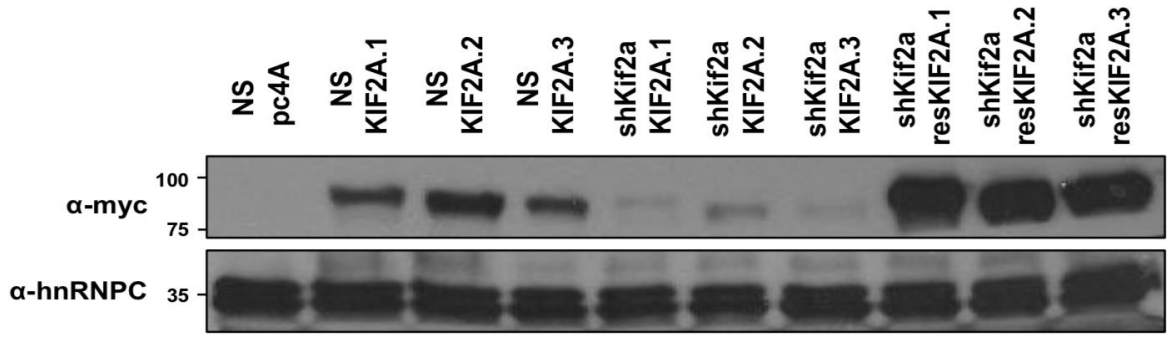

Figure 2. 21: shKif2a can suppress KIF2A isoforms expression but not the resKIF2 in comparison to control (NS) in HEK293T cells.

Immunoblotting against the myc-epitope indicates that the protein expression of myc-tagged *Kif2a* isoforms were silenced by co-expression of shKif2a (lanes 5, 6 and 7) whereas *resKif2a-myc* isoform expressions were resistant to silencing by shKif2a (lanes 8, 9 and 10). Co-transfection of non-silencing (NS) with pcDNA4A (pc4A) was used as negative control (lane 1) and NS has no effect on expression of KIF2A isoforms (lane 2, 3 and 4). Anti-hnRNPC immunoblotting is used as loading control.

2.3.6 KIF2A isoforms are interchangeable in their roles for dendritic arborization of primary mice cortical neurons

Dendrites are the branched projections of neurons which transmit electrochemical stimulation received from upstream neurons (generally axons). Dendrites have crucial role in combining inputs from synapses and they determine the extent to which action potentials are produced by the neuron. In human cortex, soon after neurons reach their destined layer, they start growing dendrites. Dendrite development is a multistep process which can be divided into several steps; neurite initiation, outgrowth and guidance, branching. and synapse formation and stabilization. Dendritic branching is a process by which neurons form new dendritic arbors in order to form new synapses. This process is important in determining which signals neurons receive and how these signals are integrated [120]. During the formation of proper dendritic branching, there is a very tight control of actin and MT cytoskeleton organization [121]. Moreover, defects in dendrite development may cause neurological disorders such as Down's syndrome, autism, schizophrenia, and fragile X syndrome [122, 123].

Previous studies have shown that KIF2A regulates pruning of axon collaterals of both cortical and sensory neurons in mice [30, 67]. Since MT dynamics are also tightly modulated in dendrite development [121], I hypothesized that KIF2A isoforms may have an effect on dendrite growth and branching. For this purpose, I cultured E14.5 primary cortical neurons and transfected them with shKif2a to achieve knockdown or with NS shRNA as a control. Dendritic arbors of transfected cells were marked by GFP expression and were quantified by Sholl analysis which is a quantitative method used to measure the extent of dendritic branching of a neuron [8] **(Figure 2.22A)**. Our results showed a significant increase in the number of primary dendrites protruding from soma in neurons where *Kif2a* expression was

silenced suggesting that in the absence of KIF2A there is a diminished dendritic MT depolymerization capacity **(Figure 2.22A and B)**. To demonstrate specificity of this effect and also to test whether different KIF2A isoforms can carry out dendritic pruning function, I cultured E14.5 primary cortical neurons and co-transfected with shKif2a to achieve knockdown along with one of the resKIF2A constructs (*resKif2a.1*, *resKif2a.2* and *resKif2a.3*) to achieve rescue in isolated cortical neurons at 2 days *in vitro* (2 DIV) and then performed Sholl analysis after fixing the neurons at 4 DIV **(Figure 2.22A)**. Sholl analysis revealed that the number of dendritic intersections was similar to those of controls when we expressed resKIF2A isoforms in *Kif2a* silenced neurons meaning that all three KIF2A isoforms have the capacity to reverse the KIF2A loss-of-function phenotype by suppressing dendrite branching **(Figure 2.22C, D and E)**. I observed even more pruning in higher order dendritic branches where the NS and shKif2a transfections showed no significant difference. Collectively these data suggested that, KIF2A is required for normal dendrite development in primary cortical neurons and all three KIF2A isoforms can support this function.

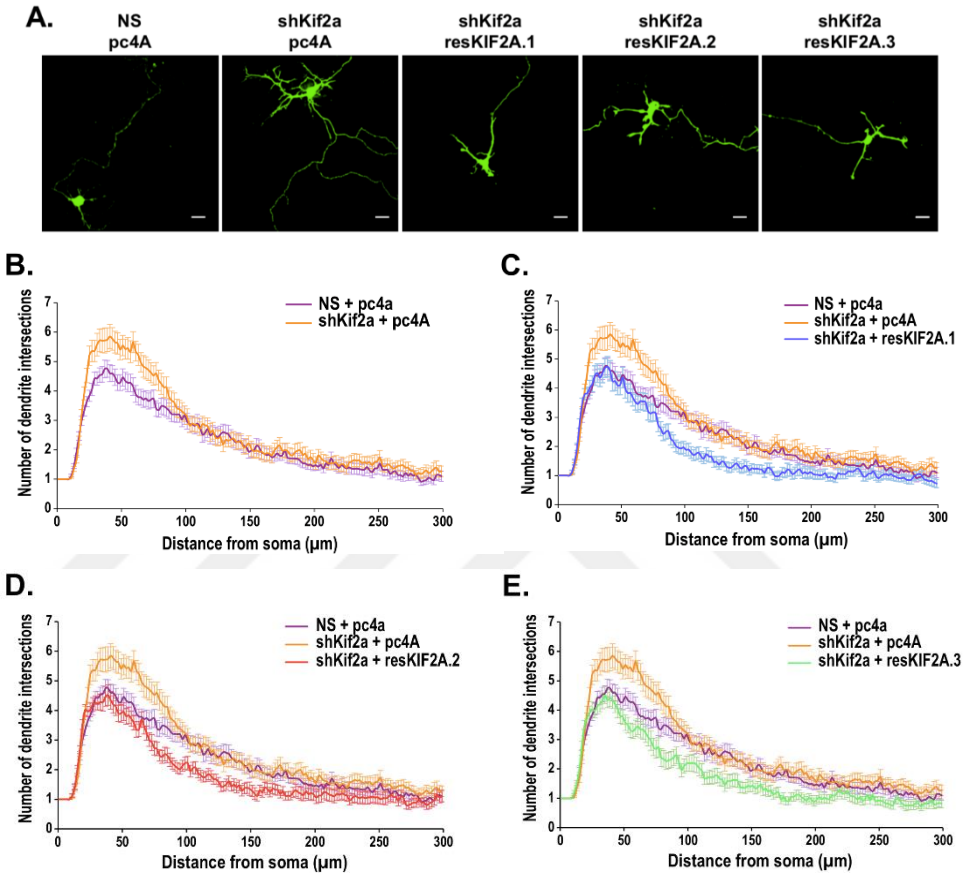

Figure 2. 22: All three KIF2A isoforms function in proper dendritic growth and branching.

A. Representative images of E14.5 primary cortical neurons co-transfected with either NS or shKif2a along with either pcDNA4A (pc4A) or resKIF2A isoforms at 2 DIV, fixed with 4% PFA at 4 DIV and images were captured with confocal microscopy for Sholl analysis. Scale bar, 10 µm. **B., C., D. and E.** Dendritic branching was quantified by Sholl analysis [113, 114]. **(B)**, NS-shKif2a; **(C)**, NS-shKif2a-resKIF2A.1; **(D)**, NS-shKif2a-resKIF2A.2; and **(E)**, NS-shKif2a-resKIF2A.3. n=60 for each condition derived from two separate neuronal cultures. Bars represent S.E.M. Unpaired two-tailed *t* test, p value: * $p<0.05$, ** $p<0.005$.

2.3.7 KIF2A's role in radial cortical neuronal migration is isoform-dependent

Past studies have suggested that KIF2A is required for radial neuronal migration during cerebral cortex development and mutations in *Kif2a* cause malformations of cortical development (MCD) by affecting neuronal positioning in the cerebral cortex [2, 8, 88]. Therefore, I asked whether KIF2A's requirement in cortical neuronal migration is isoform-dependent. In order to assess this, I performed *in utero* electroporation which is a widely used protocol to investigate the neuronal migration process. Using this approach, I knocked down the expression of endogenous *Kif2a* by shKif2a electroporation and re-introduced one isoform at a time by electroporating *resKif2a* cDNAs into subpopulations of aRG cells in the VZ of the E14.5 embryonic mouse brain. Along with these constructs, I also electroporated a marker plasmid (pCAGGS_IRES_tdTomato) expressing tdTomato to observe transfected neurons. Transfected aRG cells undergo neurogenesis and newly formed neurons migrate radially to their destinations at the CP. At three days post-electroporation (E17.5), I quantified the number of tdTomato-positive neurons in different cortical layers by confocal microscopy **(Figure 2.23A and B)**. As expected, tdTomato-positive neurons migrated throughout the cortex in control samples (NS). Approximately 45% of tdTomato-positive neurons migrated into the CP, 50% were localized throughout the SVZ-IZ and 5% remained within the VZ **(Figure 2.23A)**. Consistent with previous observations [8, 88], in *Kif2a* knockdown neurons, there was a dramatic reduction in the relative fraction of tdTomato-positive neurons localized to the CP and most of the neurons were mainly clustered in SVZ-IZ **(Figure 2.23A)**. To understand the function of KIF2A AS in cortical neuronal migration, I performed rescue experiments using *resKif2a* constructs. I observed that, *Kif2a* silenced neurons expressing either *resKif2a.1* or *resKif2a.2* plasmids could exit the SVZ-IZ and reach to CP **(Figure 2.23C, D, F and G)**. On the other hand, *resKif2a.3* expressing neurons showed the similar phenotype of *Kif2a* silenced samples. Both conditions demonstrated severe

migration defect with significantly reduced number of migrating neurons into the CP **(Figure 2.23E and H)**. It is note-worthy to point out that, KIF2A.3 differs from the other two isoforms by 20 amino acids which are encoded by exon5. This stretch of 20 amino acids encode a disordered protein region as predicted by the IUPred2A prediction tool [124] **(Figure 2.24)**. Intriguingly, tissue specific alternative splicing of disordered protein regions is recognized as a means of increasing protein interaction networks in different tissues [125]. Taken together, my results demonstrate that KIF2A.1 and KIF2A.2 have a capacity to support neuronal migration in the developing cortex whereas the third isoform, KIF2A.3 does not.

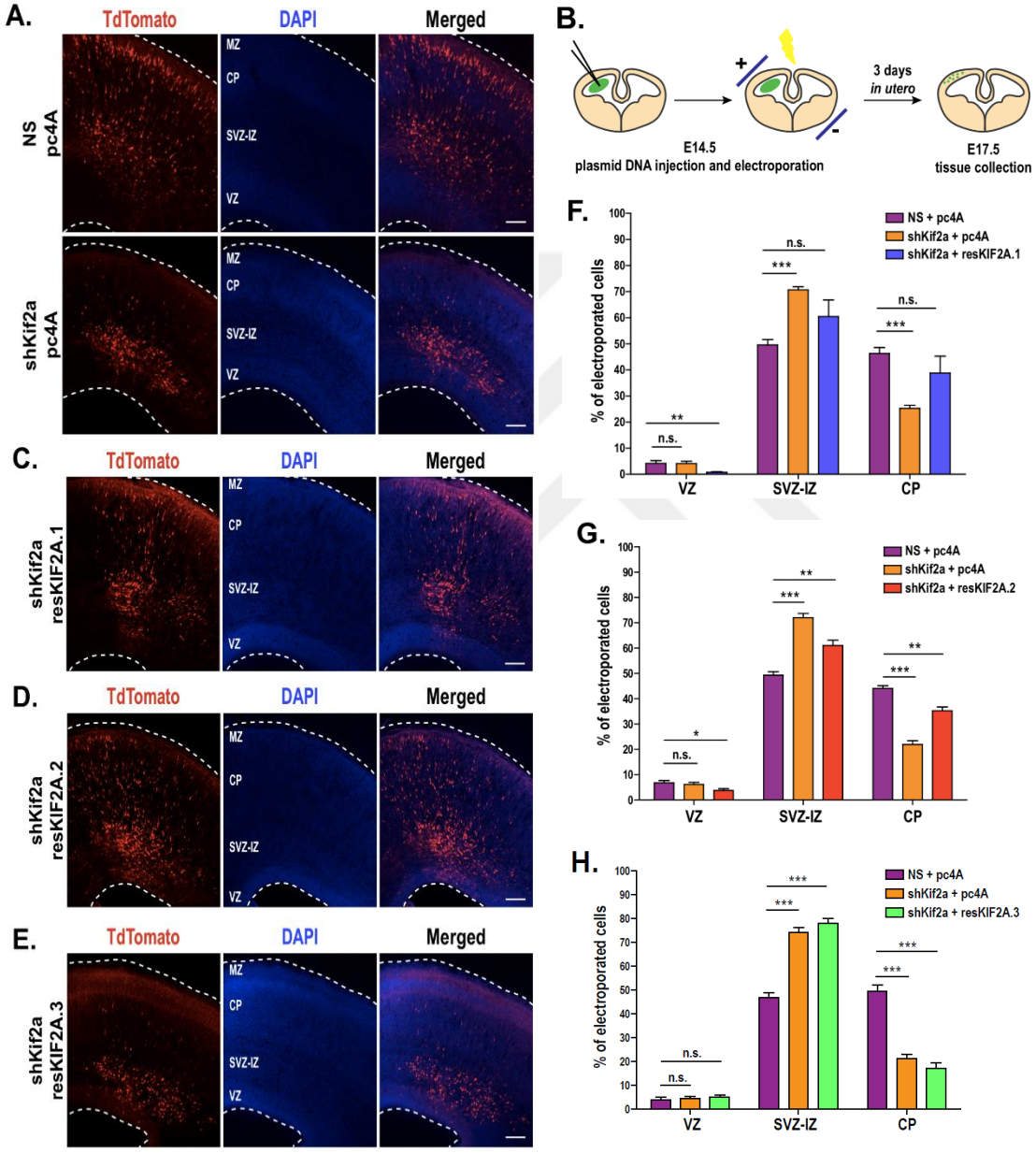
A.
TdTomato
DAPI
Merged
NS pc4A
shKif2a pc4A
MZ
CP
SVZ-IZ
VZ
B.
+
-
3 days in utero
E14.5
plasmid DNA injection and electroporation
E17.5
tissue collection
C.
shKif2a resKIF2A.1
D.
shKif2a resKIF2A.2
E.
shKif2a resKIF2A.3
F.
% of electroporated cells
NS + pc4A
shKif2a + pc4A
shKif2a + resKIF2A.1
n.s.
**
***
VZ
SVZ-IZ
CP
G.
shKif2a + resKIF2A.2
*
H.
shKif2a + resKIF2A.3

Figure 2. 23: Different KIF2A isoforms are not interchangeable for regulating the radial migration of cortical neurons.

A. DAPI staining of E17.5 coronal sections *in utero* electroporated with either mcherry-tagged NS or shKif2a along with pcDNA4A (pc4A) and tdTomato at E14.5. **B.** Schematic diagram of *in utero* electroporation. Lateral ventricle of cerebral cortex was injected with indicated plasmid DNA and embryos were electroporated at E14.5. Embryos were allowed to develop for 3 days *in utero*. Electroporated embryonic cortices were collected and the migration process was quantified at E17.5. **C., D. and E.** Embryos were electroporated with shKif2a along with one of the *resKif2a* (resKIF2A.1 **(C)**, resKIF2A.2 **(D)** or resKIF2A.3 **(E)**) and tdTomato at E14.5 and their brains were fixed at E17.5 followed by DAPI staining. Transfected cells were identified by their red color based on their co-expression of mcherry from the shRNA expressing plasmid and tdTomato signal. White dashed lines indicate boundaries of cortical sections. MZ, marginal zone; CP, cortical plate; SVZ-IZ, subventricular zone-intermediate zone; VZ, ventricular zone; NS, non-silencing, n.s. non-significant. **F., G. and H.** Quantification of *in utero* electroporation experiment of resKIF2A.1 **(F)**, resKIF2A.2 **(G)** and resKIF2A.3 **(H)**. Cortical sections were separated into zones and percentages of tdTomato-positive neurons at each neurons are counted and plotted. (For KIF2A.1 a total of n=4017 for NS, n=4572 for shKIF2A, n=2696 for resKIF2A.1 from 3 biological replicates; for KIF2A.2 a total of n=2477 for NS, n=3160 for shKIF2A, n=3558 for resKIF2A.2 from 2 biological replicates; for KIF2A.3 a total of n=3189 for NS, n=4456 for shKIF2A, n=3549 for resKIF2A.3 from 3 biological replicates). Data is represented as bar graphs. Lines represent S.E.M. Unpaired two-tailed *t* test, p value: *p<0.05, **p<0.005, ***p<0.0001. Scale bar in A, C, D and E, 100 μm.

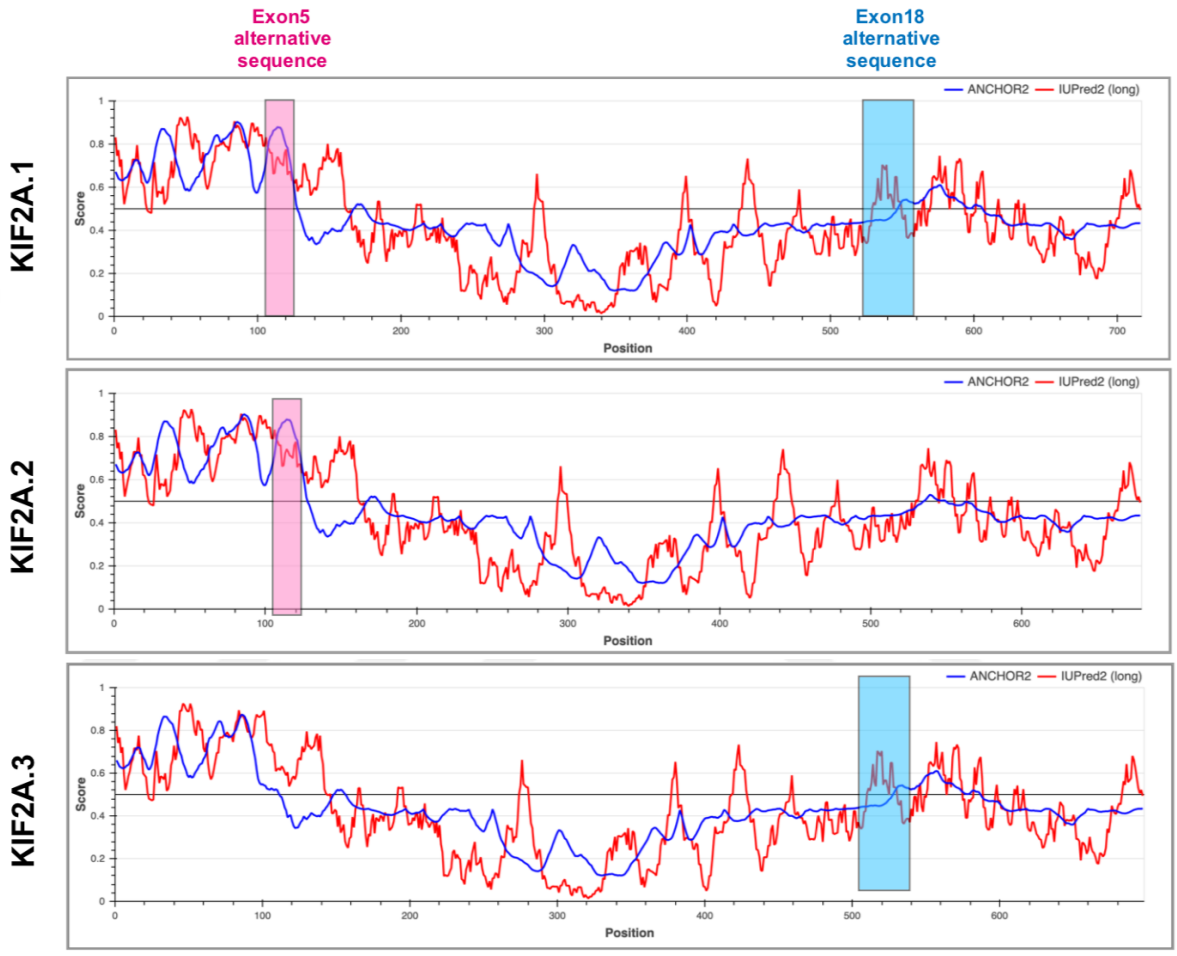

Figure 2. 24: Disorder protein segments of individual KIF2A isoforms were identified with IUPred2 and ANCHOR2 algorithms [124].

Alternative sequences are labeled in pink for exon5 and blue for exon18.

2.3.8 Proximity-labeling protein interactome analysis of alternatively spliced KIF2A isoforms uncover novel isoform-specific interactors

At the organismal level, AS generates increased proteomic and phenotypic complexity by expanding the interactome [125-127]. For that reason, I next asked whether different KIF2A isoforms indeed had divergent protein interaction networks. Toward this aim, I performed the BioID method which identifies proximal proteins by expressing promiscuous biotin-ligase (the *BirA** gene) fusion protein of interest in cells, followed by streptavidin based affinity purification and mass spectrometric characterization [128]. To use this technique, initially, I cloned *Kif2a* cDNAs (*Kif2a.1, Kif2a.2, Kif2a.3*) into pcDNA3.1 (-) mycBirA* (mycBirA*) by using a PCR based method. This vector allowed the expression of KIF2A as a mycBirA* fusion protein (KIF2A-BirA*). For BioID experiments, instead of neurons, I selected easily transfectable Neuro2A neuronal cell line in order to collect sufficient amounts of total biotinylated protein. Before starting the large-scale BioID approach, I confirmed the functionality of KIF2A-BirA* fusion proteins. For this purpose, I transiently transfect KIF2A-BirA* fusions for each of the three isoforms into Neuro2A cells and treated the cells with 0.05mM biotin and performed immunofluorescence. My immunofluorescence results showed a strong biotinylation only in KIF2A-BirA* transfected cells which confirmed the functionality of the KIF2A-BirA* fusion proteins **(Figure 2.25)**. Moreover, to confirm that biotinylation was dependent upon the external biotin treatment, I cultured transfected cells with or without supplemental biotin and then performed immunoblotting. I observed KIF2A-BirA* expression in all transfected cells independent from biotin treatment **(Figure 2.26, top panel)** and biotinylation of proteins only upon biotin supplementation (**Figure 2.26, middle panel)**. Next, to verify the streptavidin pull-down, I transfected Neuro2A cells with *Kif2a-BirA** constructs and treated them with or without supplemental biotin. Then I performed affinity purification of biotinylated proteins by

streptavidin pull-down **(Figure 2.27)**. I detected only endogenous biotinylation around 72-75 kDa and residual KIF2A-BirA* proteins in the absence of external biotin and this background signal was very low **(Figure 2.27, pull-down panel, - biotin lanes)**. With biotin treatment, I observed not only biotinylation of multiple proteins by all KIF2A-BirA* proteins **(Figure 2.27, + biotin lanes)**, but also enrichment of these biotinylated proteins which showed a successful streptavidin pulldown **(Figure 2.27, pull-down panel)**.

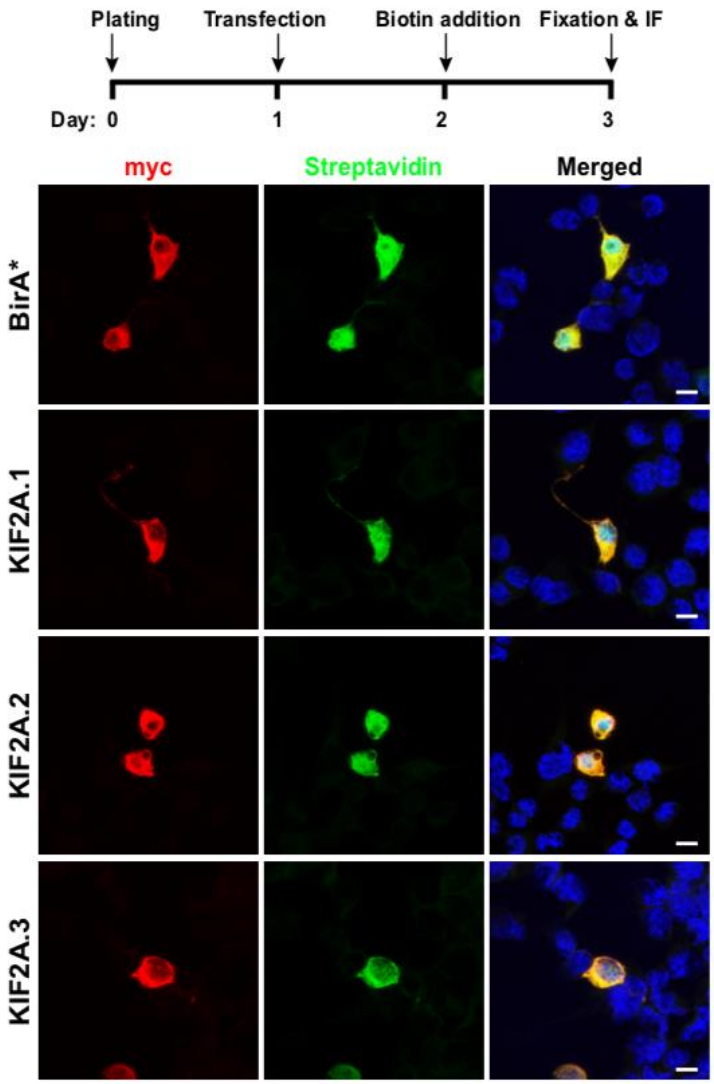

Figure 2. 25: Immunofluorescence staining confirms biotinylation of transfected cells. Neuro2A cells were transfected with myc*BirA**, myc*BirA*-Kif2a.1*, *mycBirA*-Kif2a.2* and *mycBirA*-Kif2a.3* separately and immunofluorescently stained with myc (red), Streptavidin (green) and DNA (blue). Myc immunostaining identifies transfected cells and streptavidin stains the biotinylated cells. Scale bar, 10 µm.

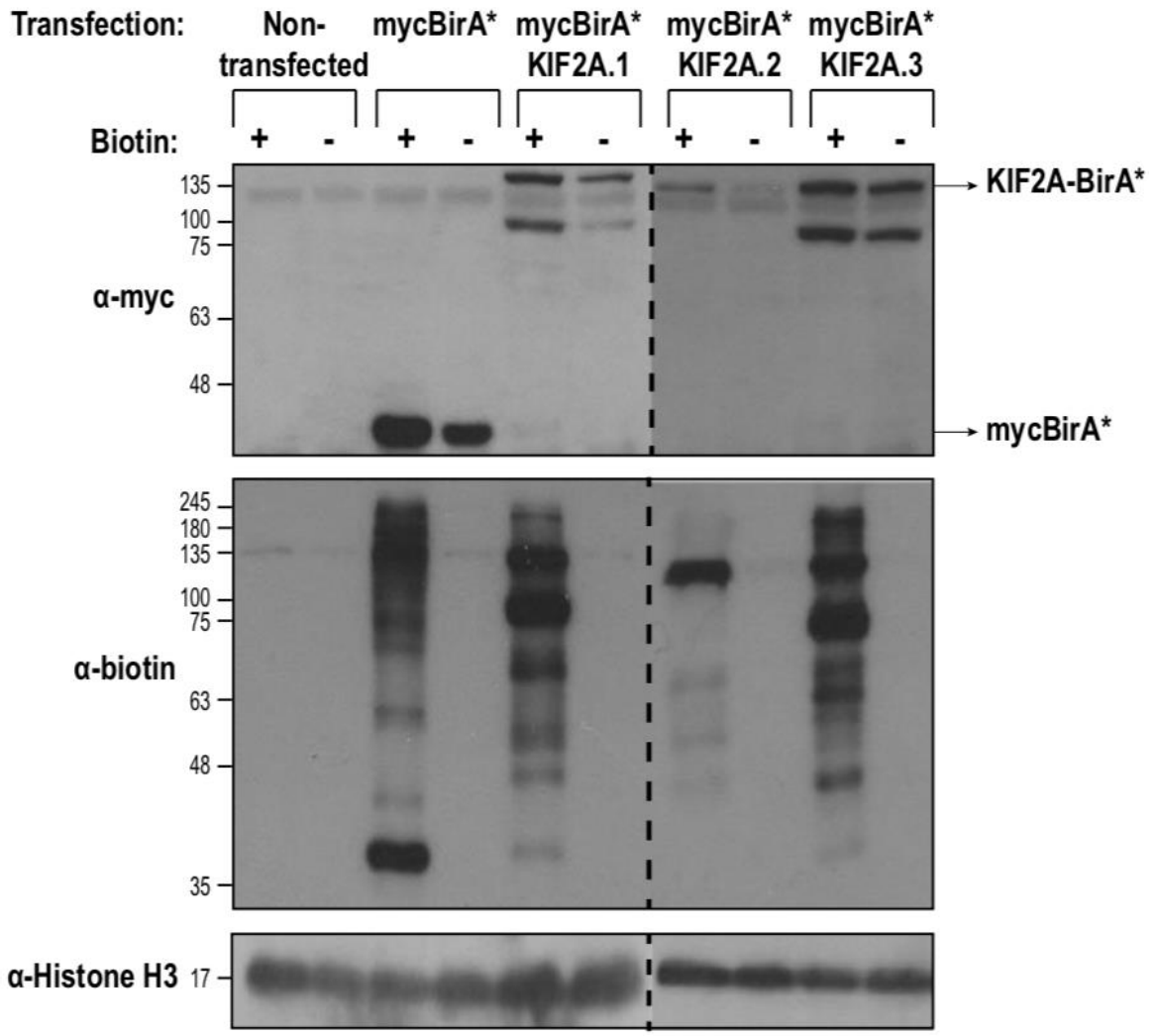

Figure 2. 26: Immunoblotting confirms that external biotin supplementation caused protein biotinylation only in BirA* expressing Neuro2A cells.

Top panel: Immunoblotting with anti-myc shows expression of mycBirA*-KIF2A isoforms. **Middle panel:** Immunoblotting with anti-biotin confirms biotinylation upon treatment with external biotin. **Bottom panel:** Anti-Histone H3 is used as a loading control. Non-transfected, (-) biotin and *mycBirA** transfected lanes are negative controls.

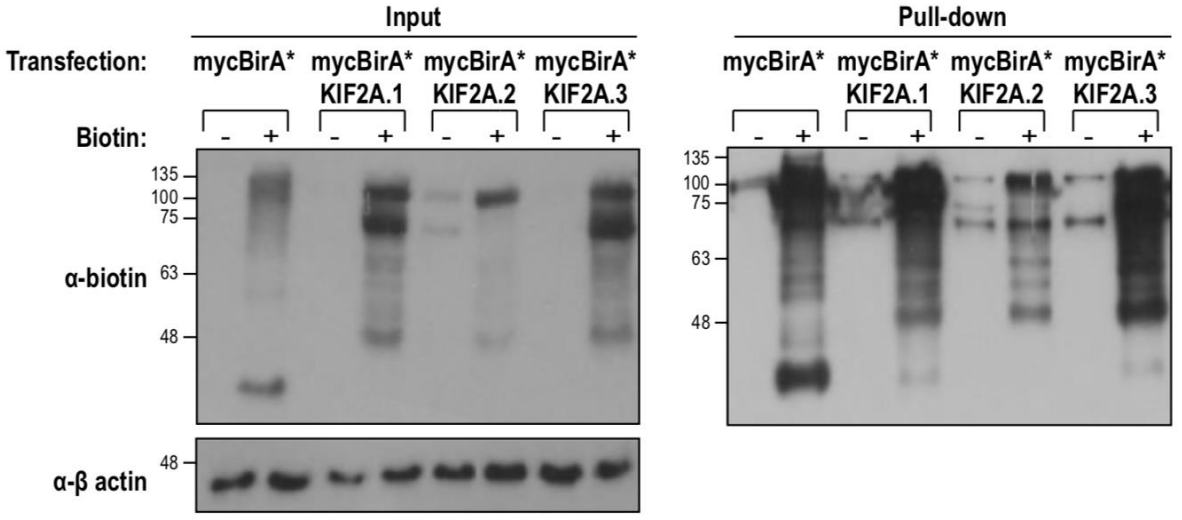

Figure 2. 27: Immunoblotting with anti-biotin antibody validates the pull-down of biotinylated proteins with streptavidin.

Input blot (left panel) shows the biotinylation of proteins after treatment with supplemental biotin and pull-down blot (right panel) indicates that biotinylated proteins were enriched and eluted successfully with streptavidin beads. Anti-β-actin is used as a loading control.

After validating the BioID approach, I applied large scale BioID protocol and proteins were eluted by Stage Tip protocol using C18 columns for analysis in Thermo Scientific Q-Exactive LC-MS/MS mass spectrometer. I used non-transfected Neuro2A cells as a control for background subtraction and for each isoform I performed the experiment as three biological replicates. For the analysis, based on their PSM (peptide spectra match) values, I filtered out proteins found in less than two replicates, those with FDR<0.05 and then those with fold-change<1.5 and created a final list **(Appendix A)**. In the final list, as expected, KIF2A was among the top hits with 90, 96 and 193 PSM values for KIF2A.1, KIF2A.2 and KIF2A.3, respectively. Following these cut-off criteria, I identified a total of 63 potential interactors for KIF2A.1, 37 for KIF2A.2, and 40 for KIF2A.3 **(Figure 2.28A and Appendix A)**. I generated both a heat-map **(Figure 2.28B)** and an interactome map **(Figure 2.29)** using Cytoscape version 3.6.1. Moreover, I identified isoform-specific interactors, as well as proteins that were common in all three KIF2A isoforms, shared in all possible pairwise combinations **(Figure 2.28, Figure 2.29 and Appendix A)**.

Next I used the String Database to perform gene ontology and interactome analysis with candidate interactors of each KIF2A isoforms [109-111, 129] **(Figure 2.30A, B and C)**. KIF2A is a MT depolymerizer and it is localized to spindle poles in mitotic cells [26, 81, 85]. Since Neuro2A cells are mitotic, as expected, all three isoforms were proximal to MT-associated proteins that function at the spindle poles during mitosis (eg. NUMA1, MAP4, CKAP5 and CEP170). Interestingly, I identified several eukaryotic translation factors as interactors of all three KIF2A isoforms (EEF1B2, EIF3E, EIF4G2 and EIF5) **(Figure 2.28, Figure 2.29 and Figure 2.30A, B and C)**. As mentioned above KIF2A.1 had the highest number of interactors. Interestingly, these interactors were enriched for nuclear RNA regulation (eg. HNRNPA1, SRRM2, SRSF3 and SRSF4), mitochondrial proteins which have roles in mitochondrial metabolism (eg. OAT, SUCLG2, SUCLA4, GLS and ALDH2) and

gene expression (PNPR1, TSFM, TIMM44, RARS2 and LARS2) **(Figure 2.28, Figure 2.29 and Figure 2.30A)**. For KIF2A.2, I identified the least number of interactors, many of which were common with interactors of KIF2A.1 and with similar functions in nuclear RNA transport and mitochondrial metabolism **(Figure 2.28, Figure 2.29 and Figure 2.30B)**. Finally, for KIF2A.3, I identified the highest relative fraction of unique interactors which were functioning in nuclear RNA transport and control. Intriguingly, KIF2A.3 was largely devoid of genes which function in the mitochondria **(Figure 2.28, Figure 2.29 and Figure 2.30C)**. Together, my data identifies both common and unique protein interactors of all three KIF2A isoforms.

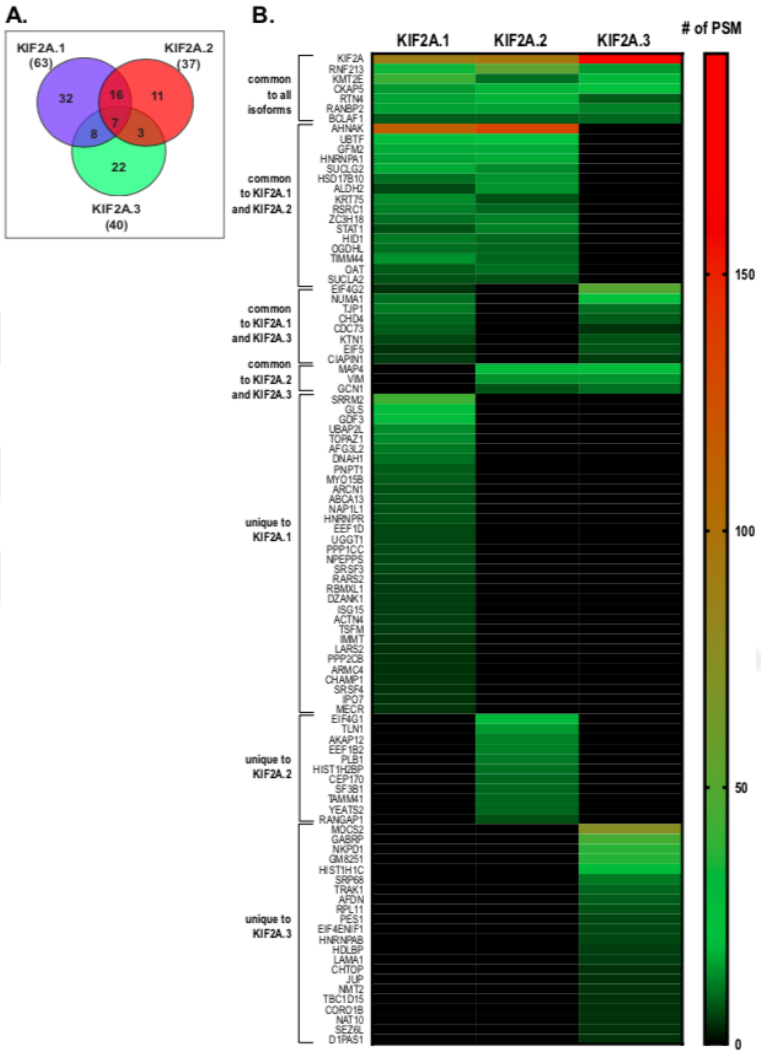

Figure 2. 28: Protein interaction partners of KIF2A isoforms are identified by a proximity-labeling method.

A. *Venn* diagram representing the number of unique and common proximal protein interactors of KIF2A isoforms. n=3 biological x 2 technical replicates. **B.** Heat map created using PSM values of proteins that were identified with BioID protocol for three KIF2A isoforms.

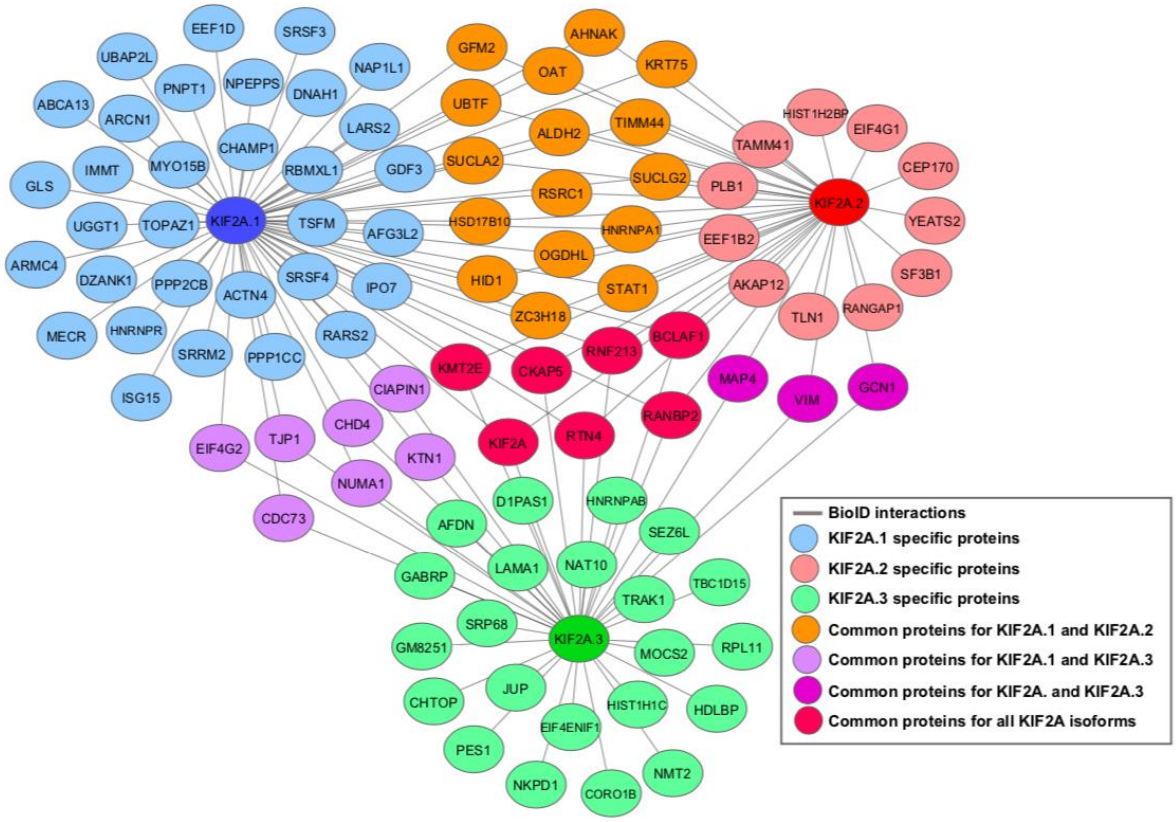

Figure 2. 29: Interactome map reveals the unique and common interactors of all KIF2A isoforms.

Comparison of three KIF2A isoforms (KIF2A.1, KIF2A.2 and KIF2A.3) proximity interactomes by creating an interactome map using Cytoscape 3.6.1 StringApp [109].

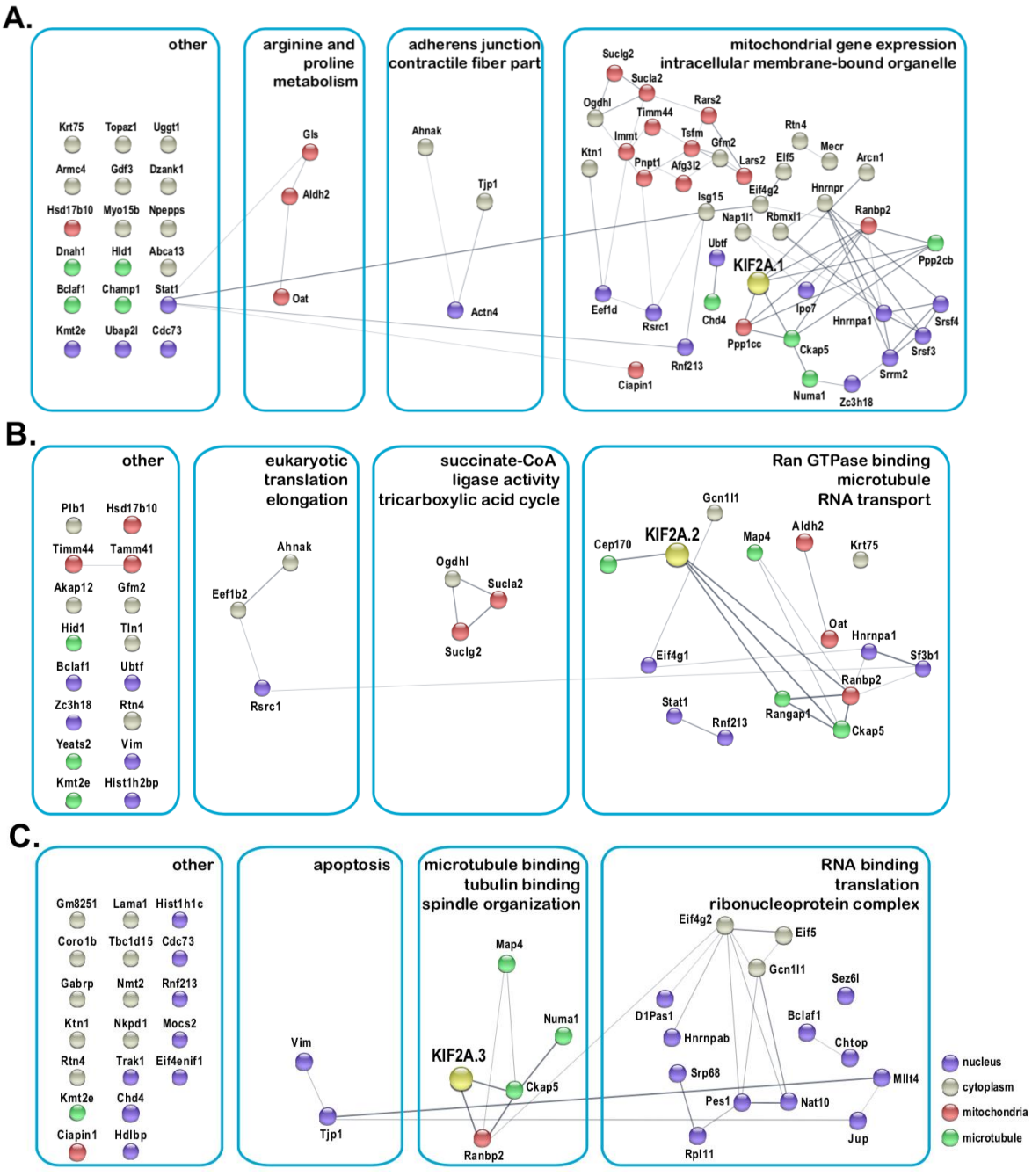
A.
other
Krt75
Topaz1
Uggt1
Armc4
Gdf3
Dzank1
Hsd17b10
Myo15b
Npepps
Dnah1
Hid1
Abca13
Bclaf1
Champ1
Stat1
Kmt2e
Ubap2l
Cdc73
arginine and proline metabolism
Gls
Aldh2
Oat
adherens junction contractile fiber part
Ahnak
Tjp1
Actn4
mitochondrial gene expression intracellular membrane-bound organelle
Suclg2
Sucla2
Ogdhl
Rars2
Timm44
Immt
Tsfm
Gfm2
Rtn4
Mecr
Ktn1
Pnpt1
Afg3l2
Lars2
Elf5
Arcn1
Eif4g2
Hnrnpr
Isg15
Nap1l1
Rbmxl1
Ranbp2
Ubtf
KIF2A.1
Ppp2cb
Eef1d
Rsrc1
Chd4
Ipo7
Hnrnpa1
Srsf4
Ppp1cc
Ckap5
Srsf3
Rnf213
Srrm2
Ciapin1
Numa1
Zc3h18
B.
other
Plb1
Hsd17b10
Timm44
Tamm41
Akap12
Gfm2
Hid1
Tln1
Bclaf1
Ubtf
Zc3h18
Rtn4
Yeats2
Vim
Kmt2e
Hist1h2bp
eukaryotic translation elongation
Ahnak
Eef1b2
Rsrc1
succinate-CoA ligase activity tricarboxylic acid cycle
Ogdhl
Sucla2
Suclg2
Ran GTPase binding microtubule RNA transport
Gcn1l1
KIF2A.2
Cep170
Map4
Aldh2
Krt75
Oat
Hnrnpa1
Sf3b1
Eif4g1
Ranbp2
Stat1
Rangap1
Rnf213
Ckap5
C.
other
Gm8251
Lama1
Hist1h1c
Coro1b
Tbc1d15
Cdc73
Gabrp
Nmt2
Rnf213
Ktn1
Nkpd1
Mocs2
Rtn4
Trak1
Eif4enif1
Kmt2e
Chd4
Ciapin1
Hdlbp
apoptosis
Vim
Tjp1
microtubule binding tubulin binding spindle organization
Map4
Numa1
KIF2A.3
Ckap5
Ranbp2
RNA binding translation ribonucleoprotein complex
Eif4g2
Eif5
Gcn1l1
Sez6l
D1Pas1
Bclaf1
Hnrnpab
Chtop
Srp68
Mllt4
Pes1
Nat10
Jup
Rpl11
nucleus
cytoplasm
mitochondria
microtubule

Figure 2. 30: Gene ontology and interactome analysis for each of the KIF2A isoforms are constructed.

A., B. and C. Interaction networks are created based upon the significant enrichment of proteins for KIF2A.1 **(A)**, KIF2A.2 **(B)** and KIF2A.3 **(C)** by STRING database [129]. Highly interconnected subnetworks are framed with blue rectangles and each network is grouped using enriched GO and KEGG terms [110, 111]. Yellow circles represent KIF2A isoforms. Proteins are colored according to their localization in the cell; gray: cytoplasm, blue: nucleus, green: microtubule, and red: mitochondria. Known interactions from STRING database are represented with gray lines and the increase in interaction confidence is indicated with an increase in thickness.

Next I focused on one of the interacting proteins, and chose Reticulon-4 (RTN4 or also known as NOGO) protein which I identified in all three KIF2A isoforms. I decided to investigate its interaction with endogenous KIF2A. RTN4 localizes both to the plasma membrane and to the ER membrane. It has been demonstrated that RTN4 controls structural stabilization of the ER network and also vesicular transport in the ER [130]. In the nervous system, RTN4 has been identified as an inhibitor of neurite outgrowth and is expressed mainly by neurons during neural development. It inhibits migration and sprouting of endothelial cells and axons in central nervous system (CNS) by supplying inhibitory signals [131-133]. To test whether endogenous RTN4 and KIF2A co-localize, I performed immunofluorescence in Neuro2A cells and quantified these immunofluorescence images by calculating the Manders' Coefficient, using JACoP plugin of ImageJ. Manders' Coefficient measures the fraction of total RTN4 fluorescence that overlaps with the fluorescence of KIF2A [115-117]. My immunofluorescence images showed that RTN4 had a cytoplasmic localization, whereas KIF2A localized to both the nucleus and the cytoplasm **(Figure 2.31A)**. Moreover, my quantification analysis revealed a partial co-localization

between endogenous RTN4 and KIF2A **(Figure 2.31B)**. Next I addressed whether there is an interaction between KIF2A and RTN4 using a different method. To answer this I performed proximity ligation assay (PLA) which is an alternative method to co-immunoprecipitation (CoIP) experiments to detect and quantify transient protein interaction in intact cells with spatial resolution by immunofluorescence [118]. My PLA results revealed a strong interaction between KIF2A and RTN4 compared with negative controls incubated with only either with anti-KIF2A or anti-RTN4 primary antibodies **(Figure 2.32A and B)**.

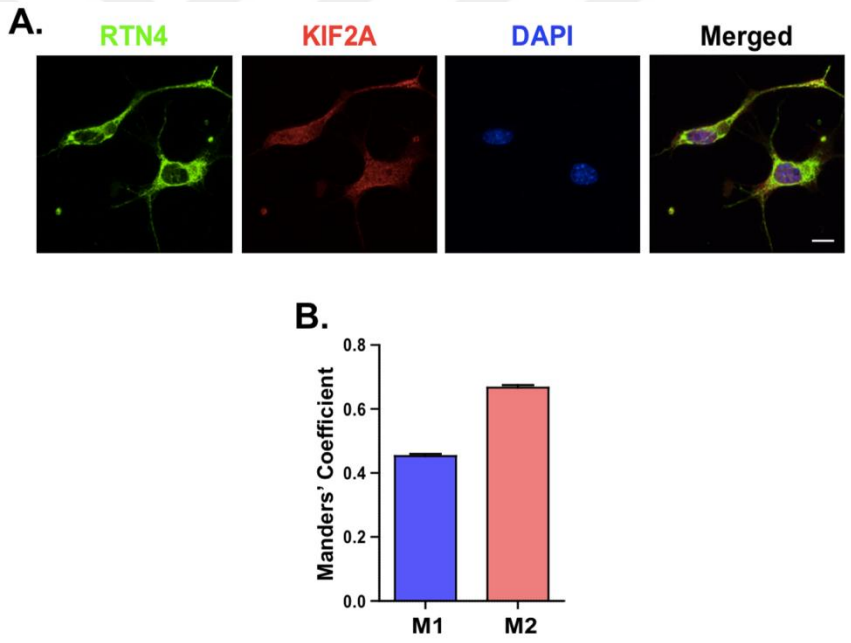

Figure 2. 31: KIF2A and RTN4 are partially co-localized in Neuro2A cells.

A. Neuro2A cells immunofluorescently stained with anti-RTN4 (green), anti-KIF2A (red), DNA (blue). Scale bar, 10µm. **B.** Manders' coefficient was calculated to quantify the co-localization of KIF2A with RTN4A [134-136]. M1: Fraction of KIF2A fluorescence overlapped with RTN4 fluorescence. M2: Fraction of RNT4 fluorescence overlapped with KIF2A fluorescence. n=219, data is represented as bar graphs. Bars represent S.E.M.

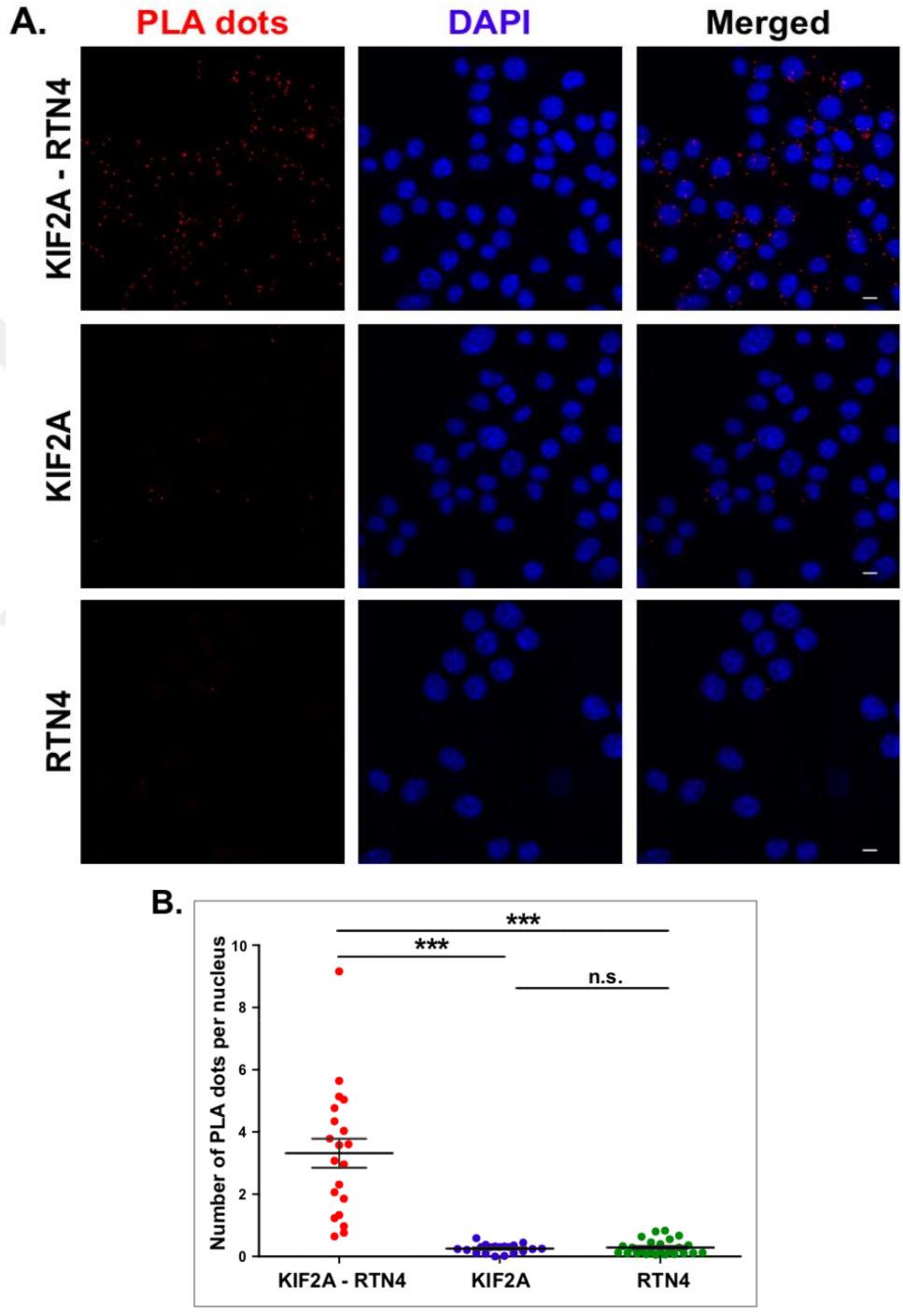
A.
PLA dots
DAPI
Merged
KIF2A - RTN4
KIF2A
RTN4
B.
Number of PLA dots per nucleus
0
2
4
6
8
10
***
***
n.s.
KIF2A - RTN4
KIF2A
RTN4

Figure 2. 32: KIF2A interacts with RTN4 (NOGO) in a spatial resolution in Neuro2A cells.

A. Neuro2A cells were fixed with 3.2% PFA and PLA dots (red), DNA (blue) were immunofluorescently stained. Scale bar, 10 μm. **B.** Spatial analysis of KIF2A-RTN4 interaction by quantification of PLA dots per nucleus. 20 image frames (n=25 frames for RTN4) chosen randomly. Fixed cells were incubated KIF2A-RTN4 antibody pairs (n=1052) for interaction analysis. Fixed cells incubated with only KIF2A (n=684) or only RTN4 (n=373) were used as control. Lines indicate the mean number of PLA dots per nucleus. Bars represent S.E.M. p value: ***p<0.0001 by one-way ANOVA with Bonferroni post hoc test.

2.3.9 KIF2A disease mutations co-localize only with MTs in Neuro2A cells

After uncovering the protein interaction network of KIF2A isoforms, I next decided to focus on KIF2A (KIF2A^{S317N} and KIF2A^{H321D}) mutations that cause developmental cortical malformations in humans [2, 8]. Initially, I cloned disease-associated point mutant *Kif2a* in the backbone of mouse *pEGFPC1_Kif2a.1* cDNA with site directed mutagenesis [103]. Next, to determine the subcellular localization of KIF2A^{S317N} and KIF2A^{H321D} mutants in both E18.5 primary cortical neurons and Neuro2A cells, I expressed EGFP-KIF2A^{S317N} and EGFP-KIF2A^{H321D} and performed immunofluorescence. Consistent with previous observations [2, 8], instead of being diffusely localized to the nucleus and cytoplasm as observed for KIF2A.1, both KIF2A^{S317N} and KIF2A^{H321D} mutants appeared to be sequestered to MTs in both primary cortical neurons [103] and Neuro2A cells **(Figure 2.33)**. Thus, my result suggested that disease-causing dominant negative mutations in *Kif2a* create an abnormal localization.

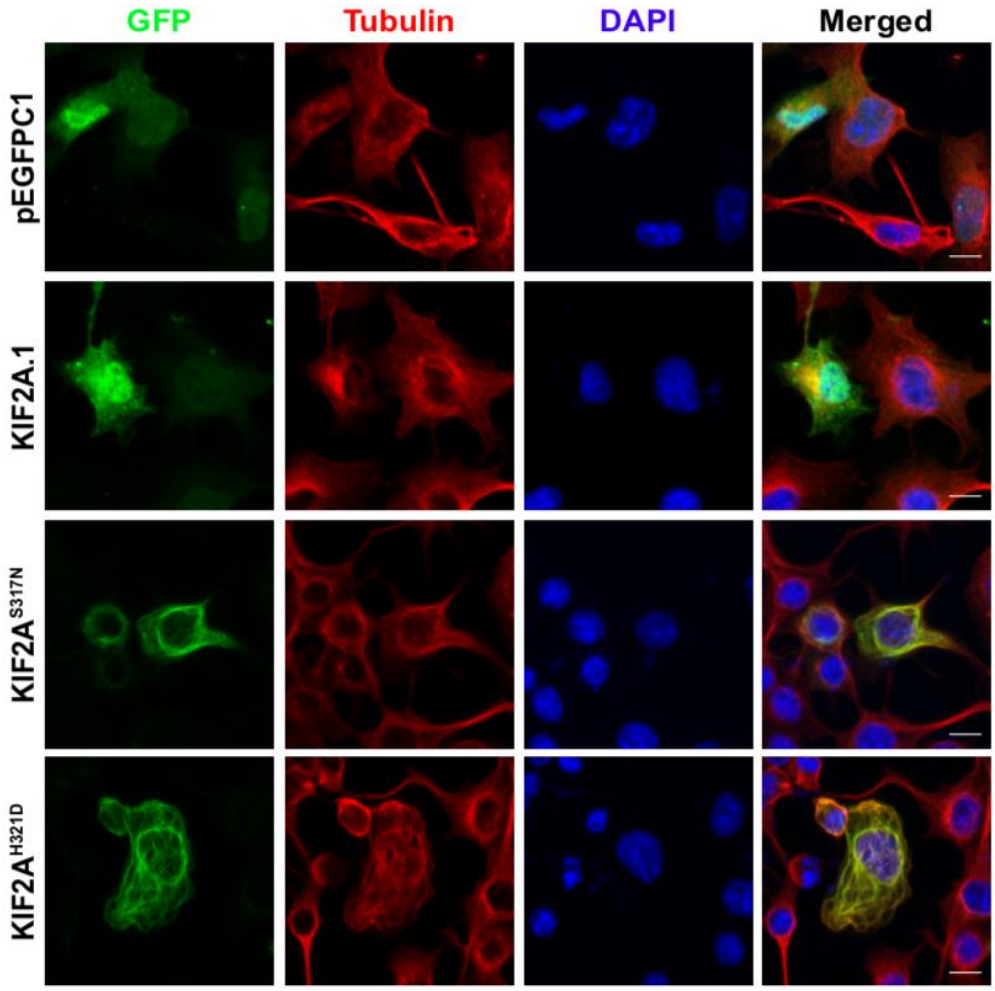

Figure 2. 33: *Kif2a* disease mutants co-localize predominantly to microtubules in Neuro2A cells.

Neuro2A cells were transfected with plasmids expressing pEGFPC1-tagged KIF2A.1, KIF2A^{S317N} or KIF2A^{H321D} 2 days after plating, fixed with 4% PFA 4 days after plating and immunostained with anti-GFP (green) to visualize transfected pEGFPC1-tagged KIF2A mutants. MTs were visualized with anti-αTubulin antibody (red) and DNA was stained with DAPI (blue) staining. Scale bar 10 μm.

2.3.10 KIF2A disease mutations have no effect on dendrite branching in mice cortical neurons

After confirming localization of KIF2A^{S317N} and KIF2A^{H321D}, I next focused on whether these dominant negative mutations affect dendrite development in cortical neurons. For this purpose, I co-transfected E14.5 primary cortical neurons with pEGFPC1 along with either one of the *Kif2a* mutants (*Kif2a*^{S317N} or *Kif2a*^{H321D}) at 2 DIV and carried out Sholl analysis after fixing them at 4 DIV. I observed that dendritic arbor development were comparable between control cultures and cultures expressing either one of the mutant KIF2A protein. Using *Kif2a* mutant plasmids in pEGFPC1 expressed neurons demonstrated that the number of dendritic intersections were similar to that of controls **(Figure 2.34A and B)**. Unexpectedly, these data suggested that disease-causing dominant negative mutations in *Kif2a* do not affect dendrite branching in primary cortical neurons.

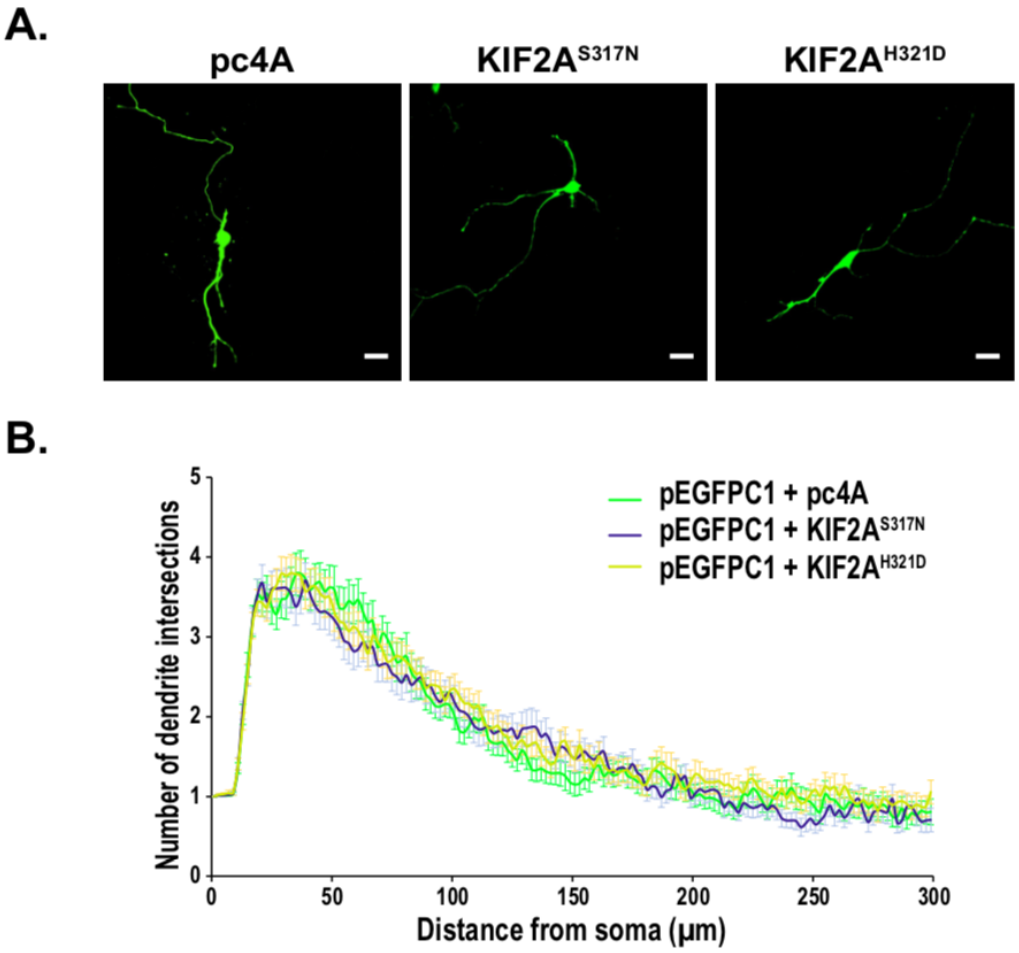

Figure 2. 34: KIF2A disease mutants do not affect dendrite development.

A. Representative images of E14.5 primary cortical neurons that were co-transfected with pEGFPC1 along with *Kif2a* mutants at 2 DIV, fixed with 4% PFA at 4 DIV and captured with confocal microscopy for Sholl analysis. Scale bar, 10 µm. **B.** Dendrite arborization was quantified by Sholl analysis [113, 114]. n=70 for each condition derived from three separate neuronal cultures. Unpaired *t* test determined the p value. *p<0.05.

2.3.11 KIF2A disease mutation resulted in protein interactome rewiring

After demonstrating altered subcellular localization of disease-causing KIF2A mutants in neurons, I next decided to identify the protein interaction partners of one of the KIF2A mutants harboring an identical mutation found in human patients ($KIF2A^{H321D}$) using the previously explained BioID method. I cloned *Kif2a*^{H321D} cDNA into mycBirA* vector with a PCR based method. Then I performed validation experiment similar to those done with the KIF2A isoforms. I compared my results with that of KIF2A.1 since the mutation was created within this isoform backbone **(Figure 2.35, Figure2.36 and Figure 2.37)**.

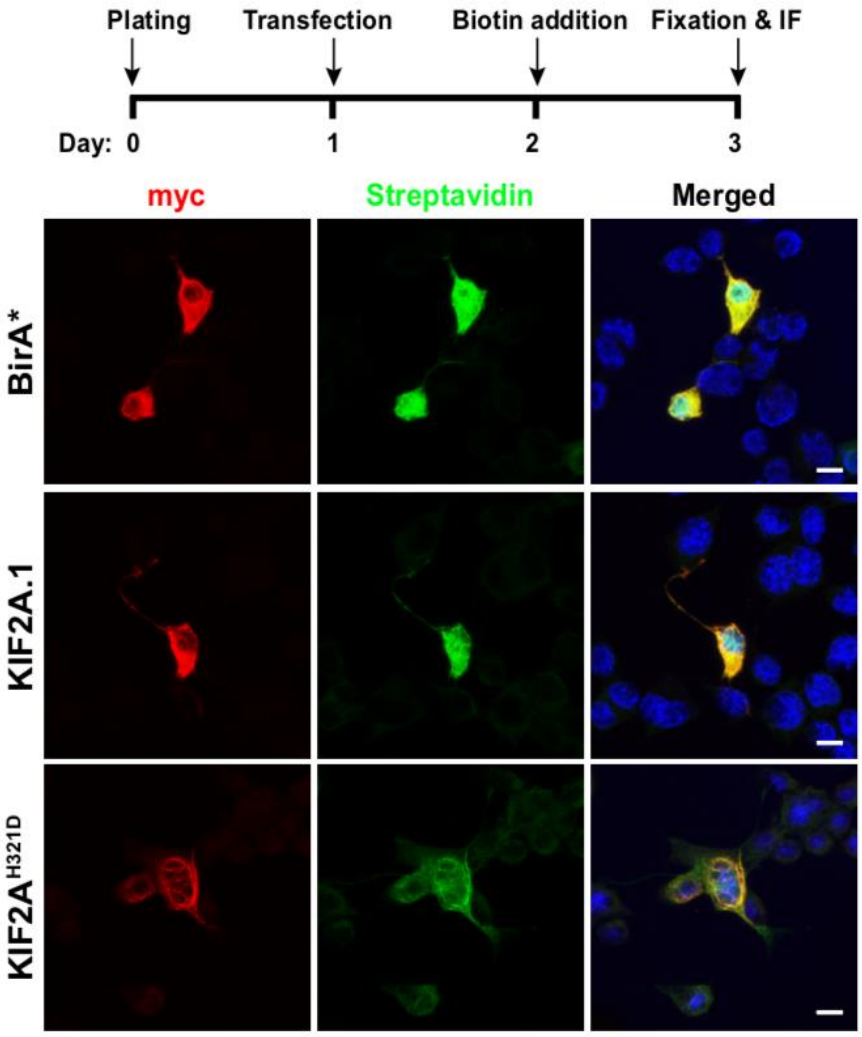

Figure 2. 35: Immunofluorescence staining confirms the biotinylation of the transfected cells.

Immunofluorescence staining of myc (red), Streptavidin (green) and DNA (blue) in Neuro2A cells that were transfected with myc*BirA**, myc*BirA*-Kif2a.1* and *mycBirA*-Kif2a*^{H321D} separately. Myc immunostaining identifies transfected cells and streptavidin stains the biotinylated cells. Scale bar, 10 μm.

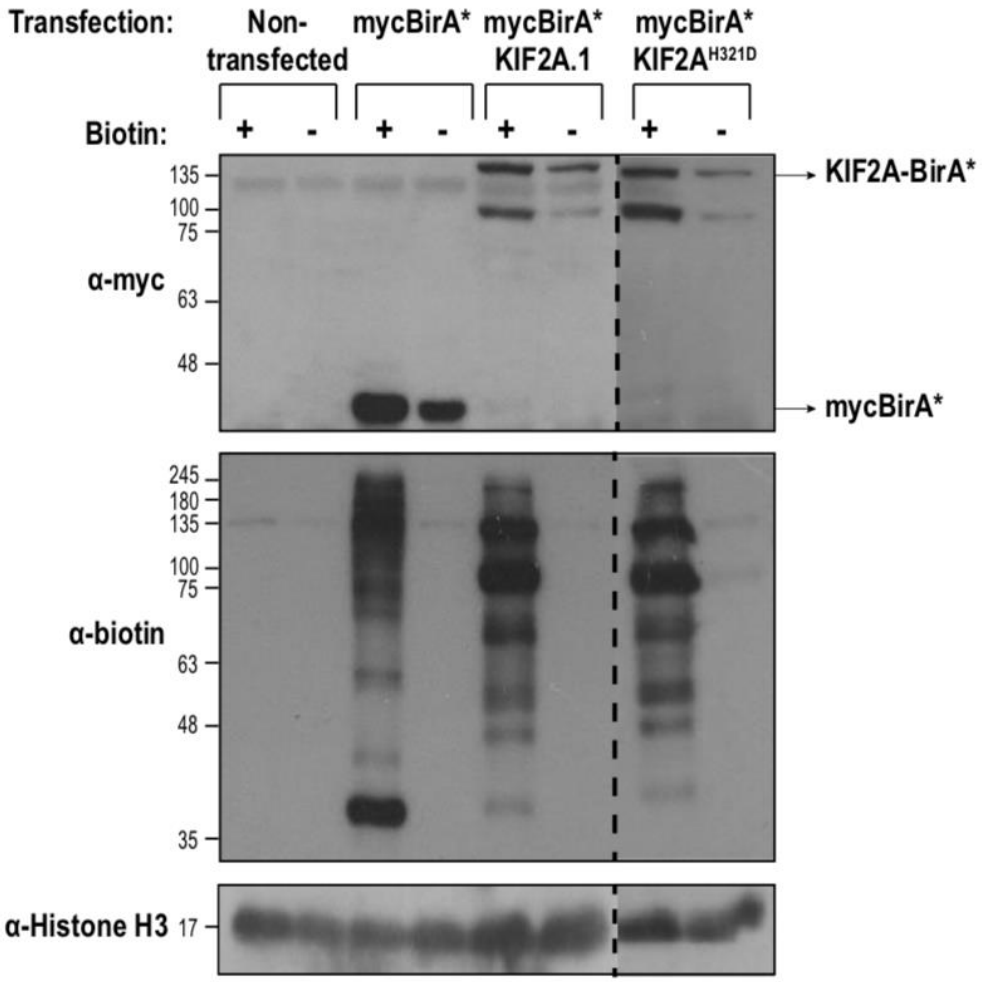

Figure 2. 36: Immunoblotting confirms only external biotin addition biotinylated the transfected Neuro2A cells.

Top panel: Immunoblotting with anti-myc shows expression of mycBirA*-KIF2A.1 and mycBirA*-KIF2A^{H321D}. **Middle panel: :** Immunoblotting with anti-biotin confirms biotinylation upon treatment with external biotin. **Bottom panel:** Anti-Histone H3 is used as a loading control. Non-transfected, (-) biotin and *mycBirA** transfected lanes are negative controls.

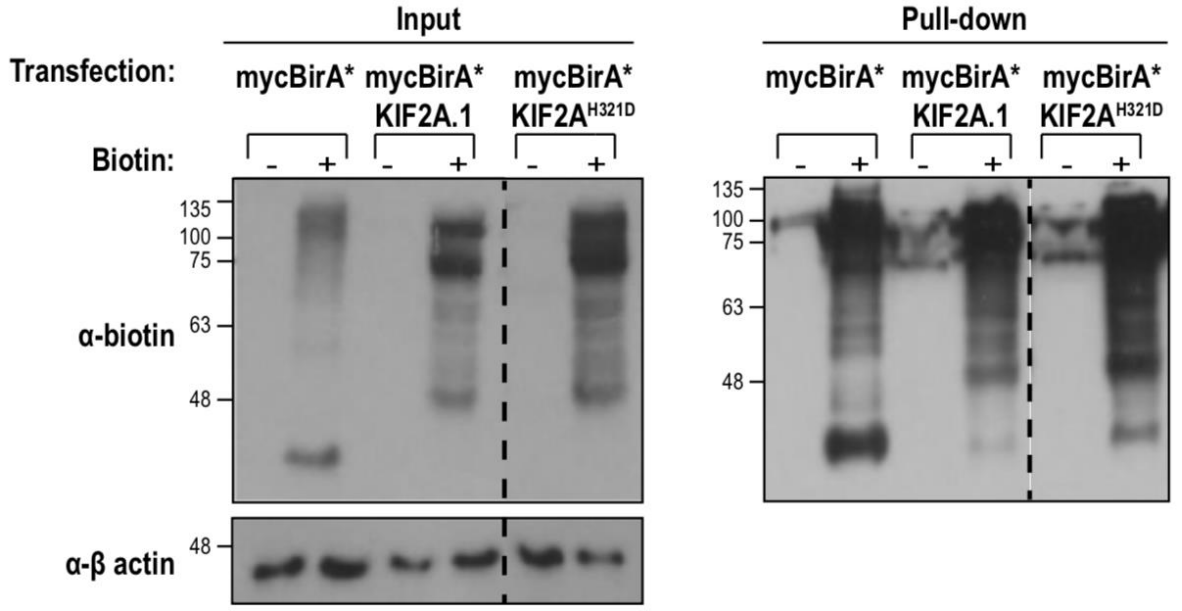

Figure 2. 37: Immunoblotting with anti-biotin antibody validates the pull-down of biotinylated proteins with streptavidin.

Input blot (left) shows the biotinylation of proteins after treatment with supplemental biotin and pull-down blot (right) indicates only biotinylated proteins were enriched and eluted with streptavidin beads. Anti-β-actin is used as a loading control.

After validation, I carried out large-scale BioID experiments by applying the same analyses I performed with the isoforms and I created a final list **(Appendix A)**. As expected, KIF2A was again among the top hits with 90 and 306 PSM values for KIF2A.1 and KIF2A^{H321D}, respectively. My comparison showed widespread rewiring of the interactome upon introducing H321D mutation. I identified 52 potential interactors that were unique for KIF2A.1, 31 unique to KIF2A^{H321D} and 11 potential interactors that were common to both **(Figure 2.38A and Appendix A)**. I generated both heat-map **(Figure 2.38B)** and interactome map **(Figure 2.39)** with Cytoscape version 3.6.1.

Next, I generated a gene ontology and interactome map for both KIF2A.1 and KIF2A^{H321D} with the String database [109-111, 129]. Even though the relative fraction of nuclear, cytoplasmic and MT-associated genes were conserved, the identities showed a differences in KIF2A^{H321D} **(Figure 2.40A and B)**. The most remarkable observation was depletion of mitochondrial protein from KIF2A^{H321D} interactome when compared to KIF2A.1. I identified a total number of 63 proteins for KIF2A.1, and among them, 16 proteins were mitochondrial. On the other hand, I identified a total number of 42 proteins for KIF2A^{H321D} and only 1 of them was a mitochondrial protein (CIAPIN1). Based on my analyses, I concluded that mutation on *Kif2a* results a change in protein interaction network.

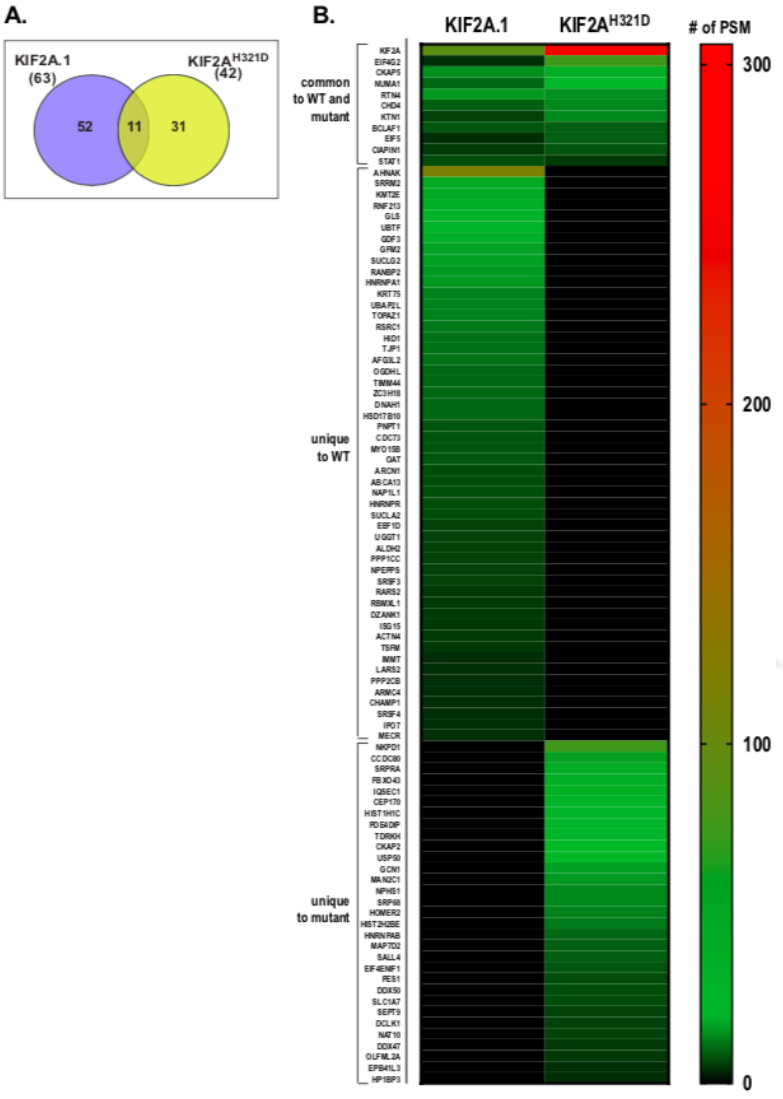

Figure 2. 38: Protein interaction partners of KIF2A^{H321D} are identified by a proximity-labeling method.

A. *Venn* diagram representing the number of common and unique proximal protein partners of KIF2A^{H321D}. n=3 biological x 2 technical replicates. **B.** Heat map created using PSM values of proteins that were identified with BioID method for KIF2A^{H321D}.

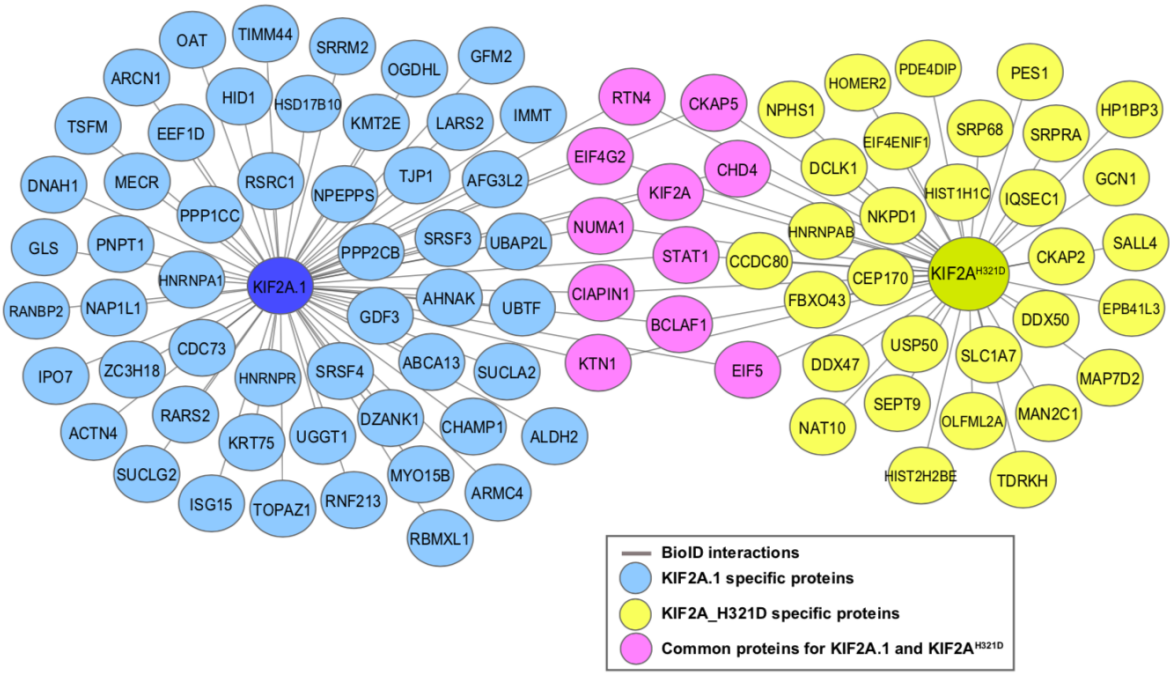

Figure 2. 39: Interactome map reveals the unique and common interactors of all KIF2A.1 and KIF2A^{H321D}.

Comparison of KIF2A.1 and KIF2A^{H321D} proximity interactomes by creating an interactome map using Cytoscape 3.6.1 StringApp [109].

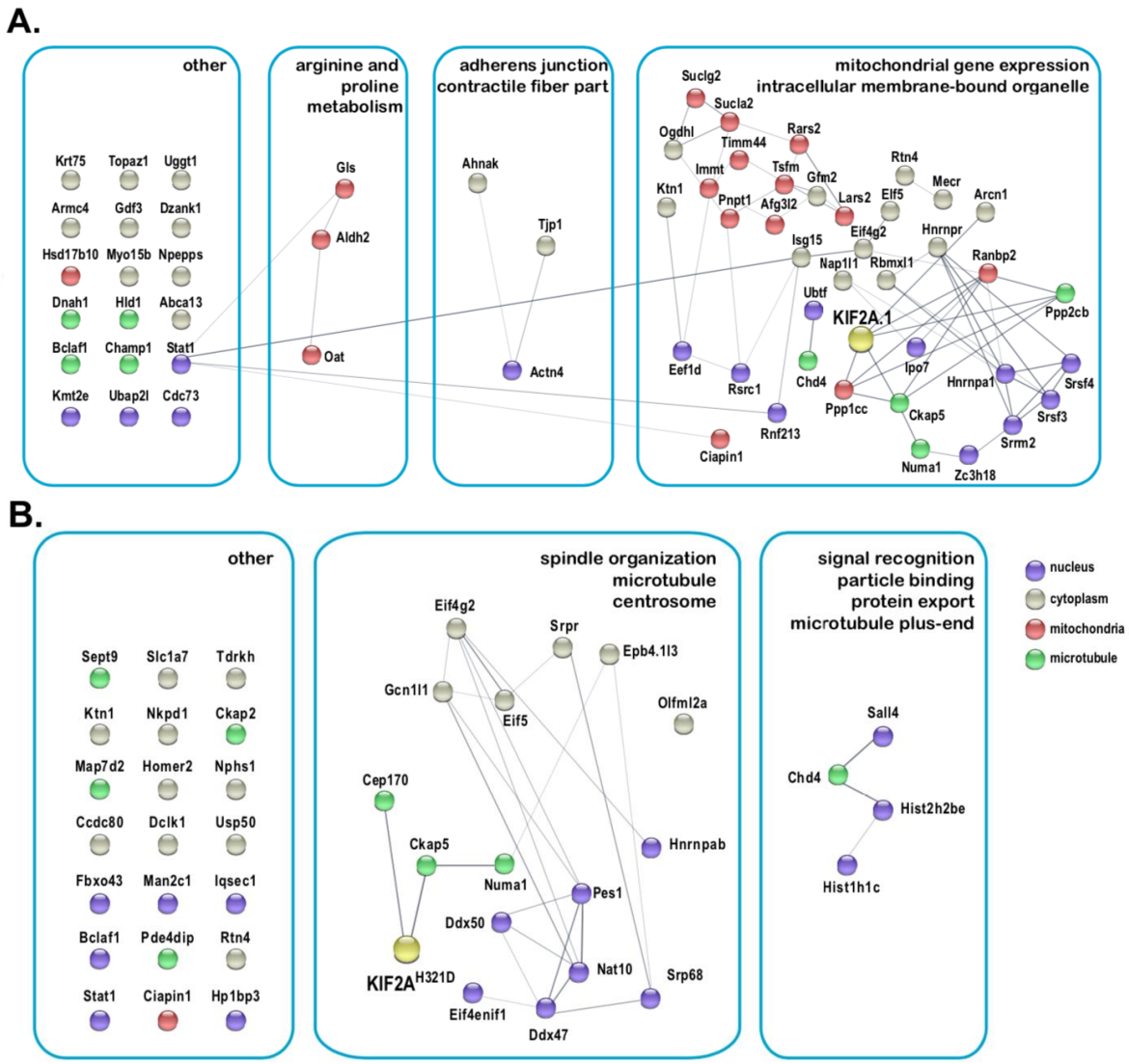

Figure 2. 40: Gene ontology and interactome analysis with interactors of KIF2A.1 and KIF2A^{H321D} are constructed.

A. and B. Interaction networks are created based upon the significant enrichment of proteins for KIF2A.1 **(A)** and KIF2A^{H321D} **(B)** by STRING database [129]. Highly interconnected

subnetworks are framed with blue rectangles and each network is grouped using enriched GO and KEGG terms [110, 111]. The ones with more than one annotated location are only illustrated with one compartment. Yellow circles indicate the KIF2A.1 and KIF2A^{H321D}. Proteins are colored according to their localization in the cell; gray: cytoplasm, blue: nucleus, green: microtubule, and red: mitochondria. Known interactions from STRING database are represented with gray lines and the increase in interaction confidence is indicated with an increase in thickness.

2.4 DISCUSSION

In this study, I investigated the role of developmentally regulated KIF2A isoforms in neuronal differentiation and radial neuronal migration in mice. In mice, *Kif2a* gene consists of 20 coding exons and it undergoes alternative splicing, a process regulated by nELAVL RNABP [31]. KIF2A is a MT depolymerizer with known roles in primary cilium formation [8, 27, 28, 88], mitosis, axon collateral branch elongation [30, 67], and radial neuronal migration during cerebral cortex development [8, 67, 102]. I demonstrated that *Kif2a* isoform expression is developmentally regulated in mouse cerebral cortex. I showed that AS splicing does not have an effect on KIF2A isoforms' subcellular localization in both primary cortical neurons [103] and Neuro2A cells. In addition to its role in axon branch elongation, I showed that KIF2A is also required for dendrite pruning in primary cortical neurons and all alternatively spliced KIF2A isoforms can perform this function equally well. Moreover, consistent with the previous observations [8, 88], I confirmed that KIF2A is required for radial neuronal migration in the developing mouse cortex and I demonstrated that only KIF2A.1 and KIF2A.2 isoforms, but not the KIF2A.3 isoform can support neuronal migration. I also found that different KIF2A isoforms indeed have different protein interacting partners by proximity biotinylation and mass spectrometry (BioID), supporting a role for AS in expanding protein interactome diversity. I confirmed the interaction of KIF2A with one of the interacting partners RNT4 protein I identified from the BioID screen. Furthermore, I showed that two dominant negative disease-causing KIF2A mutants ($KIF2A^{S317N}$ and $KIF2A^{H321D}$) localize only along the polymerized MTs and both nucleus and cytoplasm are free of these mutant proteins, and also these disease-causing KIF2A mutants do not affect dendrite development. Finally, I identified protein interaction partners of $KIF2A^{H321D}$ and found that mutation on KIF2A has changed its protein interactome. Taken

together, I proposed a model demonstrating different KIF2A isoforms have different protein interaction partners and KIF2A is required for both dendrite development in primary cortical neurons and radial neuronal migration in developing mouse embryonic cortex. The role of KIF2A in dendrite morphogenesis is not isoform dependent, all isoforms repress dendritic growth via its MT-depolymerization activity. However, the role of KIF2A in cortical neuronal migration is isoform dependent, only KIF2A.1 and KIF2A.2 can fulfill its function in radial neuronal migration **(Figure 2.41)**.

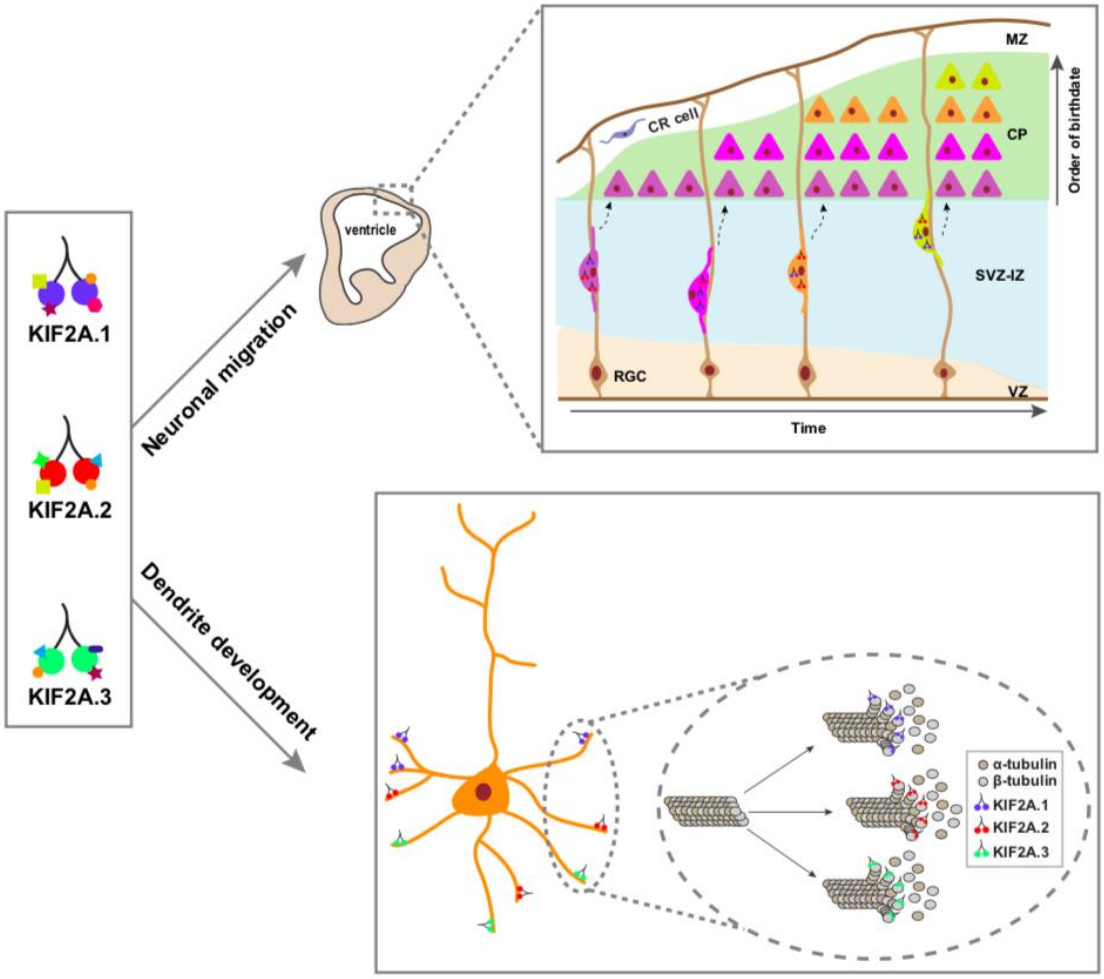

Figure 2. 41: Model of alternatively spliced KIF2A isoforms in cortical neuronal migration and dendrite arborization in mice.

Kif2a is a developmentally regulated and alternatively spliced gene. Its isoforms (KIF2A.1: blue, KIF2A.2: red, KIF2A.3: green) have common and unique protein interacting partners. Upper panel summarizes the "inside-out" radial migration of excitatory projection cortical neurons and this process is regulated by KIF2A in an isoform-dependent manner. KIF2A.1 and KIF2A.2 but not KIF2A.3 isoform can control the radial neuronal migration in mouse developing cortex. Lower panel demonstrates that KIF2A is essential for dendritic pruning and all KIF2A isoforms can promote this process equally well. RGC, radial glial cell; CR, Cajal-Retzius; MZ, marginal zone; CP, cortical plate; SVZ-IZ, subventricular zone-intermediate zone; VZ, ventricular zone.

Kif2a is an alternatively spliced gene and it has been demonstrated that nELAVL binding to U-rich intronic sequence promotes the inclusion of alternative exon 18 which has an amino acid sequence rich in Serine residues [31]. We also identified a third isoform which has the full sequence of alternative exon 18, but a truncated alternative exon 5 localized near the N-terminal of its dimerization domain. KIF2A.3 is formed as a result of alternative 5' splice site selection and it differs from KIF2A.1 by a 20 amino acid sequence. This 20 amino acid stretch encodes for a disordered protein region. Initially, I tested whether the expression of the three KIF2A isoforms were developmentally regulated at the mRNA and protein levels. My results demonstrated that *Kif2a.1* and *Kif2a.2* are the major isoforms and their mRNA expressions are high during development and decreases at postnatal stages and in adulthood. *Kif2a.3* is the minor isoform and its mRNA expression peaks in late embryogenesis and then once again in the second postnatal week. Next, I performed immunoblotting to observe overall KIF2A and nELAVL protein expression in different developmental ages. Since there is no antibody specific to each of the KIF2A isoforms I

quantified total KIF2A protein amounts. I observed a general correlation of expression between KIF2A and nELAVL at the protein level. There is a high protein expression at embryonic stages and this expression is downregulated postnatally for both proteins. This result suggested that, in addition the nELAVL proteins' role in regulating KIF2A AS, they might also regulate *Kif2a* mRNA stability. Further experiments will clarify this statement.

Since AS has many effects on cellular function, I next determined whether AS affects the subcellular localization of KIF2A isoforms. Towards this aim, I transfected either Neuro2A neuronal cell line or primary cortical neurons with three KIF2A isoforms and analyzed their localization. My immunofluorescence analysis revealed that in both primary cortical neurons and Neuro2A cells, all three KIF2A isoforms had both cytoplasmic and nuclear localization. These data suggested that AS do not affect the subcellular localization of KIF2A. Previous study had demonstrated that N-terminus of KIF2A is responsible for its localization to spindle poles in HeLa cells [86]. For all three KIF2A isoforms the N-terminal is conserved which may be the reason for observing the same localization pattern for all KIF2A isoforms. Further experiments about creating a site directed mutagenesis of N-terminus for all KIF2A isoforms and investigating the localization in primary cortical neurons and Neuro2A cells will provide further information about the domain which is responsible for its localization. As a future direction, I may further analyze the localization of endogenous KIF2A in different cell types in primary cortical cultures with immunofluorescence using different cell-type specific markers. Moreover, I will examine the localization of these KIF2A isoforms in detail in dendrite tips and protrusions, axon growth cones and MTs. In addition to these isoforms, I also investigated the subcellular localization of two disease causing KIF2A mutants ($KIF2A^{S317N}$ and $KIF2A^{H321D}$). It had been previously reported that both these mutants co-localized with dynamic MTs in Cos-7 cells. Especially, $KIF2A^{H321D}$ localization on MTs in patient-derived fibroblasts and in the cells of mouse

embryonic cortex were previously shown [2, 8]. KIF2A mutants localization to dynamic MTs was also shown in primary cortical neurons [103]. Consistent with these observations I also observed that both KIF2A mutants were sequestered along the MTs, the immunofluorescence results showed that both KIF2A mutants were co-localized with the MTs and in contrast to the WT KIF2A, both cytoplasm and nucleus were free of these two KIF2A mutants.

Control of cytoskeletal element (actin and MTs) dynamics is crucial for dendrite morphogenesis in neurons [121]. In neurons MTs localization is uniform in axons with their plus ends oriented through the axon tip. In dendrites MT polarity is mixed with both minus and plus ends positioned away from the cell body, depending on the type of the neuron and organism [137-139]. Previously, it had been demonstrated that, both axons and dendrites have dynamic MT [138, 140, 141] and recent publications also showed the dynamic MTs in dendrites of cortical neurons in adult mice [138, 142, 143]. Together, these studies pointed that both cultured and *in vivo* neurons preserve their MTs in dynamic form in their dendrites [122].

Dendritic branches are formed via either by bifurcating from growth cone-like tips or growth of new branches from an existing branch. Intrinsic signals or extrinsic factors regulate either growth or retraction of these newly formed branches [122]. For instance, nerve growth factor (NGF), neurotrophin 3 (NT-3) and brain-derived neurotrophic factor (BDNF) have roles in dendritic morphogenesis in vertebrate cortical neurons as extrinsic factors [122, 144]. Moreover, depending on the neuronal type, these factors can also either suppress or promote dendritic growth in cortical slices [122, 145]. In addition to these extrinsic factors, intrinsic signals such as transcription factors, signaling pathways and cytoskeletal elements can modulate dendritic morphology [122, 146, 147]. For example, mutations on MT motor protein dynein or its associated protein Lis1 perturb dendrite arborization and maturation in

the *Drosophila melanogaster* mushroom body neurons [148]. Moreover, in MT stabilizer *Map2* deficient mice, both decrease in length and MT density in dendrites of hippocampal neurons were observed [149]. Moreover, MT binding proteins (MAPs), motor proteins and MT plus-end tracking proteins also regulate dendrite development and stability as well as branching. Kakapo, CHO1/MKLP1, MAP1b, Lis1 and CRMP3 can be given as examples to these proteins [121, 148, 150-153]. Finally, it has been reported that cyclin-dependent kinase like-5 (CDKL5) regulates MT dynamics in dendrites via phosphorylation of MAP1S [154]. Together these studies implicate the importance of the MT dynamics in dendrite growth and branching.

It has been previously shown that KIF2A controls axon branch elongation by its MT depolymerization activity [30, 67, 74]. BDNF which was shown to regulate dendrite and neuronal morphology via activating a signaling pathway that specifically phosphorylates and inactivates KIF2A which results in promoting neurite outgrowth [80]. Moreover, in tamoxifen-inducible *Kif2a* conditional knock-out mice, in dentate granule cells, dendro-axonal conversion was observed [29]. Growth of overextended dendrites lead to a gain of axonal properties resulting in a dendro-axonal conversion. In light of all these studies, I tested whether KIF2A has a role in dendrite development. For this, I performed Sholl analysis in KIF2A knock-down neurons and observed a significant increase in the number of primary dendrites in KIF2A knock-down primary cortical neurons suggesting that KIF2A is required for dendrite development. To see whether this effect is isoform dependent, I performed rescue experiments by re-introducing KIF2A isoforms one at a time, in *Kif2a* silenced primary cortical neurons. My results showed that all three isoforms were able to rescue the loss-of-function phenotype of KIF2A. The number of dendritic intersections in primary dendrites were similar to control (NS) transfected neurons. I observed even more dendritic pruning in distal dendrites where there was no difference between KIF2A knock down and

control samples. Taken together, my results point to a role of KIF2A in dendritic pruning, possibly by promoting MT depolymerization and all three KIF2A isoforms can perform this function. Further experiments such as labeling of MT tips with EB3 marker and performing time-lapse imaging of the polymerized MTs upon KIF2A knockdown will provide important clues about whether the role of KIF2A in dendritic pruning is due to its MT depolymerization role. Finally, I also performed Sholl analysis to investigate the effect of patient mutations on *Kif2a* on dendrite development. Surprisingly, I did not observe any significant change in the number of dendritic intersections when I expressed both mutations separately in primary cortical neurons. One of the reason why I did not observe any change is because of the possibility of the inadequate expression of these mutant proteins. Both disease-causing *Kif2a* mutations are dominant-negative. Thus, in the primary cortical neurons, I expressed these mutants without silencing endogenous KIF2A. Future experiment of expressing both shRNA resistant *Kif2a* mutants in KIF2A knockdown neurons followed by Sholl analysis will give a clear result about the effect of *Kif2a* mutations on dendrite development. Alternatively, creating *Kif2a* mutant neurons from iPSC using patient fibroblasts and then performing Sholl analysis will uncover whether these mutants affect dendrite development.

KIF2A has known roles during different steps of cortex development in mice. One of the crucial step in cortex development is neuronal migration and regulation of MT dynamics. For instance, mutations in MT binding protein *Eml1* resulted in defects in primary cilia formation in apical progenitors in the VZ, neuronal migration defects and periventricular heterotopia [155]. Moreover, MT-depolymerizer KIF2A is also shown to be required for radial neuronal migration in developing mouse cortex [8, 88]. When *Kif2a* is silenced in neural progenitors either in E13.5 or E14.5, significant reduction in the number of KIF2A knock down neurons migrating to the CP was observed and most of these neurons accumulated in the VZ, SVZ and IZ region of the developing cortex. [8, 88]. In addition to

these results, mutations in *Kif2a* (*Kif2a*^{H321D} and *Kif2a*^{S317N}) which cause malformations of cortical development in humans also displayed defects in neuronal migration. *In utero* electroporation of these *Kif2a* mutant cDNAs into NPCs resulted in severe defects in neuronal migration. Nearly all transfected neurons were trapped in the VZ, SVZ and IZ and very few of them were able to reach the CP [8]. Altogether, these results point to the importance of KIF2A in cortical radial neuronal migration.

Most of studies about neuronal migration demonstrated the importance of regulation of expression of specific transcription factors [5]. For example, transcription factors SOX5 and TBR1 regulate neuronal migration and laminar positioning of early-born (deep layer) neurons, respectively [5, 156, 157], whereas transcription SATB2 modulates the neuronal migration of late-born (upper layer) neurons [5, 158, 159]. Although many studies were published about the regulation of neuronal migration by transcriptional programs, few studies were published about the control of neuronal migration via posttranscriptional mechanisms. Posttranscriptional mechanisms regulate the exact spatiotemporal expression patterns of proteins and this process is required for the normal development of the cerebral cortex [5]. For instance, the RNABP neuro-oncological ventral antigen 2 (NOVA2) controls neuronal migration by modulating AS of intracellular adaptor protein *Dab1* [160]. Together these studies highlight the importance of the combination of transcriptional and posttranscriptional mechanisms in the cortical neuronal migration.

As mentioned above, few yet significant studies demonstrated that posttranscriptional modifications regulate neuronal migration. Since KIF2A undergoes AS and it is shown to be an important protein in cortex development and control of radial neuronal migration, next I tested whether the role of KIF2A in neuronal migration is isoform dependent. Toward this goal, I silenced *Kif2a* by electroporating shKif2a into the ventricular zone NPCs at E14.5

and analyzed the migration progress at E17.5. Consistent with previous observations [8, 88], I observed a gross defect in radial neuronal migration with significantly reduced number of *Kif2a* silenced neurons reaching the cortical plate, most of them accumulated in the SVZ-IZ. When I re-introduced the each shRNA resistant *Kif2a* isoforms individually in KIF2A knock-down samples, I observed rescue in the migration phenotype only with the *resKif2a.1* and *resKif2a.2* expressing samples, but not with the *resKif2a.3* sample. My results demonstrated that only KIF2A.1 and KIF2A.2 but not KIF2A.3 can support radial neuronal migration in the developing mouse cortex. Taken together, my results show that the requirement of KIF2A in neuronal migration is isoform dependent.

Recent studies have suggested that AS increases the phenotypic and cellular complexity in eukaryotes by rewiring the protein interactome between species [48, 161-164]. Computational studies have revealed that alternatively spliced exons often encode for intrinsically disordered protein region [48, 165, 166]. AS of these disordered regions can create new protein interactions resulting in changes to the molecular or biochemical functions that are performed by the protein; and this can provide novel traits in disease evolution and development [48]. This event becomes more frequent in tissue specific AS [48, 126, 167] suggesting the inclusion or exclusion of such disordered regions can introduce modification of protein function by changing its stability or its molecular interactions [48, 126, 167, 168]. As mentioned above, KIF2A.3 contains a truncated alternative exon 5 and when I measured the disordered protein regions in all KIF2A isoforms with IUPred2A prediction tool [124], I identified a disordered protein region which is encoded by this alternative sequence of KIF2A.3. Loss in the function of the KIF2A.3 in neuronal migration might be correlated with the AS in disordered segment. Since the AS splicing of disordered regions may change the function of the protein and its protein interactome, I performed proximity biotinylation which is a method used to identify protein interacting partners of a given protein of interest (KIF2A)

by mass spectrometry. Moreover, I also performed BioID protocol by expressing *Kif2a*^{H321D} cDNA in Neuro2A cells to investigate whether a disease-causing mutation in *Kif2a* changes its protein interaction partners. In these kinds of large scale experiments, using primary cortical neurons is challenging, since it is difficult to acquire enough primary cortical neurons from mouse embryos. Also I used the PEI (Polyethylenimine) transfection reagent which can be toxic to primary neurons. Furthermore, the transfection efficiency of the neurons can be very low such that sufficient amount of biotinylated proteins might not be obtained. For all these reasons, I used the neuronal cell line Neuro2A for the BioID experiments.

BioID assay followed by LC-MS/MS mass spectrometry analysis identified known interactors of KIF2A such as centrosomal proteins CEP170 and NUMA which have roles in bipolar spindle assembly [28, 86, 169]. During mitosis, KIF2A localizes to spindle poles, regulates spindle assembly and depolymerizes MTs at their minus end for the poleward chromosome movement [26, 170, 171]. In addition to the known interactors, I also identified other novel potential interactors that are common to all KIF2A isoforms such as CKAP5, CHD4, KMT2E and RANBP2 which are also shown to be localized to bipolar spindles. Since Neuro2A is able to perform mitosis, identification of these interactors were expected. Further experiments on how KIF2A and these potential partners interact will help to understand the mechanisms of control of chromosome segregation and bipolar spindle assembly. Moreover, among these candidates, a lysine methyl transferase KMT2E has a role in modulating the methylation of lysine 4 on histone 3 (H3K4) and mutations in *KMT2E* cause a neurodevelopmental disorders such as epilepsy and microcephaly [172]. Finally, during cerebral cortex development, chromatin remodeling histone deacetylase CHD4 supports the proliferation of NPCs within the VZ [173]. Further experiments demonstrating the characterization of these candidate interactors of KIF2A will uncover crucial features of KIF2A's role in cortical development.

Several studies demonstrated the role of KIF2A in primary cilium formation. It has been suggested that primary cilium disassembly might be regulated by Cenpj through PLK1-KIF2A pathway in mouse developing cortex [88]. Depletion of Cenpj results in a delay in cell cycle of NPCs hence a reduction of the NPC pool. Cenpj controlled primary cilium formation via KIF2A might be the reason for the decrease in neurogenesis in the developing mouse cortex [88]. Furthermore, another study showed the WDR2-CEP170 interaction promotes the CEP170 localization to the basal body of the primary cilium where it recruits KIF2A. As a result, primary cilium disassembles via MT-depolymerizer KIF2A [28]. In the BioID assay, primary cilium specific proteins were not identified because Neuro2A cells are actively dividing hence do not have primary cilia. I only identified CEP170 which is a modulator of primary cilium formation and NPC division in the VZ [28] as a potential interactor specific to KIF2A.2.

Intriguingly, mass spectrometry analysis identified unexpected potential interactors of KIF2A such as translation factors, ER- or mitochondrial- targeted proteins and RNA processing enzymes. One of the reasons for the identification of these interactors is that they might be a false-positive results. However, many of these potential targets were identified as isoform specific which suggest that it is unlikely they are contaminants. A number of these interactors have known roles in MT-based cargo trafficking. For instance, KTN1 which a candidate interactor for all KIF2A isoforms and TRAK1 which is a potential interactor specific to KIF2A.3 are both adaptor proteins of kinesin with important roles in MT-based mitochondrial transport [174-178]. Moreover, KIF1B, a potential interactor specific to KIF2A.2, has a role in anterograde mitochondrial transport [179]. Conflictingly, it has been shown that in *Kif2a* knockout cells, both ER and mitochondrial subcellular distribution is not changed [67] and this result brings up the possibility of genetic redundancy amongst several kinesins while organelle trafficking.

Mass spectrometry data identifies several possible interactors of KIF2A with possible functions in cerebral cortex development. CHD4, CEP170, KMT2E and RTN4 are the examples for these interactors. I previously discussed CHD4, KMT2E and CEP170. RTN4 also known as NOGO has a role in inhibiting neurite outgrowth specific to CNS. During development, it has roles in dendritic pruning and myelin formation of oligodendrocytes; in adulthood, it has roles in long term potentiation and short term memory; and finally during lifetime, it has roles in stem cell survival and proliferation, cell migration, axon growth and synaptic plasticity [180]. Moreover, it has been demonstrated that RTN4 regulates neuronal migration negatively and in *Rtn4* knockout mice cortical lamination defects were observed [181]. I confirmed the interaction between endogenous KIF2A and RTN4 in Neuro2A cells by performing proximity ligation assay (PLA) which is a specific method to show the interactions of proteins in spatial resolution. However, how the interactions between KIF2A and RTN4 affects neuronal function such as radial neuronal migration or dendritic pruning is still not known. Further experiments of RTN4 knockdown in *Kif2a* silenced primary cortical neurons and embryonic cortex will give a clue about whether RTN4 has an additive effect of these KIF2A phenotypes.

As mentioned above, unlike the first two KIF2A isoforms, the third isoform KIF2A.3 which has a truncated alternative exon 5 cannot sustain neuronal migration. At the moment, I do not know how the spliced segment affects the function of KIF2A. However, my BioID screen suggested that the protein interaction network of KIF2A.3 isoform is different from both KIF2A.1 and KIF2A.2. I identified the highest fraction of unique interactors of KIF2A.3 compared with other two isoforms. In addition, it has been shown that expression of *Kif2a*^{H321D} cDNA in mouse embryonic cortex causes neuronal migration defects and patients with *Kif2a*^{H321D} mutation have MCD [2, 8]. Intriguingly, in my BioID results, I identified high numbers of common potential targets of KIF2A.3 and KIF2A^{H321D} that were not

identified in the interactome sets of KIF2A.1 and KIF2A.2. Among these targets, many of them are known components of ribonucleoprotein complexes such as PES1, HNRNPAB, NAT10 and EIF4ENIF1 [182-186]. Moreover, as discussed previously, many of the mitochondrial proteins were identified as potential interactors of both KIF2A.1 and KIF2A.2. In KIF2A.3 and KIF2A^{H321D} datasets, I observed a significant reduction of these mitochondrial proteins. Importantly, recent studies have suggested MT- and kinesin-dependent transport mechanisms for several mRNA populations which are targeted to mitochondria [187-190]. Moreover, I also identified several inner mitochondrial membrane or matrix proteins such as TIMM44, SUCLG2, OGDLH and SUCLA2. Previous studies also demonstrated several inner-membrane mitochondrial proteins are co-translationally targeted to mitochondria [191, 192]. KIF2A might play roles during this co-translational process, thus this mechanism might be the reason why I identified mitochondrial inner membrane or matrix proteins in our dataset. Further experiments will clarify whether KIF2A modulates the transport of MT-based RNA-protein complex directly, or instead of direct interactions it might be in the close proximity to several numbers of MT-interacting cargos while regulating the MT-dynamics. To sum up, although further experiments are necessary to reveal the biological significance of my findings, these results provide a particular example of how AS of a single gene can regulate differentially a cellular process such as radial neuronal migration.

Chapter 3

TERMINAL NEURON LOCALIZATION TO THE UPPER CORTICAL PLATE IS CONTROLLED BY THE TRANSCRIPTION FACTOR NEUROD2

3.1 LITERATURE REVIEW

3.1.1 Overview of mammalian cortex development

The fine adjustment of neurogenesis, neuronal migration, differentiation and connectivity are required for the appropriate development of the cerebral cortex [70]. The development of the architecture of the mammalian neocortex depends on coordinated developmental processes, starting with an excessive neural progenitor cell (NPC) proliferation in the ventricular zone (VZ) [8]. Glutamatergic excitatory projection neurons develop from asymmetric division of aRG cells located in the VZ. During radial migration of neocortical projection neurons toward the cortical plate (CP), neuronal morphologies transition from multipolar to bipolar state. They use radial glia fibers to migrate their final destination to form the six layered cortex structure. After reaching their final destination at the CP, they translocate from radial glial processes, obtain identities by forming axonal and dendritic extensions, establish cortical connectivity and finally six layer cerebral cortex is formed in an “inside-out” manner [5, 8, 70].

3.1.2 Neurogenins and NeuroD proteins

The neocortex is organized into six-layers, each layer is composed of neurons that have different birth-dates and also send their axons to different part of the nervous system. During the formation of cortex, there is a transition of cellular states from neural progenitor cells to neurons from the point of their proliferative potential, migratory actions, axon development, dendritogenesis and synaptogenesis [43, 193-195]. Moreover, cortical projection neurons provide the communication between the neocortex and other parts of the brain by expressing particular groups of axon guidance molecules which directs the axons to correct targets [45, 195]. Transcription factors (TFs) are key players and control neurogenesis, neuronal migration and differentiation by specific spatiotemporal and combinatorial expression. As a result, neurons are generated at the right time and they migrate towards their correct destinations **(Figure 3.1)** [5, 43, 45, 196, 197]. Proneural and neurogenic basic helix-loop-helix (bHLH) TFs are one of the major players that regulate the development of neuronal subtypes, each characterized by unique patterns of connectivity as well as characteristic morphological and physiological properties [43, 198-200]. These bHLH TFs contain proneural Neurogenins (Neurog1 and Neurog2) and neurogenic NeuroDs (Neurod1, Neurod2, Neurod4 and Neurod6) and neurogenesis is induced by their ectopic expression in the developing mammalian cortex [43, 201, 202]. At around E11.5 (onset of neurogenesis) in mice, Neurogenins are transiently expressed in neural progenitor cells which results in the differentiation to cortical projection neurons [199, 203, 204] and activates the expression of downstream TFs such as NeuroD family. This expression induces genetic programs for neurogenesis of excitatory neurons and suppresses other cell fates [194, 205, 206]. Moreover, various neurological disorders are identified with their loss-of-function mutations [200, 207].

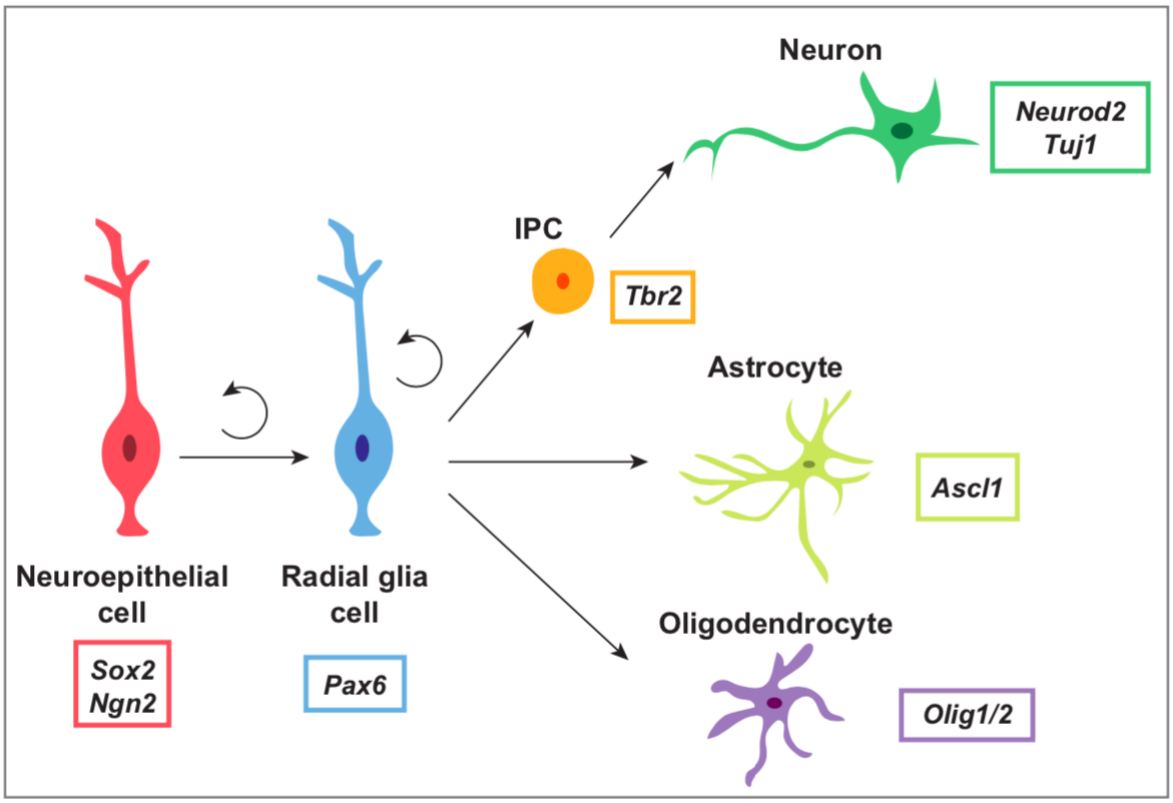

Figure 3. 1: Transcriptional regulation in progenitor maintenance, non-neuronal differentiation and neuronal differentiation.

Examples of transcription factors that regulate neuroepithelial cell (*Sox2, Ngn2*) and radial glia cell (*Pax6*) maintenance; intermediate progenitor cell (IPC) (*Tbr2*) production; neuronal fate specification (*Neurod2, Tuj1*); non-neuronal cells such as astrocyte (*Ascl1*) and oligodendrocyte (*Olig1/2*) differentiation (Adapted from [104]).

3.1.3 Neurogenic Differentiation 2 (NEUROD2)

Neurogenic Differentiation 2 (NEUROD2) is a prominent member of the NeuroD family which binds to phylogenetically conserved sites which is composed of consensus E-box elements (CANNTG). It modulates various fundamental properties during brain development. *Neurod2* is expressed outside of the proliferative zones of the mammalian cortex from embryonic day 11.5 (start of neurogenesis) and is expression is sustained in excitatory projection neurons throughout adulthood. NEUROD2 is a potential modulator of both maintenance and differentiation of various types of cortical projection neurons [43-45, 208, 209]. It has been demonstrated that NEUROD2 is required for hippocampal neuron dendrite and synapse maturation as well as layer II/III callosal projection neurons' commissural axon pathfinding and granular neurons' cortical somatosensory map formation within layer VI [210-212]. Moreover, the failure of differentiation of GABAergic projection neurons is observed when NEUROD2 is ectopically expressed in NPCs in the ventral telencephalon [206]. *Neurod2* knock out mice show deficiencies in thalamocortical connections, amygdalar nuclei development, axonal guidance of callosal axons and synaptogenesis in the hippocampus [44, 210-213]. Moreover, early cell cycle exit which leads to premature differentiation is observed when *Neurod2* is overexpressed [195]. It has also been shown that, NEUROD2 binds to large number of target genes that regulate functions such as radial neuronal migration, layer-specific differentiation and axon guidance which are required for normal cortex development [45].

In our previous studies, we identified genome-wide targets of transcription factor NEUROD2 that is expressed in projection neurons of cortex during E14.5 (mid-embryogenesis and also peak of cortical excitatory neurogenesis) and P0 (onset of dendritogenesis, synaptogenesis and differentiation) using chromatin-immunoprecipitation and sequencing (ChIP-Seq) approach [43, 45]. E14.5 ChIP-Seq analysis showed that NEUROD2 binds and regulates key target genes which are involved in the REELIN signaling pathway [45]. We also demonstrated that NEUROD2 binds and controls the expression of radial neuronal migration regulator *Cdk5r1* and a transcription factor *Cux1* that has a role in regulating the upper layer (II/III and IV) neuron differentiation [45]. Furthermore, our ChIP-seq analysis of P0 mouse cortex revealed that NEUROD2 binds to an intronic element of the stromal interaction molecule 1 (*Stim1*) gene. STIM1 is a sensor for calcium levels in endoplasmic reticulum (ER) and it is also a crucial regulator of store-operated calcium entry (SOCE) [43, 214, 215]. It has also been shown that binding of NEUROD2 to intron 2 of *Stim1* suppresses its expression hence a downregulation in SOCE response [43]. All these studies show that NEUROD2 has a crucial role in regulating the neurodevelopment and neuronal calcium homeostasis in various cortical developmental stage.

3.1.4 REELIN signaling pathway

REELIN is an extracellular glycoprotein secreted by Cajal-Retzius (CR) cells located in the marginal zone (MZ) and has roles in neuronal migration and cortical lamination by creating a stop signal for migrating neurons in the cortex [32, 33, 216] **(Figure 3.2A)**. Migrating neurons in the developing cerebral cortex express VLDLR (very low density lipoprotein receptor) and LRP8 (also known as APOER2, apolipoprotein E receptor 2) receptors to which the ligand REELIN binds to and becomes internalized. This binding activates the differential tyrosine (Tyr, Y) phosphorylation of the cytosolic adaptor protein DAB1 by Src-family kinases (SFKs) which leads to the activation of downstream signaling pathways [14, 32] **(Figure 3.2B)**. REELIN signaling pathway activation prompts migration termination, neuronal cell shape stabilization and anchorage of nascent primary dendrites to the marginal zone's extracellular matrix [33-37, 217]. As mentioned above, REELIN is mainly secreted by CR cells in MZ but small amount of REELIN is also observed in the IZ [32, 218-220]. Moreover, receptors of REELIN are expressed in migrating neurons localized to the SVZ-IZ [32, 219] which suggests that REELIN also binds to its receptors in the deep part of the cortex to perform its function in early developmental stages.

Mutations in genes (*Reln*, *Vldlr*, *Apoer2* or *Dab1*) which play essential roles in REELIN signaling pathway lead to severe central nervous system defects including profound neuronal positioning defects during brain development as well as abnormal lamination of cortex, and disorganized hippocampus and cerebellum [35], lissencephaly and cerebellar hypoplasia (characterized by ataxia, mild epilepsy and mental retardation) in humans [34, 36]. *Reeler* mouse has an inverted ("outside-in") cortical lamination pattern which is arises by incorrect localization of early- and late-born neurons to upper and deep layers of cortex, respectively [32, 37, 216, 221-224]. This suggests that REELIN has a crucial role in modulating the proper "inside-out" formation of six-layer mammalian cerebral cortex.

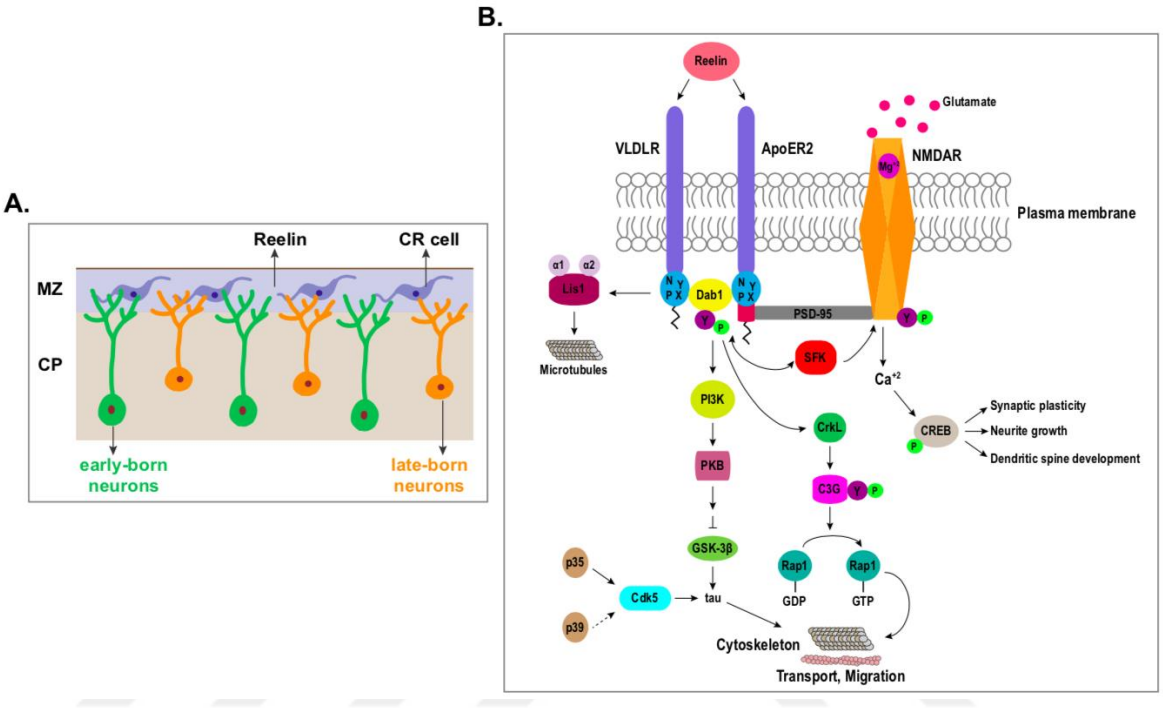

Figure 3. 2: REELIN signaling pathway in neurons.

A. REELIN is secreted by CR cells (blue) located in the MZ. Early-born (green) and late-born (orange) neurons located into CP, extend their apical leading processes into MZ. MZ, marginal zone; CP cortical plate; CR, Cajal-Retzius (Adapted from [32]). **B.** REELIN binds to VLDLR and APOER2 on the cell surface and induces the phosphorylation (P) hence the activation of DAB1 adaptor protein. DAB1 interacts with NPxY motifs in both receptors and activates Src-family kinases (SFKs) which leads to tyrosine (Y) phosphorylation of DAB1. Phosphorylation of DAB1 induces the recruitment and activation PI3K and protein kinase B (PKB). PKB activation leads to inhibition of glycogen synthase kinase-3β (GSK-3β) followed by reduction of tau phosphorylation which is also regulated by cyclin-dependent kinase 5 (Cdk5) and its activators p35 and p39. Phosphorylation of DAB1 can also induce recruitment of Crk-like (CrkL) that phosphorylates tyrosine on C3G, a guanine nucleotide exchange factor. Phosphorylated C3G induces the formation of Rap1-GTP that regulates

cytoskeleton reorganization hence migration or transport. Lis1 can also modulate MT dynamics by binding to phosphorylated DAB1. Finally, APOER2 interacts with postsynaptic scaffolding protein PSD95 through alternatively spliced exon and this association is crucial for combining the REELIN signaling complex with NMDAR. SFK is activated by REELIN binding and it phosphorylates tyrosine on NMDAR receptor. Phosphorylation increases intracellular Ca^{+2} by inducing Ca^{+2} influx and phosphorylates the cAMP-response element binding protein (CREB). Active CREB induces gene expression which is crucial for synaptic plasticity, neurite growth, and dendritic spine development (Adapted from [225, 226]).

3.2 MATERIAL AND METHODS

3.2.1 *In utero* electroporation, immunofluorescence and image analysis

In utero electroporation protocol was explained in detail in **Section 2.2.13**. DNA solution was composed of 500 ng NS (control) or shRNA plasmid (shNeurod2-1), 500 ng of pCAGGS-IRES-tdTomato and 0.1% Fast Green FCF (All plasmids were prepared using QIAGEN endofree plasmid maxi kit). Pregnant mice was sacrificed using CO_2 and electroporated brains were harvested in 1X cold PBS. Brains were fixed with 4% PFA in PBS at 4^{o}C overnight and next day they were transferred into 30% sucrose in PBS solution and incubated at 4^{o}C. Brains were embedded into cryostat embedding medium and coronal sections were taken as 50 μm thickness onto Polysine coated slides using cryostat. Sections were dried onto 37^{o}C heat block for one hour and at 4^{o}C for another one hour. A general frame was drawn with a liquid blocker pen and tissues were rehydrated with 1X cold PBS. Sections were blocked with blocking solution (3% BSA, 0.3% Triton X-100 in 1X PBS) and incubated with primary antibody at 4^{o}C overnight. Next day, sections were washed with 1X cold PBS for 20 minutes, 3 times and incubated with secondary antibody at room temperature for 3 hours. Sections were washed with 1X cold PBS for 20 minutes three times. In the second wash DAPI was added (1:500 in PBS). LEICA DMI8 SP8 CS/DLS microscope was used to capture optical z-series through 50 μm images and LasX Life Science software was used to create maximum intensity projections. Analysis was performed as explained in **Section 2.2.13**. For immunofluorescence protocol, antibodies used as follow; Reelin (Abcam, Cat. #78540, Host: mouse, 1:1000) as primary antibody and Donkey Anti-Mouse IgG (H+L) Alexa Fluor®488 (Invitrogen, Cat. #A21202, 1:1000) as secondary antibody.

3.3 RESULTS

3.3.1 NEUROD2 affects REELIN protein levels in marginal zone of developing cortex

After performing ChIP-Seq analysis using E14.5 and P0 mice cortices [43, 45], we wanted to further analyze expression of genes controlled by NEUROD2. Towards this aim, we performed RNA-Seq by silencing *Neurod2* using two different confirmed shRNAs (shNeurod2-1 and shNeurod2-2) in primary cortical cultures and found that 9 genes were upregulated and 25 genes were downregulated upon NEUROD2 knock-down [42]. Among these targets, we were interested in the *Reln* gene (460 kb of genomic sequence) which has crucial roles in cortical neuronal migration and consists of 65 exons in mice [227]. We found four prominent NEUROD2 binding sites at introns 21, 22, 55 and 63 of *Reln* and also confirmed these sites by performing ChIP followed by quantitative PCR (ChIP-qPCR) using E14.5 and P0 cortical tissue [42]. During radial neuronal migration, *Reln* is expressed ectopically by CR cells located in the MZ which do not express *Neurod2* [216, 228, 229]. However, migrating neurons express *Neurod2*, REELIN receptor genes such as *Apoer2 (Lrp8)* and *Vldlr* and adaptor protein *Dab1* which is the downstream element of REELIN signaling pathway. Moreover, recent studies using RNA-Seq analysis demonstrate that there is a mutually exclusive expression pattern of *Neurod2* and *Reln* within the CR cells and projection cortical neurons of developing cortex [230]. Intriguingly, our RNA-Seq results demonstrated that NEUROD2 acts as a negative regulator of *Reln* expression and to confirm this we silenced *Neurod2* in primary cortical neurons and then performed RT-qPCR [42]. We observed that upon silencing of *Neurod2* there is a significant upregulation of *Reln* mRNA levels. Moreover, to determine how NEUROD2 affects the REELIN protein expression, we performed immunoblotting in *Neurod2* silenced primary cortical neuron lysates. Interestingly, we observed a slight yet significant ($p=0.02$) upregulation of REELIN

in *Neurod2* knock-down neurons compared to control and we eliminated off-target effects by rescuing the REELIN increase by co-expressing an shRNA resistant *Neurod2* cDNA [42]. Collectively, our results indicated that NEUROD2 significantly suppresses *Reln* mRNA expression and this control only moderately influence REELIN protein levels in cortical neurons [42].

Next I asked whether REELIN protein expression is regulated upon NEUROD2 knock down in the embryonic mouse cortex. Towards this aim, I performed *in utero* electroporation by injecting either NS or shNeurod2-1 into the lateral ventricle of E14.5 embryo and electroporated to transfect plasmid DNA into radial glia cells located in the VZ. Then I collected and fixed the electroporated embryo brains at E17.5 with PFA and performed immunofluorescence staining with an anti-REELIN antibody in cortical sections. I observed increased levels of REELIN in the MZ but not in CP or SVZ-IZ in *Neurod2* silenced sections compared to control samples **(Figure 3.3A and B)**. Next, I quantified the immunofluorescence signal intensity of REELIN in both control and *Neurod2* silenced tissue sections and I observed a small but significant upregulation of REELIN signal intensity in the MZ, mainly localized to the cell body **(Figure 3.3A-C)**. In addition, I observed no difference in REELIN intensity within the CP and SVZ-IZ in *Neurod2* silenced samples when compared to control **(Figure 3.3D and E)**. My results bring up the questions about the cellular source of this ectopic REELIN protein expression. Although there is a small numbers of over-migrating neurons into the MZ, a huge majority of the neurons are located to CP in the *Neurod2* silenced neurons. It is worth investigating whether the increase in REELIN protein in MZ is due to a secondary response of CR cells or it emerges from the projecting dendrites of cortical neurons upon *Neurod2* suppression [42].

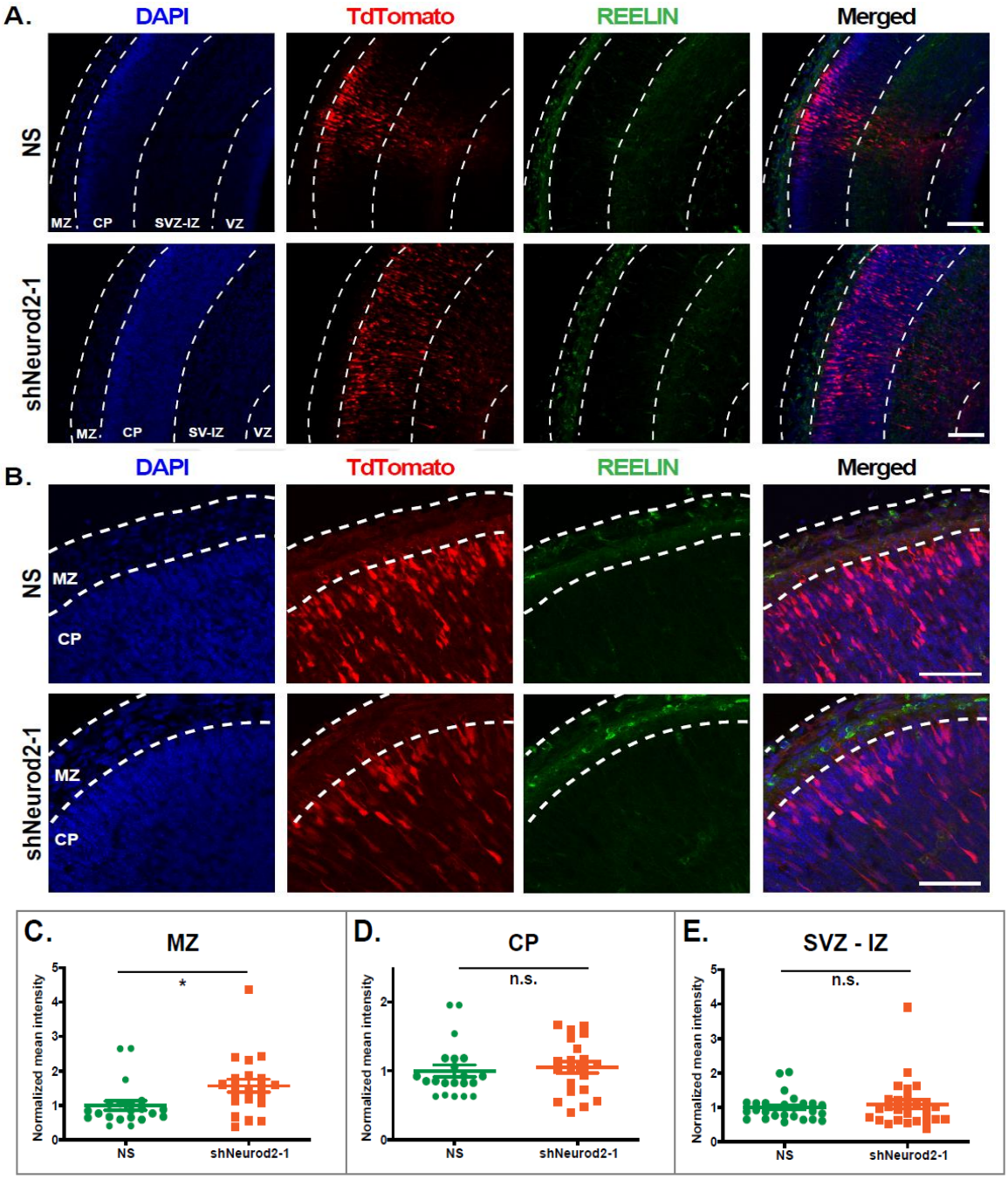
A.
DAPI
TdTomato
REELIN
Merged
NS
shNeurod2-1
MZ
CP
SVZ-IZ
VZ
B.
C.
MZ
*
D.
CP
n.s.
E.
SVZ - IZ
n.s.
Normalized mean intensity
NS
shNeurod2-1

Figure 3. 3: REELIN protein levels are affected in MZ upon *Neurod2* suppression in the developing cortex.

A. *In utero* electroporation of E14.5 embryos with either non-silencing (NS) or shNeurod2-1 along with tdTomato marker gene. Cortices were harvested and fixed with 4% PFA at E17.5, coronally sectioned and REELIN immunofluorescent staining (green) followed by image capturing with confocal microscope were performed. Transfected neurons were visualized by tdTomato marker (red) and nucleus was stained with DAPI (blue). White dashed lines indicate boundaries of each cortical layer. Scale bar, 100 μm. **B.** Higher magnification images displayed in **(A)**. White dashed lines indicate boundaries of each MZ. Scale bar, 50 μm. **C., D. and E.** *In vivo* quantification of images displayed in **(A)** and **(B)**. A total of 21 images obtained from n=3 embryos per each condition were used for quantification. Lines indicate the mean intensity. Bars represent S.E.M. Unpaired two-tailed *t* test with *p=0.02. MZ, marginal zone; CP, cortical plate; SVZ-IZ, subventricular zone-intermediate zone; VZ, ventricular zone; NS, non-silencing; n.s., non-significant.

3.3.2 NEUROD2 regulates terminal stages of radial neuronal migration by controlling the neuronal soma placement to primitive cortical zone

Since we identified NEUROD2 target genes that have roles in neuronal migration coupled with experiments showing the control of *Reln* expression, I decided to investigate whether *Neurod2* silencing affected neuronal migration. Toward this aim, I transfected either NS or shNeurod2-1 along with tdTomato marker *in utero* into NPCs in E14.5 embryos and then I quantified the number of tdTomato-positive neurons at E17.5 by confocal microscopy **(Figure 3.4A and B)**. As expected, I observed tdTomato-positive neurons within the VZ, throughout the SVZ-IZ and also at the CP. In *Neurod2* suppressed tissue samples, I did not observe large defects in neuronal migration. I observed tdTomato-positive neurons within the VZ and most of them could able to migrate away from VZ toward the CP which were similar to control samples. However, I observed significantly low numbers of tdTomato-positive neurons in the primitive cortical zone which is the place located immediately below the MZ. My results demonstrated that NEUROD2 affects the terminal stage of neuronal migration in the developing cortex **(Figure 3.4A and B)**. In addition to this result, I also detected over-migrated neurons into the MZ in NEUROD2 knock down samples **(Figure 3.4B and C)**. Collectively, these data suggested that NEUROD2 has a role in controlling terminal stage of neuronal migration by modulating the neuronal soma positioning at the primitive cortical zone [42].

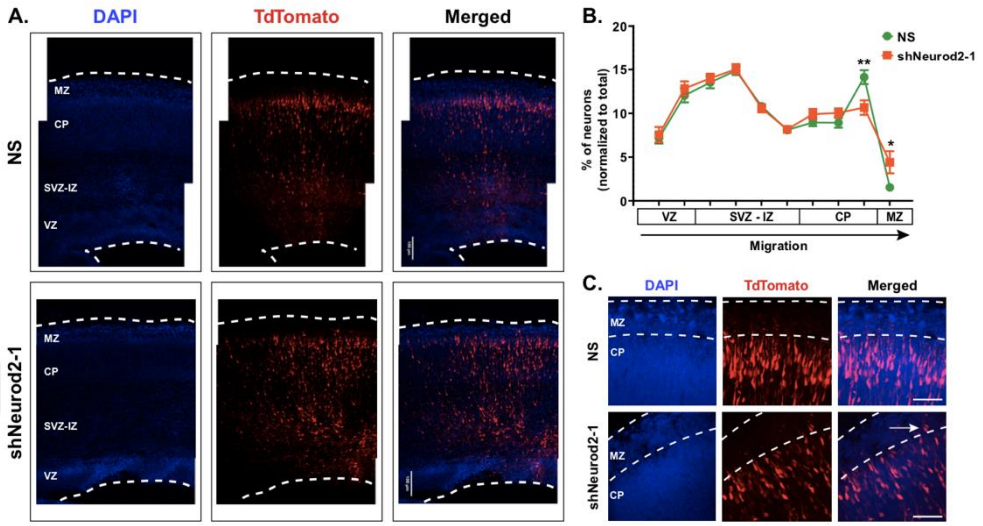

Figure 3. 4: NEUROD2 controls the soma positioning of the neurons to the primitive cortical zone.

A. *In utero* electroporation of E14.5 embryos with NS or shNeurod2-1 along with TdTomato. Electroporated brains were collected and fixed with paraformaldehyde at E17.5 and transfected neurons were imaged based on their tdTomato expression using confocal microscopy. Boundaries of cortex were marked with white dashed lines. Scale bar, 100 µm. **B.** Quantification of *in utero* electroporation shown in **(A)**. A total of n=16,184 for NS and n=19,339 for shNeurod2-1 transfected neurons from seven littermate embryos from five independent pregnant mice were counted. Normalized percentages of tdTomato-positive neurons counted in each cortical zones are plotted as line graph. Bars represent S.E.M. Two-way ANOVA with $p<0.0001$ and *$p=0.0165$ and **$p=0.0015$ by post hoc Sidak's test. C. Higher magnification images of the MZ and CP in control (NS) and shNeurod2-1 transfected samples. Neuron that over-migrate in the MZ in *Neurod2* silenced cortex is indicated with white arrow. White dashed lines identify boundaries of each MZ. Scale bar, 50 µm. VZ, ventricular zone; SVZ-IZ, subventricular zone-intermediate zone; CP, cortical plate; MZ, marginal zone; NS, non-silencing.

3.4 DISCUSSION

In this study, based on our previous RNA-Seq analysis of transcription factor NEUROD2, we showed a new role for Neurod2 in the terminal stage of neuronal radial migration during cerebral cortex development. We focused on the *Reln* gene, which encodes an extracellular glycoprotein REELIN secreted by CR cells located in the MZ and has crucial roles in neuronal migration. Previously, we found that NEUROD2 binds to conserved E-box elements in multiple introns. Moreover, we reported that there is a significant upregulation of *Reln* gene expression at mRNA level upon NEUROD2 knockdown in primary cortical neurons and a slight yet significant upregulation of REELIN protein levels. When I knocked down NEUROD2 *in utero* in embryonic mice cortices REELIN is upregulated in MZ. Finally, I demonstrated that NEUROD2 has a role in the terminal stages of radial neuronal migration by promoting the migrating neurons to localize to the primitive cortical plate. My data uncover a novel role for transcription factor NEUROD2 in the terminal stages of radial neuronal migration in developing cortex [42].

REELIN signaling pathway is well studied. Binding of glycoprotein REELIN ligand to its lipoprotein receptors VLDLR and APOER2 activates DAB1 followed by the activation of its downstream signaling pathways that leads to cytoskeleton modifications as well as synaptic plasticity, neurite outgrowth and dendritic spine development in neurons [231-234]. Moreover mutations in *Vldlr, ApoEr2* and *Dab1* show the same phenotypes with *Reeler* mice. *Reeler* (*Reln* mutant) mice show several brain malformations such as lamination defects in cerebellum, hippocampus and neocortex and these phenotypes resemble the phonotypes of patients that have *Reln* mutations [234, 235]. Especially in neocortex, there is a defect in splitting of the preplate as well as migration defects, such as the late-born neurons failing to bypass early-born neurons during migration. It has been shown that, “mirror image” laminar

structure was observed in *reeler* mice, where neurons of layer II/III are located in the middle of the cortex, whereas neurons of layers IV/V/VI are misplaced above and below. Because of these results, *reeler* phenotype is described as a "partial inversion" of layers [234, 236]. Moreover, it has been suggested that REELIN signaling regulates neuronal migration through controlling several steps such as terminal translocation, transition from multipolar to bipolar stage and migration termination below the MZ. It has also been demonstrated that REELIN regulates somal translocation through distinct mechanisms such as controlling cellular adhesion and actin cytoskeleton [32, 34, 237, 238]. The proper stabilization of the actin cytoskeleton may create a stop signal for migrating neurons, so the cause of neuronal migration defects in the absence of REELIN may be due to the absence of stabilization of actin which may create leading process misorientation and instability in the migrating neurons [36, 233, 234].

By carrying out ChIP-Seq analyses, we reported binding of NEUROD2 to the promoters of various genes which has a role in REELIN signaling pathway such as *Dab1, ApoEr2 (Lrp8)* and *Fyn* [45]. In this study, we also demonstrated that NEUROD2 controls *Reln* mRNA expression. Unexpectedly, when we knocked down NERUOD2 in primary cortical neurons, we did not observe similar changes of REELIN upregulation at the protein level. We observe slight, yet significant REELIN upregulation upon NEUROD2 knockdown in primary cortical neurons. Taken together, we conclude that NEUROD2 regulates *Reln* expression primarily at the mRNA level. Previous research has shown that in *Neurod2/6* double knockout mice embryonic cortex, *Reln* expression is upregulated [239] which supports our findings. Moreover, our previous studies reported NEUROD2 as a potential transcriptional repressor in primary cortical neurons [43]. Although, NEUROD2 has usually been reported as transcriptional activator [44, 211, 240], our recent and previous studies also considered NEUROD2 as transcription repressor in a context-dependent manner which

shows the possible dual function for NEUROD2. Further investigations will reveal important insight about how NEUROD2 controls transcriptional activity in different gene loci. Furthermore, it is not clear that this effect is caused by NEUROD2 directly binding to the *Reln* introns or a secondary response and it will be interesting to perform site-directed mutagenesis to these binding sites and reveal the mechanism.

When I knocked down NEUROD2 in embryonic cortex, I observed no change in the REELIN level in the CP or SVZ-IZ. However, I performed REELIN immunofluorescence and quantified signal intensities for the embryonic sections. Since immunofluorescence is a semi-quantitative method, it might not show small changes accurately. In addition, in the *in utero* electroporation protocol, not all the neurons are transfected which means only a part of the neurons in CP or SVZ-IZ have silenced *Neurod2* which may affect the overall REELIN expression in these cortical zones. Unfortunately, with my confocal images, I cannot quantify the REELIN expression with each NEUROD2-knocked down neuron. It has been shown that REELIN may also induce the migrating neurons to detach from the RG basal processes [37, 234, 241]. Upon NEUROD2 knockdown, REELIN upregulation might cause an early detachment of the migrating neurons from the RG fibers which can lead to reduced neuron localization to the primitive cortical zone. Furthermore, *in utero* electroporation experiments with thinner cortical sections and increased resolution will likely provide an answer to that question.

Moreover, when I silenced *Neurod2* in mouse cortex, I observed an increase in the REELIN intensity levels at MZ. The upregulation of REELIN protein level in MZ but not the other regions of cortex drew my attention to the extracellular source of this ectopic REELIN expression. I observed the small numbers of over-migrating NEUROD2 knocked-down neurons in the MZ but most of the neurons were localized to the CP and SVZ-IZ. It has been demonstrated that over-migrating neurons into the MZ are associated with REELIN

creating a stop signal for migrating neurons [224, 234, 242]. It has also been shown that regulation of cytoskeleton with several both intracellular and extracellular elements is one of the key factors for cerebral cortex development such as neuronal migration regulation as well cortical lamination [90] and sometimes both overexpression and knockdown of the gene which is related with cytoskeletal elements can show similar phenotypes. For example, both knock down and overexpression of MT depolymerizer KIF2A in neuronal progenitors by *in utero* electroporation result in accumulation of neurons in the IZ compared to controls [8]. Moreover, mutations in the *Eml1* (Echinoderm microtubule-associated protein-like 1) gene encoding for a MT-binding protein expression in apical progenitors in the VZ cause a reduction in MT growth and this leads to heterotopia which is a MCD caused by neuronal migration defects. In addition overexpression of EML1 also reduces MT growth which may result in a similar phenotype. Thus, *Eml1* is important in MT dynamics and these results show that overexpression, mutation or absence of EML1 result in the reduction of MT growth in apical progenitors which may cause neuronal migration defects at the end [243]. Since REELIN signaling pathway results in cytoskeleton modifications [231-234], increase in ectopic REELIN protein levels in MZ due to NEUROD2 knockdown might change the cytoskeletal dynamics and this can also be the reason for over-migrating neurons in the MZ. However, the source this extra ectopic REELIN in the MZ, whether it is from the leading processes of over-migrating neurons or a secondary effect of CR cells in response the decreased level of NEUROD2 expression in cortical neurons, is not clear at the moment, but is a great interest for future investigations.

Previous studies also demonstrated that expression of *Reln* gene is tightly controlled by several other TFs. For instance, deletion of *Foxg1* gene, as well as knockdown of histone methyltransferase *Ezh2* lead to derepression of *Reln* expression and in both cases radial migration and cerebral cortex development defects were observed [244, 245]. Moreover, double knockout of TF *Pbx1/2* in mice display ectopic *Reln* expression and this phenocopies *reeler* mice, both phenotype resembles an inverted cortical lamination [246]. Finally, overexpression of ectopic REELIN in apical progenitor cells by *in utero* electroporation leads to migration defects such as accumulation of neuronal aggregation in deep cortical layers [247]. Collectively, these findings support the significance of the precise regulation of *Reln* gene expression in correct cortical layer formation. In addition to these results our findings suggest NEUROD2 as an additional transcriptional modulator of *Reln* gene such as deficiencies in function of NEUROD2 may affect only one level of control against ectopic REELIN instead of complete change and in migrating neurons this might create some extra genetic interactions with other genes that have roles in REELIN signaling.

Previous studies had shown that NEUROD2 might have a role in modulating radial neuronal migration [45, 195, 210]. In addition to these findings, our comprehensive analysis revealing NEUROD2 targets which have known roles in neuronal migration, prompted us to test whether NEUROD2-modulated transcription functions had an effect on radial neuronal migration. Toward this goal, I performed *in utero* electroporation protocol and silenced *Neurod2* in NPCs that are located in the VZ by electroporating shNeurod2-1 *in utero*. I found that silencing *Neurod2* did not show a gross migration defect in mice. However, I observed less neurons located at the uppermost layer of the primitive cortical zone which is the place immediately below the MZ. I reported significantly reduced number of neurons localized to the uppermost layer of primitive cortical zone upon *in utero* knockdown of NEUROD2. Thus, NEUROD2 is crucial for final stages of neuronal migration by regulating the proper

somal positioning of neurons upon arrival at the primitive cortical zone. Collectively, these data suggested that NEUROD2 regulates various components of the REELIN signaling pathway and/or other pathways and this regulation might affect the cortical lamination in developing cerebral cortex in mice. Further investigations will provide important clues about how target genes of NEUROD2 control this crucial step during cortical development. To sum up, transcription factor NEUROD2 regulates the terminal stages of radial neuronal migration by promoting the neurons to localize the uppermost layer of the primitive cortical zone and our comparative and compressive analyses of RNA-Seq and ChIP-Seq datasets contribute novel candidate genes that may regulate the cortical lamination in several aspects.

BIBLIOGRAPHY

1. Caviness, V.S., Jr., T. Takahashi, and R.S. Nowakowski, *Numbers, time and neocortical neuronogenesis: a general developmental and evolutionary model.* Trends in Neurosciences, 1995. **18**(9): p. 379-383.
2. Poirier, K., et al., *Mutations in TUBG1, DYNC1H1, KIF5C and KIF2A cause malformations of cortical development and microcephaly.* Nature Genetics, 2013. **45**(6): p. 639-647.
3. Rakic, P. and V.S. Caviness, Jr., *Cortical development: View from neurological mutants two decades later.* Neuron, 1995. **14**(6): p. 1101-1104.
4. Florio, M. and W.B. Huttner, *Neural progenitors, neurogenesis and the evolution of the neocortex.* Development, 2014. **141**(11): p. 2182-2194.
5. Kwan, K.Y., N. Šestan, and E.S. Anton, *Transcriptional co-regulation of neuronal migration and laminar identity in the neocortex.* Development, 2012. **139**(9): p. 1535-1546.
6. Kriegstein, A.R. and S.C. Noctor, *Patterns of neuronal migration in the embryonic cortex.* Trends in Neurosciences, 2004. **27**(7): p. 392-399.
7. Barkovich, A.J., et al., *A developmental and genetic classification for malformations of cortical development: update 2012.* Brain : a journal of neurology, 2012. **135**(Pt 5): p. 1348-1369.
8. Broix, L., et al., *Ciliogenesis and cell cycle alterations contribute to KIF2A-related malformations of cortical development.* Human Molecular Genetics, 2018. **27**(2): p. 224-238.
9. Cavallin, M., et al., *Recurrent KIF2A mutations are responsible for classic lissencephaly.* neurogenetics, 2017. **18**(2): p. 73-79.
10. Colombrita, C., V. Silani, and A. Ratti, *ELAV proteins along evolution: Back to the nucleus?* Molecular and Cellular Neuroscience, 2013. **56**: p. 447-455.
11. Spitz, F. and E.E.M. Furlong, *Transcription factors: from enhancer binding to developmental control.* Nature Reviews Genetics, 2012. **13**(9): p. 613-626.
12. Mansfield, K.D. and J.D. Keene, *The ribonome: a dominant force in co-ordinating gene expression.* Biology of the Cell, 2009. **101**(3): p. 169-181.
13. D, D., K.-Y. Hung, and W.-Y. Tarn, *RBM4 Modulates Radial Migration via Alternative Splicing of Dab1 during Cortex Development.* Molecular and Cellular Biology, 2018. **38**(12): p. e00007-18.
14. Su, C.-H., D. D, and W.-Y. Tarn, *Alternative Splicing in Neurogenesis and Brain Development.* Frontiers in Molecular Biosciences, 2018. **5**(12).
15. Zhang, X., et al., *Cell-Type-Specific Alternative Splicing Governs Cell Fate in the Developing Cerebral Cortex.* Cell, 2016. **166**(5): p. 1147-1162.e15.

16. Zhang, Y., et al., *An RNA-sequencing transcriptome and splicing database of glia, neurons, and vascular cells of the cerebral cortex.* The Journal of neuroscience : the official journal of the Society for Neuroscience, 2014. **34**(36): p. 11929-11947.
17. Pan, Q., et al., *Deep surveying of alternative splicing complexity in the human transcriptome by high-throughput sequencing.* Nature Genetics, 2008. **40**(12): p. 1413-1415.
18. Wang, E.T., et al., *Alternative isoform regulation in human tissue transcriptomes.* Nature, 2008. **456**(7221): p. 470-476.
19. Irimia, M., et al., *A Highly Conserved Program of Neuronal Microexons Is Misregulated in Autistic Brains.* Cell, 2014. **159**(7): p. 1511-1523.
20. Scotti, M.M. and M.S. Swanson, *RNA mis-splicing in disease.* Nature Reviews Genetics, 2016. **17**(1): p. 19-32.
21. Raj, B. and Benjamin J. Blencowe, *Alternative Splicing in the Mammalian Nervous System: Recent Insights into Mechanisms and Functional Roles.* Neuron, 2015. **87**(1): p. 14-27.
22. Yeo, G., et al., *Variation in alternative splicing across human tissues.* Genome Biology, 2004. **5**(10): p. R74.
23. Desai, A., et al., *Kin I Kinesins Are Microtubule-Destabilizing Enzymes.* Cell, 1999. **96**(1): p. 69-78.
24. Noda, Y., et al., *KIF2 is a new microtubule-based anterograde motor that transports membranous organelles distinct from those carried by kinesin heavy chain or KIF3A/B.* Journal of Cell Biology, 1995. **129**(1): p. 157-167.
25. Wordeman, L. and T.J. Mitchison, *Identification and partial characterization of mitotic centromere-associated kinesin, a kinesin-related protein that associates with centromeres during mitosis.* Journal of Cell Biology, 1995. **128**(1): p. 95-104.
26. Ganem, N.J. and D.A. Compton, *The KinI kinesin Kif2a is required for bipolar spindle assembly through a functional relationship with MCAK.* The Journal of cell biology, 2004. **166**(4): p. 473-478.
27. Miyamoto, T., et al., *The Microtubule-Depolymerizing Activity of a Mitotic Kinesin Protein KIF2A Drives Primary Cilia Disassembly Coupled with Cell Proliferation.* Cell Reports, 2015. **10**(5): p. 664-673.
28. Zhang, W., et al., *Modeling microcephaly with cerebral organoids reveals a WDR62–CEP170–KIF2A pathway promoting cilium disassembly in neural progenitors.* Nature Communications, 2019. **10**(1): p. 2612.
29. Homma, N., et al., *KIF2A regulates the development of dentate granule cells and postnatal hippocampal wiring.* eLife, 2018. **7**: p. e30935.
30. Maor-Nof, M., et al., *Axonal Pruning Is Actively Regulated by the Microtubule-Destabilizing Protein Kinesin Superfamily Protein 2A.* Cell Reports, 2013. **3**(4): p. 971-977.

31. Ince-Dunn, G., et al., *Neuronal Elav-like (Hu) Proteins Regulate RNA Splicing and Abundance to Control Glutamate Levels and Neuronal Excitability.* Neuron, 2012. **75**(6): p. 1067-1080.
32. Hirota, Y. and K. Nakajima, *Control of Neuronal Migration and Aggregation by Reelin Signaling in the Developing Cerebral Cortex.* Frontiers in Cell and Developmental Biology, 2017. **5**(40).
33. Chai, X., et al., *Reelin Induces Branching of Neurons and Radial Glial Cells during Corticogenesis.* Cerebral Cortex, 2014. **25**(10): p. 3640-3653.
34. Franco, S.J., et al., *Reelin Regulates Cadherin Function via Dab1/Rap1 to Control Neuronal Migration and Lamination in the Neocortex.* Neuron, 2011. **69**(3): p. 482-497.
35. Matsuki, T., et al., *Reelin and Stk25 Have Opposing Roles in Neuronal Polarization and Dendritic Golgi Deployment.* Cell, 2010. **143**(5): p. 826-836.
36. Olson, E.C., S. Kim, and C.A. Walsh, *Impaired Neuronal Positioning and Dendritogenesis in the Neocortex after Cell-Autonomous Dab1 Suppression.* The Journal of Neuroscience, 2006. **26**(6): p. 1767.
37. Sanada, K., A. Gupta, and L.-H. Tsai, *Disabled-1-Regulated Adhesion of Migrating Neurons to Radial Glial Fiber Contributes to Neuronal Positioning during Early Corticogenesis.* Neuron, 2004. **42**(2): p. 197-211.
38. Sekine, K., et al., *The Outermost Region of the Developing Cortical Plate Is Crucial for Both the Switch of the Radial Migration Mode and the Dab1-Dependent "Inside-Out" Lamination in the Neocortex.* The Journal of Neuroscience, 2011. **31**(25): p. 9426.
39. Hand, R., et al., *Phosphorylation of Neurogenin2 Specifies the Migration Properties and the Dendritic Morphology of Pyramidal Neurons in the Neocortex.* Neuron, 2005. **48**(1): p. 45-62.
40. Heng, J.I.-T., et al., *Neurogenin 2 controls cortical neuron migration through regulation of Rnd2.* Nature, 2008. **455**(7209): p. 114-118.
41. Pacary, E., et al., *Proneural Transcription Factors Regulate Different Steps of Cortical Neuron Migration through Rnd-Mediated Inhibition of RhoA Signaling.* Neuron, 2011. **69**(6): p. 1069-1084.
42. Guzelsoy, G., et al., *Terminal neuron localization to the upper cortical plate is controlled by the transcription factor NEUROD2.* Scientific Reports, 2019. **9**(1): p. 19697.
43. Guner, G., et al., *NEUROD2 Regulates Stim1 Expression and Store-Operated Calcium Entry in Cortical Neurons.* eneuro, 2017. **4**(1): p. ENEURO.0255-16.2017.
44. Olson, J.M., et al., *NeuroD2 Is Necessary for Development and Survival of Central Nervous System Neurons.* Developmental Biology, 2001. **234**(1): p. 174-187.

45. Bayam, E., et al., *Genome-wide target analysis of NEUROD2 provides new insights into regulation of cortical projection neuron migration and differentiation.* BMC Genomics, 2015. **16**(1): p. 681.
46. Ule, J., et al., *Nova regulates brain-specific splicing to shape the synapse.* Nature Genetics, 2005. **37**(8): p. 844-852.
47. Babu, M.M., *The contribution of intrinsically disordered regions to protein function, cellular complexity, and human disease.* Biochemical Society Transactions, 2016. **44**(5): p. 1185-1200.
48. Buljan, M., et al., *Alternative splicing of intrinsically disordered regions and rewiring of protein interactions.* Current Opinion in Structural Biology, 2013. **23**(3): p. 443-450.
49. Dlamini, Z., F. Mokoena, and R. Hull, *Abnormalities in alternative splicing in diabetes: therapeutic targets.* 2017. **59**(2): p. R93.
50. Camp, J.G., et al., *Human cerebral organoids recapitulate gene expression programs of fetal neocortex development.* Proceedings of the National Academy of Sciences, 2015. **112**(51): p. 15672.
51. Buckanovich, R., Y.Y.L. Yang, and R. Darnell, *The onconeural antigen Nova-1 is a neuron-specific RNA-binding protein, the activity of which is inhibited by paraneoplastic antibodies.* The Journal of neuroscience : the official journal of the Society for Neuroscience, 1996. **16**: p. 1114-22.
52. Gehman, L.T., et al., *The splicing regulator Rbfox1 (A2BP1) controls neuronal excitation in the mammalian brain.* Nature Genetics, 2011. **43**(7): p. 706-711.
53. Yang, Y.Y., G.L. Yin, and R.B. Darnell, *The neuronal RNA-binding protein Nova-2 is implicated as the autoantigen targeted in POMA patients with dementia.* Proceedings of the National Academy of Sciences of the United States of America, 1998. **95**(22): p. 13254-13259.
54. McKee, A.E., et al., *A genome-wide in situhybridization map of RNA-binding proteins reveals anatomically restricted expression in the developing mouse brain.* BMC Developmental Biology, 2005. **5**(1): p. 14.
55. Okano, H.J. and R.B. Darnell, *A Hierarchy of Hu RNA Binding Proteins in Developing and Adult Neurons.* The Journal of Neuroscience, 1997. **17**(9): p. 3024-3037.
56. Samson, M.-L. and F. Chalvet, *found in neurons, a third member of the Drosophila elav gene family, encodes a neuronal protein and interacts with elav.* Mechanisms of Development, 2003. **120**(3): p. 373-383.
57. Zheng, S. and D.L. Black, *Alternative pre-mRNA splicing in neurons: growing up and extending its reach.* Trends in Genetics, 2013. **29**(8): p. 442-448.

58. Gao, Z., et al., *Splice-Mediated Motif Switching Regulates Disabled-1 Phosphorylation and SH2 Domain Interactions.* Molecular and Cellular Biology, 2012. **32**(14): p. 2794-2808.
59. Boutz, P.L., et al., *A post-transcriptional regulatory switch in polypyrimidine tract-binding proteins reprograms alternative splicing in developing neurons.* Genes Dev, 2007. **21**(13): p. 1636-52.
60. Vuong, C.K., D.L. Black, and S. Zheng, *The neurogenetics of alternative splicing.* Nature Reviews Neuroscience, 2016. **17**(5): p. 265-281.
61. Dalmau, J., et al., *The expression of the Hu (paraneoplastic encephalomyelitis/sensory neuronopathy) antigen in human normal and tumor tissues.* The American journal of pathology, 1992. **141**(4): p. 881-886.
62. Szabo, A., et al., *HuD, a paraneoplastic encephalomyelitis antigen, contains RNA-binding domains and is homologous to Elav and sex-lethal.* Cell, 1991. **67**(2): p. 325-333.
63. Beckel-Mitchener, A.C., et al., *Poly(A) tail length-dependent stabilization of GAP-43 mRNA by the RNA-binding protein HuD.* J Biol Chem, 2002. **277**(31): p. 27996-8002.
64. Simone, L.E. and J.D. Keene, *Mechanisms coordinating ELAV/Hu mRNA regulons.* Current Opinion in Genetics & Development, 2013. **23**(1): p. 35-43.
65. Wang, X. and T.M. Tanaka Hall, *Structural basis for recognition of AU-rich element RNA by the HuD protein.* Nature Structural Biology, 2001. **8**(2): p. 141-145.
66. Akamatsu, W., et al., *The RNA-binding protein HuD regulates neuronal cell identity and maturation.* Proceedings of the National Academy of Sciences of the United States of America, 2005. **102**(12): p. 4625.
67. Homma, N., et al., *Kinesin Superfamily Protein 2A (KIF2A) Functions in Suppression of Collateral Branch Extension.* Cell, 2003. **114**(2): p. 229-239.
68. Talje, L., et al., *DHTP is an allosteric inhibitor of the kinesin-13 family of microtubule depolymerases.* FEBS Letters, 2014. **588**(14): p. 2315-2320.
69. Walczak, C.E., S. Gayek, and R. Ohi, *Microtubule-Depolymerizing Kinesins.* Annual Review of Cell and Developmental Biology, 2013. **29**(1): p. 417-441.
70. Jaglin, X.H. and J. Chelly, *Tubulin-related cortical dysgeneses: microtubule dysfunction underlying neuronal migration defects.* Trends in Genetics, 2009. **25**(12): p. 555-566.
71. Desai, A. and T.J. Mitchison*, *MICROTUBULE POLYMERIZATION DYNAMICS.* Annual Review of Cell and Developmental Biology, 1997. **13**(1): p. 83-117.
72. Hirokawa, N., et al., *Kinesin superfamily motor proteins and intracellular transport.* Nature Reviews Molecular Cell Biology, 2009. **10**(10): p. 682-696.
73. Mazumdar, M., M.-H. Sung, and T. Misteli, *Chromatin maintenance by a molecular motor protein.* Nucleus, 2011. **2**(6): p. 591-600.

74. Hirokawa, N., S. Niwa, and Y. Tanaka, *Molecular Motors in Neurons: Transport Mechanisms and Roles in Brain Function, Development, and Disease.* Neuron, 2010. **68**(4): p. 610-638.
75. Aizawa, H., et al., *Kinesin family in murine central nervous system.* Journal of Cell Biology, 1992. **119**(5): p. 1287-1296.
76. Hall, D.H. and E.M. Hedgecock, *Kinesin-related gene unc-104 is required for axonal transport of synaptic vesicles in C. elegans.* Cell, 1991. **65**(5): p. 837-847.
77. Niwa, S., *Kinesin superfamily proteins and the regulation of microtubule dynamics in morphogenesis.* Anatomical Science International, 2014. **90**(1): p. 1-6.
78. Cross, R.A. and A. McAinsh, *Prime movers: the mechanochemistry of mitotic kinesins.* Nature Reviews Molecular Cell Biology, 2014. **15**(4): p. 257-271.
79. Hirokawa, N. and Y. Noda, *Intracellular Transport and Kinesin Superfamily Proteins, KIFs: Structure, Function, and Dynamics.* Physiological Reviews, 2008. **88**(3): p. 1089-1118.
80. Ogawa, T. and N. Hirokawa, *Microtubule Destabilizer KIF2A Undergoes Distinct Site-Specific Phosphorylation Cascades that Differentially Affect Neuronal Morphogenesis.* Cell Reports, 2015. **12**(11): p. 1774-1788.
81. Jang, C.-Y., et al., *Plk1 and Aurora A regulate the depolymerase activity and the cellular localization of Kif2a.* Journal of Cell Science, 2009. **122**(9): p. 1334-1341.
82. Kline-Smith, S.L. and C.E. Walczak, *Mitotic Spindle Assembly and Chromosome Segregation: Refocusing on Microtubule Dynamics.* Molecular Cell, 2004. **15**(3): p. 317-327.
83. Arzate-Mejía, R.G., F. Recillas-Targa, and V.G. Corces, *Developing in 3D: the role of CTCF in cell differentiation.* Development, 2018. **145**(6): p. dev137729.
84. Cameron, L.A., et al., *Kinesin 5-independent poleward flux of kinetochore microtubules in PtK1 cells.* The Journal of cell biology, 2006. **173**(2): p. 173-179.
85. Jang, C.-Y., et al., *DDA3 recruits microtubule depolymerase Kif2a to spindle poles and controls spindle dynamics and mitotic chromosome movement.* The Journal of cell biology, 2008. **181**(2): p. 255-267.
86. Welburn, J.P.I. and I.M. Cheeseman, *The microtubule-binding protein Cep170 promotes the targeting of the kinesin-13 depolymerase Kif2b to the mitotic spindle.* Molecular biology of the cell, 2012. **23**(24): p. 4786-4795.
87. Noda, Y., et al., *Phosphatidylinositol 4-phosphate 5-kinase alpha (PIPKα) regulates neuronal microtubule depolymerase kinesin, KIF2A and suppresses elongation of axon branches.* Proceedings of the National Academy of Sciences, 2012. **109**(5): p. 1725-1730.

88. Ding, W., et al., *Cenpj Regulates Cilia Disassembly and Neurogenesis in the Developing Mouse Cortex.* The Journal of neuroscience : the official journal of the Society for Neuroscience, 2019. **39**(11): p. 1994-2010.
89. Douglas, R.J. and K.A.C. Martin, *NEURONAL CIRCUITS OF THE NEOCORTEX*. Annual Review of Neuroscience, 2004. **27**(1): p. 419-451.
90. Buchsbaum, I.Y. and S. Cappello, *Neuronal migration in the CNS during development and disease: insights from in vivo and in vitro models.* Development, 2019. **146**(1): p. dev163766.
91. Tan, X. and S.-H. Shi, *Neocortical neurogenesis and neuronal migration.* WIREs Developmental Biology, 2013. **2**(4): p. 443-459.
92. Götz, M. and W.B. Huttner, *The cell biology of neurogenesis.* Nature Reviews Molecular Cell Biology, 2005. **6**(10): p. 777-788.
93. Ramanathan, A. *With Great Power Comes Great Responsibility: Neural Stem Cells*. 2014; Available from: https://knowingneurons.com/2014/11/18/with-great-power-comes-great-responsibility-neural-stem-cells/neuralstemcells/.
94. Noctor, S.C., V. Martinez-Cerdeno, and A.R. Kriegstein, *Neural stem and progenitor cells in cortical development.* Novartis Found Symp, 2007. **288**: p. 59-73; discussion 73-8, 96-8.
95. Sun, T. and R.F. Hevner, *Growth and folding of the mammalian cerebral cortex: from molecules to malformations.* Nature Reviews Neuroscience, 2014. **15**(4): p. 217-232.
96. Taverna, E., M. Gotz, and W.B. Huttner, *The cell biology of neurogenesis: toward an understanding of the development and evolution of the neocortex.* Annu Rev Cell Dev Biol, 2014. **30**: p. 465-502.
97. Komuro, H. and P. Rakic, *Distinct Modes of Neuronal Migration in Different Domains of Developing Cerebellar Cortex.* The Journal of Neuroscience, 1998. **18**(4): p. 1478-1490.
98. Dwyer, N.D., et al., *Neural Stem Cells to Cerebral Cortex: Emerging Mechanisms Regulating Progenitor Behavior and Productivity.* The Journal of Neuroscience, 2016. **36**(45): p. 11394.
99. Ohtaka-Maruyama, C. and H. Okado, *Molecular Pathways Underlying Projection Neuron Production and Migration during Cerebral Cortical Development.* Frontiers in Neuroscience, 2015. **9**(447).
100. Saillour, Y., et al., *Beta tubulin isoforms are not interchangeable for rescuing impaired radial migration due to Tubb3 knockdown.* Human Molecular Genetics, 2013. **23**(6): p. 1516-1526.
101. Tian, G., et al., *A patient with lissencephaly, developmental delay, and infantile spasms, due to de novo heterozygous mutation of KIF2A.* Molecular Genetics & Genomic Medicine, 2016. **4**(6): p. 599-603.

102. Gilet, J.G., et al., *Conditional switching of KIF2A mutation provides new insights into cortical malformation pathogeny.* Human Molecular Genetics, 2020.
103. Akkaya, C., *Effects of KIF2A protein isoforms and Kif2a disease mutations on neuronal function* in *Molecular Biology and Genetics*. 2015, Koç University. p. 102.
104. Baffet, A. *Cell Biology of Mammalian Neurogenesis*. Available from: https://science.institut-curie.org/research/multiscale-physics-biology-chemistry/umr144-subcellular-structure-and-cellular-dynamics/team-baffet/.
105. dal Maschio, M., et al., *High-performance and site-directed in utero electroporation by a triple-electrode probe.* Nature Communications, 2012. **3**(1): p. 960.
106. Rappsilber, J., M. Mann, and Y. Ishihama, *Protocol for micro-purification, enrichment, pre-fractionation and storage of peptides for proteomics using StageTips.* Nature Protocols, 2007. **2**(8): p. 1896-1906.
107. Uniprot, *UniProt: The Universal Protein Knowledgebase.* Nucleic Acids Res., 2017. **45**(D1): p. D158.
108. Szklarczyk, D., et al., *STRING v11: protein–protein association networks with increased coverage, supporting functional discovery in genome-wide experimental datasets.* Nucleic Acids Research, 2018. **47**(D1): p. D607-D613.
109. Doncheva, N.T., et al., *Cytoscape StringApp: Network Analysis and Visualization of Proteomics Data.* Journal of Proteome Research, 2019. **18**(2): p. 623-632.
110. Cline, M.S., et al., *Integration of biological networks and gene expression data using Cytoscape.* Nature Protocols, 2007. **2**(10): p. 2366-2382.
111. Raudvere, U., et al., *g:Profiler: a web server for functional enrichment analysis and conversions of gene lists (2019 update).* Nucleic Acids Research, 2019. **47**(W1): p. W191-W198.
112. Ueda, S., et al., *Force Dependent Biotinylation of Myosin IIA by α-Catenin Tagged with a Promiscuous Biotin Ligase.* PLOS ONE, 2015. **10**(3): p. e0122886.
113. Ferreira, T.A., et al., *Neuronal morphometry directly from bitmap images.* Nature Methods, 2014. **11**(10): p. 982-984.
114. Schindelin, J., et al., *Fiji: an open-source platform for biological-image analysis.* Nature Methods, 2012. **9**(7): p. 676-682.
115. Dunn, K.W., M.M. Kamocka, and J.H. McDonald, *A practical guide to evaluating colocalization in biological microscopy.* American Journal of Physiology-Cell Physiology, 2011. **300**(4): p. C723-C742.
116. Manders, E.M.M., F.J. Verbeek, and J.A. Aten, *Measurement of co-localization of objects in dual-colour confocal images.* Journal of Microscopy, 1993. **169**(3): p. 375-382.
117. Zinchuk, V. and O. Zinchuk, *Quantitative Colocalization Analysis of Confocal Fluorescence Microscopy Images.* Current Protocols in Cell Biology, 2008. **39**(1): p. 4.19.1-4.19.16.

118. Debaize, L., et al., *Optimization of proximity ligation assay (PLA) for detection of protein interactions and fusion proteins in non-adherent cells: application to pre-B lymphocytes.* Molecular cytogenetics, 2017. **10**: p. 27-27.
119. *How Proximity Ligation Assay (PLA) Works*. Available from: https://www.sigmaaldrich.com/technical-documents/protocols/biology/how-pla-works.html.
120. Tavosanis, G., *Dendritic structural plasticity*. Developmental Neurobiology, 2012. **72**(1): p. 73-86.
121. Urbanska, M., M. Blazejczyk, and J. Jaworski, *Molecular basis of dendritic arborization.* Acta Neurobiol Exp (Wars), 2008. **68**(2): p. 264-88.
122. Jan, Y.-N. and L.Y. Jan, *The Control of Dendrite Development.* Neuron, 2003. **40**(2): p. 229-242.
123. Moffat, J.J., et al., *Genes and brain malformations associated with abnormal neuron positioning.* Molecular brain, 2015. **8**(1): p. 72-72.
124. Dosztányi, *Z., Prediction of protein disorder based on IUPred.* 2018. **27**(1): p. 331-340.
125. Buljan, M., et al., *Alternative splicing of intrinsically disordered regions and rewiring of protein interactions.* Curr Opin Struct Biol, 2013. **23**(3): p. 443-50.
126. Ellis, Jonathan D., et al., *Tissue-Specific Alternative Splicing Remodels Protein-Protein Interaction Networks.* Molecular Cell, 2012. **46**(6): p. 884-892.
127. Kandoi, G. and J.A. Dickerson, *Tissue-specific mouse mRNA isoform networks.* Scientific Reports, 2019. **9**(1): p. 13949.
128. Roux, K.J., D.I. Kim, and B. Burke, *BioID: A Screen for Protein-Protein Interactions.* 2013. **74**(1): p. 19.23.1-19.23.14.
129. Szklarczyk, D., et al., *STRING v11: protein–protein association networks with increased coverage, supporting functional discovery in genome-wide experimental datasets.* Nucleic Acids Research, 2019. **47**(D1): p. D607-D613.
130. Oertle, T. and M.E. Schwab, *Nogo and its paRTNers.* Trends in Cell Biology, 2003. **13**(4): p. 187-194.
131. Chen, M.S., et al., *Nogo-A is a myelin-associated neurite outgrowth inhibitor and an antigen for monoclonal antibody IN-1.* Nature, 2000. **403**(6768): p. 434-439.
132. Huber, A.B. and M.E. Schwab, *Nogo-A, a Potent Inhibitor of Neurite Outgrowth and Regeneration*, in *Biological Chemistry*. 2000. p. 407.
133. Schmandke, A., A. Schmandke, and M.E. Schwab, *Nogo-A:Multiple Roles in CNS Development, Maintenance, and Disease.* 2014. **20**(4): p. 372-386.
134. Dunn, K.W., M.M. Kamocka, and J.H. McDonald, *A practical guide to evaluating colocalization in biological microscopy.* 2011. **300**(4): p. C723-C742.
135. Manders, E.M.M., F.J. Verbeek, and J.A. Aten, *Measurement of co-localization of objects in dual-colour confocal images.* 1993. **169**(3): p. 375-382.

136. Zinchuk, V. and O. Zinchuk, *Quantitative Colocalization Analysis of Confocal Fluorescence Microscopy Images.* 2008. **39**(1): p. 4.19.1-4.19.16.
137. Baas, P.W., et al., *Polarity orientation of microtubules in hippocampal neurons: uniformity in the axon and nonuniformity in the dendrite.* Proceedings of the National Academy of Sciences, 1988. **85**(21): p. 8335.
138. Dent, E.W., *Of microtubules and memory: implications for microtubule dynamics in dendrites and spines.* Molecular biology of the cell, 2017. **28**(1): p. 1-8.
139. Kelliher, M.T., H.A.J. Saunders, and J. Wildonger, *Microtubule control of functional architecture in neurons.* Current Opinion in Neurobiology, 2019. **57**: p. 39-45.
140. Baas, P.W., et al., *Microtubule dynamics in axons and dendrites.* Journal of Neuroscience Research, 1991. **30**(1): p. 134-153.
141. Brown, A., et al., *Composite microtubules of the axon: quantitative analysis of tyrosinated and acetylated tubulin along individual axonal microtubules.* Journal of Cell Science, 1993. **104**(2): p. 339.
142. Kleele, T., et al., *An assay to image neuronal microtubule dynamics in mice.* Nature Communications, 2014. **5**(1): p. 4827.
143. Yau, K.W., et al., *Dendrites In Vitro and In Vivo Contain Microtubules of Opposite Polarity and Axon Formation Correlates with Uniform Plus-End-Out Microtubule Orientation.* J Neurosci, 2016. **36**(4): p. 1071-85.
144. McAllister, A.K., D.C. Lo, and L.C. Katz, *Neurotrophins regulate dendritic growth in developing visual cortex.* Neuron, 1995. **15**(4): p. 791-803.
145. McAllister, A.K., L.C. Katz, and D.C. Lo, *Opposing Roles for Endogenous BDNF and NT-3 in Regulating Cortical Dendritic Growth.* Neuron, 1997. **18**(5): p. 767-778.
146. Gao, F.-B. and B.A. Bogert, *Genetic control of dendritic morphogenesis in Drosophila.* Trends in Neurosciences, 2003. **26**(5): p. 262-268.
147. Scott, E.K. and L. Luo, *How do dendrites take their shape?* Nature Neuroscience, 2001. **4**(4): p. 359-365.
148. Liu, Z., R. Steward, and L. Luo, *Drosophila Lis1 is required for neuroblast proliferation, dendritic elaboration and axonal transport.* Nature Cell Biology, 2000. **2**(11): p. 776-783.
149. Harada, A., et al., *MAP2 is required for dendrite elongation, PKA anchoring in dendrites, and proper PKA signal transduction.* The Journal of cell biology, 2002. **158**(3): p. 541-549.
150. Prokop, A., et al., *The kakapo mutation affects terminal arborization and central dendritic sprouting of Drosophila motorneurons.* The Journal of cell biology, 1998. **143**(5): p. 1283-1294.
151. Quach, T.T., et al., *CRMP3 is required for hippocampal CA1 dendritic organization and plasticity.* FASEB journal : official publication of the Federation of American Societies for Experimental Biology, 2008. **22**(2): p. 401-409.

152. Teng, J., et al., *Synergistic effects of MAP2 and MAP1B knockout in neuronal migration, dendritic outgrowth, and microtubule organization.* J Cell Biol, 2001. **155**(1): p. 65-76.
153. Yu, W., et al., *Depletion of a microtubule-associated motor protein induces the loss of dendritic identity.* The Journal of neuroscience : the official journal of the Society for Neuroscience, 2000. **20**(15): p. 5782-5791.
154. Baltussen, L.L., et al., *Chemical genetic identification of CDKL5 substrates reveals its role in neuronal microtubule dynamics.* The EMBO Journal, 2018. **37**(24): p. e99763.
155. Uzquiano, A., et al., *Mutations in the Heterotopia Gene Eml1/EML1 Severely Disrupt the Formation of Primary Cilia.* Cell Reports, 2019. **28**(6): p. 1596-1611.e10.
156. Hevner, R.F., et al., *Tbr1 Regulates Differentiation of the Preplate and Layer 6.* Neuron, 2001. **29**(2): p. 353-366.
157. Kwan, K.Y., et al., *SOX5 postmitotically regulates migration, postmigratory differentiation, and projections of subplate and deep-layer neocortical neurons.* Proceedings of the National Academy of Sciences, 2008. **105**(41): p. 16021.
158. Alcamo, E.A., et al., *Satb2 regulates callosal projection neuron identity in the developing cerebral cortex.* Neuron, 2008. **57**(3): p. 364-77.
159. Britanova, O., et al., *Satb2 Is a Postmitotic Determinant for Upper-Layer Neuron Specification in the Neocortex.* Neuron, 2008. **57**(3): p. 378-392.
160. Yano, M., et al., *Nova2 Regulates Neuronal Migration through an RNA Switch in Disabled-1 Signaling.* Neuron, 2010. **66**(6): p. 848-858.
161. Barbosa-Morais, N.L., et al., *The Evolutionary Landscape of Alternative Splicing in Vertebrate Species.* Science, 2012. **338**(6114): p. 1587.
162. Graveley, B.R., *Alternative splicing: increasing diversity in the proteomic world.* Trends in Genetics, 2001. **17**(2): p. 100-107.
163. Merkin, J., et al., *Evolutionary Dynamics of Gene and Isoform Regulation in Mammalian Tissues.* Science, 2012. **338**(6114): p. 1593.
164. Papasaikas, P. and J. Valcárcel, *Splicing in 4D.* Science, 2012. **338**(6114): p. 1547.
165. Hegyi, H., et al., *Verification of alternative splicing variants based on domain integrity, truncation length and intrinsic protein disorder.* Nucleic Acids Research, 2010. **39**(4): p. 1208-1219.
166. Romero, P.R., et al., *Alternative splicing in concert with protein intrinsic disorder enables increased functional diversity in multicellular organisms.* Proceedings of the National Academy of Sciences, 2006. **103**(22): p. 8390.
167. Buljan, M., et al., *Tissue-specific splicing of disordered segments that embed binding motifs rewires protein interaction networks.* Molecular cell, 2012. **46**(6): p. 871-883.
168. Weatheritt, R.J., N.E. Davey, and T.J. Gibson, *Linear motifs confer functional diversity onto splice variants.* Nucleic Acids Research, 2012. **40**(15): p. 7123-7131.

169. Gaetz, J. and T.M. Kapoor, *Dynein/dynactin regulate metaphase spindle length by targeting depolymerizing activities to spindle poles.* J Cell Biol, 2004. **166**(4): p. 465-71.
170. Ali, A., et al., *MLL/WDR5 Complex Regulates Kif2A Localization to Ensure Chromosome Congression and Proper Spindle Assembly during Mitosis.* Developmental Cell, 2017. **41**(6): p. 605-622.e7.
171. Manning, A.L., et al., *The Kinesin-13 Proteins Kif2a, Kif2b, and Kif2c/MCAK Have Distinct Roles during Mitosis in Human Cells.* 2007. **18**(8): p. 2970-2979.
172. O'Donnell-Luria, A.H., et al., *Heterozygous Variants in KMT2E Cause a Spectrum of Neurodevelopmental Disorders and Epilepsy.* The American Journal of Human Genetics, 2019. **104**(6): p. 1210-1222.
173. Nitarska, J., et al., *A Functional Switch of NuRD Chromatin Remodeling Complex Subunits Regulates Mouse Cortical Development.* Cell Reports, 2016. **17**(6): p. 1683-1698.
174. MacAskill, A.F., et al., *Miro1 Is a Calcium Sensor for Glutamate Receptor-Dependent Localization of Mitochondria at Synapses.* Neuron, 2009. **61**(4): p. 541-555.
175. Tanaka, Y., et al., *Targeted Disruption of Mouse Conventional Kinesin Heavy Chain kif5B, Results in Abnormal Perinuclear Clustering of Mitochondria.* Cell, 1998. **93**(7): p. 1147-1158.
176. Barel, O., et al., *Deleterious variants in TRAK1 disrupt mitochondrial movement and cause fatal encephalopathy.* Brain, 2017. **140**(3): p. 568-581.
177. Brickley, K. and F.A. Stephenson, *Trafficking kinesin protein (TRAK)-mediated transport of mitochondria in axons of hippocampal neurons.* J Biol Chem, 2011. **286**(20): p. 18079-92.
178. López-Doménech, G., et al., *Miro proteins coordinate microtubule- and actin-dependent mitochondrial transport and distribution.* The EMBO Journal, 2018. **37**(3): p. 321-336.
179. Nangaku, M., et al., *KIF1B, a novel microtubule plus end-directed monomeric motor protein for transport of mitochondria.* Cell, 1994. **79**(7): p. 1209-1220.
180. Seiler, S. and H.R. Widmer, *Nogo-A and its functions beyond axonal inhibition: the controversial role of Nogo-A in Parkinson's disease.* Neural regeneration research, 2015. **10**(8): p. 1223-1224.
181. Mathis, C., et al., *Nogo-A Regulates Neural Precursor Migration in the Embryonic Mouse Cortex.* Cerebral Cortex, 2010. **20**(10): p. 2380-2390.
182. Andrei, M.A., et al., *A role for eIF4E and eIF4E-transporter in targeting mRNPs to mammalian processing bodies.* Rna, 2005. **11**(5): p. 717-27.

183. Dominissini, D. and G. Rechavi, *N⁴-acetylation of Cytidine in mRNA by NAT10 Regulates Stability and Translation.* Cell, 2018. **175**(7): p. 1725-1727.
184. Lampasona, A.A. and K. Czaplinski, *Hnrnpab regulates neural cell motility through transcription of Eps8.* Rna, 2019. **25**(1): p. 45-59.
185. Lapik, Y.R., et al., *Physical and Functional Interaction between Pes1 and Bop1 in Mammalian Ribosome Biogenesis.* Molecular Cell, 2004. **15**(1): p. 17-29.
186. Lerch-Gaggl, A., et al., *Pescadillo is essential for nucleolar assembly, ribosome biogenesis, and mammalian cell proliferation.* J Biol Chem, 2002. **277**(47): p. 45347-55.
187. Fazal, F.M., et al., *Atlas of Subcellular RNA Localization Revealed by APEX-Seq.* Cell, 2019. **178**(2): p. 473-490.e26.
188. Gagnon, J.A. and K.L. Mowry, *Molecular motors: directing traffic during RNA localization.* Critical Reviews in Biochemistry and Molecular Biology, 2011. **46**(3): p. 229-239.
189. Kanai, Y., N. Dohmae, and N. Hirokawa, *Kinesin Transports RNA: Isolation and Characterization of an RNA-Transporting Granule.* Neuron, 2004. **43**(4): p. 513-525.
190. Messitt, T.J., et al., *Multiple Kinesin Motors Coordinate Cytoplasmic RNA Transport on a Subpopulation of Microtubules in Xenopus Oocytes.* Developmental Cell, 2008. **15**(3): p. 426-436.
191. Fox, T.D., *Mitochondrial protein synthesis, import, and assembly.* Genetics, 2012. **192**(4): p. 1203-1234.
192. Williams, C.C., C.H. Jan, and J.S. Weissman, *Targeting and plasticity of mitochondrial proteins revealed by proximity-specific ribosome profiling.* Science, 2014. **346**(6210): p. 748.
193. Kohwi, M. and C.Q. Doe, *Temporal fate specification and neural progenitor competence during development.* Nature Reviews Neuroscience, 2013. **14**(12): p. 823-838.
194. Pataskar, A., et al., *NeuroD1 reprograms chromatin and transcription factor landscapes to induce the neuronal program.* The EMBO Journal, 2016. **35**(1): p. 24-45.
195. Telley, L., et al., *Sequential transcriptional waves direct the differentiation of newborn neurons in the mouse neocortex.* Science, 2016. **351**(6280): p. 1443.
196. Greig, L.C., et al., *Molecular logic of neocortical projection neuron specification, development and diversity.* Nature Reviews Neuroscience, 2013. **14**(11): p. 755-769.
197. Leone, D.P., et al., *The determination of projection neuron identity in the developing cerebral cortex.* Current Opinion in Neurobiology, 2008. **18**(1): p. 28-35.
198. Imayoshi, I. and R. Kageyama, *bHLH Factors in Self-Renewal, Multipotency, and Fate Choice of Neural Progenitor Cells.* Neuron, 2014. **82**(1): p. 9-23.

199. Mattar, P., et al., *Basic Helix-Loop-Helix Transcription Factors Cooperate To Specify a Cortical Projection Neuron Identity.* Molecular and Cellular Biology, 2008. **28**(5): p. 1456.
200. Wilkinson, G., D. Dennis, and C. Schuurmans, *Proneural genes in neocortical development.* Neuroscience, 2013. **253**: p. 256-273.
201. Farah, M.H., et al., *Generation of neurons by transient expression of neural bHLH proteins in mammalian cells.* Development, 2000. **127**(4): p. 693.
202. Noda, T., et al., *Transduction of NeuroD2 protein induced neural cell differentiation.* Journal of Biotechnology, 2006. **126**(2): p. 230-236.
203. Fode, C., et al., *A role for neural determination genes in specifying the dorsoventral identity of telencephalic neurons.* Genes Dev, 2000. **14**(1): p. 67-80.
204. Kim, E.J., et al., *Spatiotemporal fate map of neurogenin1 (Neurog1) lineages in the mouse central nervous system.* Journal of Comparative Neurology, 2011. **519**(7): p. 1355-1370.
205. Jo, A.Y., et al., *Contrasting and brain region-specific roles of neurogenin2 and mash1 in GABAergic neuron differentiation in vitro.* Experimental Cell Research, 2007. **313**(19): p. 4066-4081.
206. Roybon, L., et al., *GABAergic Differentiation Induced by Mash1 Is Compromised by the bHLH Proteins Neurogenin2, NeuroD1, and NeuroD2.* Cerebral Cortex, 2009. **20**(5): p. 1234-1244.
207. Yuan, L. and B.A. Hassan, *Neurogenins in brain development and disease: An overview.* Archives of Biochemistry and Biophysics, 2014. **558**: p. 10-13.
208. McCormick, M.B., et al., *NeuroD2 and neuroD3: distinct expression patterns and transcriptional activation potentials within the neuroD gene family.* Molecular and Cellular Biology, 1996. **16**(10): p. 5792.
209. Schuurmans, C., et al., *Sequential phases of cortical specification involve Neurogenin-dependent and -independent pathways.* The EMBO Journal, 2004. **23**(14): p. 2892-2902.
210. Bormuth, I., et al., *Neuronal Basic Helix–Loop–Helix Proteins Neurod2/6 Regulate Cortical Commissure Formation before Midline Interactions.* The Journal of Neuroscience, 2013. **33**(2): p. 641.
211. Ince-Dunn, G., et al., *Regulation of Thalamocortical Patterning and Synaptic Maturation by NeuroD2.* Neuron, 2006. **49**(5): p. 683-695.
212. Wilke, S.A., et al., *NeuroD2 regulates the development of hippocampal mossy fiber synapses.* Neural Development, 2012. **7**(1): p. 9.
213. Chen, F., et al., *The transcription factor NeuroD2 coordinates synaptic innervation and cell intrinsic properties to control excitability of cortical pyramidal neurons.* The Journal of Physiology, 2016. **594**(13): p. 3729-3744.

214. Kraft, R., *STIM and ORAI proteins in the nervous system.* Channels (Austin), 2015. **9**(5): p. 245-52.
215. Moccia, F., et al., *Stim and Orai proteins in neuronal Ca2+ signaling and excitability.* Frontiers in Cellular Neuroscience, 2015. **9**(153).
216. D'Arcangelo, G., et al., *A protein related to extracellular matrix proteins deleted in the mouse mutant reeler.* Nature, 1995. **374**(6524): p. 719-723.
217. Sekine, K., et al., *Reelin Controls Neuronal Positioning by Promoting Cell-Matrix Adhesion via Inside-Out Activation of Integrin α5β1.* Neuron, 2012. **76**(2): p. 353-369.
218. Hirota, Y., et al., *Reelin receptors ApoER2 and VLDLR are expressed in distinct spatiotemporal patterns in developing mouse cerebral cortex.* J Comp Neurol, 2015. **523**(3): p. 463-78.
219. Uchida, T., et al., *Downregulation of Functional Reelin Receptors in Projection Neurons Implies That Primary Reelin Action Occurs atEarly/Premigratory Stages.* The Journal of Neuroscience, 2009. **29**(34): p. 10653.
220. Yoshida, M., et al., *Massive loss of Cajal-Retzius cells does not disrupt neocortical layer order.* Development, 2006. **133**(3): p. 537.
221. Caviness Jr., V.S. and R.L. Sidman, *Time of origin of corresponding cell classes in the cerebral cortex of normal and reeler mutant mice: An autoradiographic analysis.* Journal of Comparative Neurology, 1973. **148**(2): p. 141-151.
222. González, J.L., et al., *Birthdate and Cell Marker Analysis of Scrambler: A Novel Mutation Affecting Cortical Development with a Reeler-Like Phenotype.* The Journal of Neuroscience, 1997. **17**(23): p. 9204.
223. Howell, B.W., et al., *Neuronal position in the developing brain is regulated by mouse disabled-1.* Nature, 1997. **389**(6652): p. 733-737.
224. Trommsdorff, M., et al., *Reeler/Disabled-like Disruption of Neuronal Migration in Knockout Mice Lacking the VLDL Receptor and ApoE Receptor 2.* Cell, 1999. **97**(6): p. 689-701.
225. Herz, J., et al., *Expanding functions of lipoprotein receptors.* J Lipid Res, 2009. **50 Suppl**: p. S287-92.
226. Lussier, A.L., E.J. Weeber, and G.W. Rebeck, *Reelin Proteolysis Affects Signaling Related to Normal Synapse Function and Neurodegeneration.* Frontiers in Cellular Neuroscience, 2016. **10**(75).
227. O'Leary, N.A., et al., *Reference sequence (RefSeq) database at NCBI: current status, taxonomic expansion, and functional annotation.* Nucleic Acids Research, 2015. **44**(D1): p. D733-D745.
228. Ogawa, M., et al., *The reeler gene-associated antigen on Cajal-Retzius neurons is a crucial molecule for laminar organization of cortical neurons.* Neuron, 1995. **14**(5): p. 899-912.

229. Yamazaki, H., et al., *Distinct ontogenic and regional expressions of newly identified Cajal-Retzius cell-specific genes during neocorticogenesis.* Proceedings of the National Academy of Sciences of the United States of America, 2004. **101**(40): p. 14509.
230. Fan, X., et al., *Spatial transcriptomic survey of human embryonic cerebral cortex by single-cell RNA-seq analysis.* Cell Research, 2018. **28**(7): p. 730-745.
231. Belvindrah, R., M. Nosten-Bertrand, and F. Francis, *Neuronal migration and its disorders affecting the CA3 region.* Frontiers in cellular neuroscience, 2014. **8**: p. 63-63.
232. Folsom, T.D. and S.H. Fatemi, *The involvement of Reelin in neurodevelopmental disorders.* Neuropharmacology, 2013. **68**: p. 122-135.
233. Frotscher, M., *Role for Reelin in stabilizing cortical architecture.* Trends in Neurosciences, 2010. **33**(9): p. 407-414.
234. Stouffer, M.A., J.A. Golden, and F. Francis, *Neuronal migration disorders: Focus on the cytoskeleton and epilepsy.* Neurobiology of disease, 2016. **92**(Pt A): p. 18-45.
235. Guerrini, R. and E. Parrini, *Neuronal migration disorders.* Neurobiology of Disease, 2010. **38**(2): p. 154-166.
236. Boyle, M.P., et al., *Cell-type-specific consequences of reelin deficiency in the mouse neocortex, hippocampus, and amygdala.* Journal of Comparative Neurology, 2011. **519**(11): p. 2061-2089.
237. Chai, X., et al., *Reelin Stabilizes the Actin Cytoskeleton of Neuronal Processes by Inducing n-Cofilin Phosphorylation at Serine3.* The Journal of Neuroscience, 2009. **29**(1): p. 288.
238. Gil-Sanz, C., et al., *Cajal-Retzius Cells Instruct Neuronal Migration by Coincidence Signaling between Secreted and Contact-Dependent Guidance Cues.* Neuron, 2013. **79**(3): p. 461-477.
239. Bormuth, I., *Roles of bHLH transcription factors Neurod1, Neurod2 and Neurod6 in cerebral cortex development and commissure formation*. 2015, Georg-August Universität.
240. Aizawa, H., et al., *Dendrite Development Regulated by CREST, a Calcium-Regulated Transcriptional Activator.* Science, 2004. **303**(5655): p. 197.
241. Dulabon, L., et al., *Reelin Binds α3β1 Integrin and Inhibits Neuronal Migration.* Neuron, 2000. **27**(1): p. 33-44.
242. Hack, I., et al., *Divergent roles of ApoER2 and Vldlr in the migration of cortical neurons.* Development, 2007. **134**(21): p. 3883.
243. Bizzotto, S., et al., *Eml1 loss impairs apical progenitor spindle length and soma shape in the developing cerebral cortex.* Scientific Reports, 2017. **7**(1): p. 17308.
244. Cargnin, F., et al., *FOXG1 Orchestrates Neocortical Organization and Cortico-Cortical Connections.* Neuron, 2018. **100**(5): p. 1083-1096.e5.

245. Zhao, L., et al., *Ezh2 is involved in radial neuronal migration through regulating Reelin expression in cerebral cortex.* Scientific Reports, 2015. **5**(1): p. 15484.
246. Golonzhka, O., et al., *Pbx Regulates Patterning of the Cerebral Cortex in Progenitors and Postmitotic Neurons.* Neuron, 2015. **88**(6): p. 1192-1207.
247. Kubo, K.-i., et al., *Ectopic Reelin Induces Neuronal Aggregation with a Normal Birthdate-Dependent "Inside-Out" Alignment in the Developing Neocortex.* The Journal of Neuroscience, 2010. **30**(33): p. 10953.

VITA

Cansu Akkaya was born on October 17, 1991, in Izmir, Turkey. She graduated from TED Aliağa High School in 2009 and received her major B.Sc. degree in Molecular Biology and Genetics from Middle East Technical University (METU), Ankara, Turkey in 2013. From September 2013 to July 2015 she worked as both teaching and research assistant at Koç University, Istanbul, Turkey and received her M.Sc. degree in Molecular Biology and Genetics under the supervision of Assoc. Prof. Gülayşe İnce Dunn with the thesis titled as "Effects of KIF2A protein isoforms and *Kif2a* disease mutations on neuronal function" on July 31, 2015. She graduated from master's with 3.90/4.00 cumulative GPA. Then, she continued to work as research assistant at Koç University, Istanbul, Turkey from September 2015 to July 2020 with receiving the BIDEB Scholarship from TUBITAK, and a full-tuition waiver and accommodation scholarship from Koç University. She carried out her thesis project under the joint supervision of Assoc. Prof. Gülayşe İnce Dunn and Assoc. Prof. Nurhan Özlü. She received 4.00/4.00 cumulative GPA and passed Ph.D. qualification exam in her second year. During her Ph.D., she also carried out duties as a teaching assistant for many different molecular biology courses and laboratories and was awarded the *Outstanding Teaching Award* (Fall 2017) by Koç University. Her work has led to two first author and one middle author publications. She received her Ph.D. degree in Molecular Biology and Genetics with the dissertation titled as "Control of gene expression and cytoskeleton in migrating neurons during cerebral cortex development" on July 13, 2020.

Appendix A: Proximal interaction partners of KIF2A isoforms (KIF2A.1, KIF2A.2 and KIF2A.3) and disease-causing KIF2A mutant ($KIF2A^{H321D}$)

Table A. 1: KIF2A isoform specific proximal protein interaction partners

KIF2A.1 specific	PSM_average
Srrm2	42
Gls	27
Gdf3	19
Ubap2l	13
Topaz1	13
Afg3l2	11
Dnah1	10
Pnpt1	8
Myo15b	8
Arcn1	7
Abca13	7
Nap1l1	7
Hnrnpr	7
Eef1d	6
Uggt1	6
Ppp1cc	6
Npepps	6
Srsf3	6
Rars2	5
Rbmxl1	5
Dzank1	5
Isg15	5
Actn4	5
Tsfm	5
Immt	4
Lars2	4
Ppp2cb	4
Armc4	4
Champ1	4
Srsf4	4
Ipo7	4
Mecr	4

KIF2A.2 specific	PSM_average
Eif4g1	30
Tln1	15
Akap12	12
Eef1b2	12
Plb1	11
Hist1h2bp	10
Cep170	9
Sf3b1	9
Tamm41	9
Yeats2	9
Rangap1	7

KIF2A.3 specific	PSM_average
Mocs2	73
Gabrp	43
Nkpd1	37
Gm8251	36
Hist1h1c	19
Srp68	11
Trak1	9
Afdn	8
Rpl11	7
Pes1	6
Eif4enif1	6
Hnrnpab	6
Hdlbp	5
Lama1	5
Chtop	4
Jup	4
Nmt2	4
Tbc1d15	4
Coro1b	4
Nat10	4
Sez6l	4
D1Pas1	4

Table A. 2: Common proximal protein interaction partners of KIF2A isoforms

KIF2A.1-KIF2A.2	PSM_average
Ahnak	132
Ubtf	25
Gfm2	17
Hnrnpa1	17
Suclg2	17
Hsd17b10	14
Aldh2	14
Krt75	13
Rsrc1	12
Zc3h18	12
Stat1	12
Hid1	11
Ogdhl	10
Timm44	10
Oat	10
Sucla2	7

KIF2A.1-KIF2A.3	PSM_average
Eif4g2	49
Numa1	21
Tjp1	11
Chd4	9
Cdc73	8
Ktn1	7
Eif5	7
Ciapin1	5

KIF2A.2-KIF2A.3	PSM_average
Map4	28
Vim	14
Gcn1	10

All isoforoms	PSM_average
Kif2a	193
Rnf213	53
Kmt2e	40
Ckap5	22
Rtn4	18
Ranbp2	16
Bclaf1	9

Table A. 3: KIF2A.1 and KIF2A^{H321D} specific proximal protein interaction partners

KIF2A.1 specific	PSM_average	KIF2A^{H321D} specific	PSM_average
Ahnak	115	Nkpd1	75
Srrm2	42	Ccdc80	59
Kmt2e	40	Srpra	37
Rnf213	33	Fbxo43	36
Gls	27	Iqsec1	32
Ubtf	25	Cep170	25
Gdf3	19	Hist1h1c	22
Gfm2	17	Pde4dip	22
Suclg2	17	Tdrkh	22
Ranbp2	16	Ckap2	21
Hnrnpa1	16	Usp50	20
Krt75	13	Gcn1	17
Ubap2l	13	Man2c1	16
Topaz1	13	Nphs1	14
Rsrc1	12	Srp68	14
Hid1	11	Homer2	13
Tjp1	11	Hist2h2be	12
Afg3l2	11	Hnrnpab	10
Ogdhl	10	Map7d2	9
Timm44	10	Sall4	9
Zc3h18	10	Eif4enif1	8
Dnah1	10	Pes1	7
Hsd17b10	10	Ddx50	7
Pnpt1	8	Slc1a7	7
Cdc73	8	Sept9	6
Myo15b	8	Dclk1	6
Oat	8	Nat10	6
Arcn1	7	Ddx47	5
Abca13	7	Olfml2a	5
Nap1l1	7	Epb41l3	4
Hnrnpr	7	Hp1bp3	4
Sucla2	7		
Eef1d	6		
Uggt1	6		
Aldh2	6		
Ppp1cc	6		
Npepps	6		
Srsf3	6		
Rars2	5		
Rbmxl1	5		
Dzank1	5		
Isg15	5		
Actn4	5		
Tsfm	5		
Immt	4		
Lars2	4		
Ppp2cb	4		
Armc4	4		
Champ1	4		
Srsf4	4		
Ipo7	4		
Mecr	4		

Table A. 4: Common proximal protein interaction partners of KIF2A.1 and KIF2A^{H321D}

KIF2A.1-KIF2A^{H321D}	PSM_average
Kif2a	306
Eif4g2	75
Ckap5	36
Numa1	21
Rtn4	16
Chd4	14
Ktn1	14
Bclaf1	9
Eif5	9
Ciapin1	8
Stat1	7

Appendix B: Role of Protocadherin 7 (PCDH7) in radial neuronal migration

Lysate preparation and western blot analysis from mouse cortex tissue

Brains from mice at different time points (embryonic day 14, 17, 18, postnatal day 0, 7, 14, 28 and adult) were collected and their cortices were dissected in ice-cold 1X PBS. Cortex lysates were prepared as explained **Section 2.2.1** and western blot was performed as described in **Section 2.2.19**. For western blot protocol, antibodies used as follow; PCDH7 (Abcam, Cat. #ab139274, Host: mouse, 1:200), β-actin (Abcam, Cat. #6276, Host: mouse, 1:5000) as primary antibodies and Anti-mouse IgG HRP-linked (Cell Signaling, Cat. #7076S, 1:2000) as secondary antibody. Western blot analysis revealed the PCDH7 expression was very low at embryonic cortex. Protein abundance was increased at P0 stage and exhibited elevated expression postnatally **(Figure B.1)**.

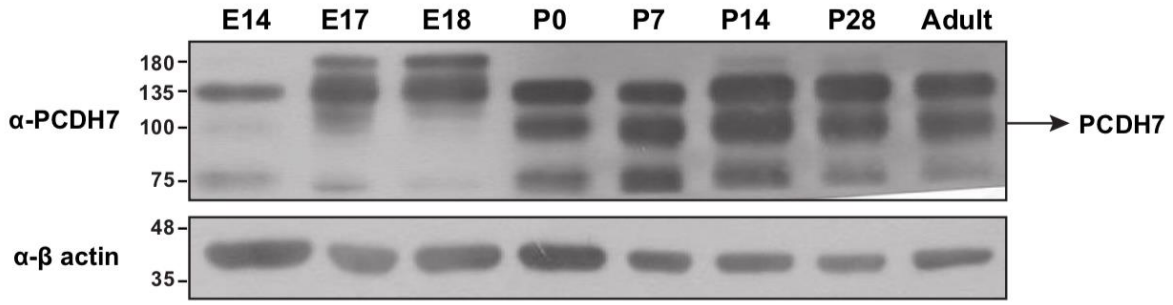

Figure B. 1: PCDH7 protein expression is controlled developmentally at mouse cortex. Immunoblotting analysis showed very low levels of PCDH7 at embryonic stages and expression level is increased postnatally. β-actin is used as loading control.

In utero electroporation and image analysis

In utero electroporation procedure was explained in **Section 2.2.13**. Injection solution was composed of 500 ng pEGFPN1 (control) or one the PCDH7 isoform (PCDH7-b or PCDH7-c **(Figure B.2**)), 500 ng of pCAGGS-IRES-GFP and 0.1% Fast Green FCF (All plasmids were prepared using QIAGEN endofree plasmid maxi kit). Immunofluorescence protocol was performed according to **Section 3.2.1** and antibodies used as follow; GFP (Aves Labs, Cat. #GFP-1020, Host: chick, 1:1000) as primary antibody and Goat Anti-Chick IgG (H+L) Alexa Fluor®488 (Life Technologies, Cat. # A11039, 1:1000) as secondary antibody. Optical z-series through 50 µm were captured using Nikon Eclipse 90i microscope and NIS Elements AR software and maximum intensity property of the software was used to project into a flattened plane. Analysis was performed as explained in **Section 2.2.13**.

As expected, GFP-positive neurons migrate throughout the cortex in pEGFPN1 control samples with approximately 40% of tdTomato-positive neurons migrate into CP, 50% are throughout the SVZ-IZ and 10% are remained within the VZ **(Figure B.3A)**. When I overexpressed PCDH7-b isoform in mouse embryonic cortex, I observed a slight yet significant over-migration of GFP-positive neurons towards the CP. Significantly less number of GFP-positive neurons are located in VZ which means more neurons exited the VZ and migrated toward to CP **(Figure B.3A and B)**. Interestingly, this significance is lost when I overexpressed PCDH7-c isoform which has an extra exon **(Figure B.3A and C)**. The reason why inclusion of an extra exon cause a loss-of-function is worth to investigate.

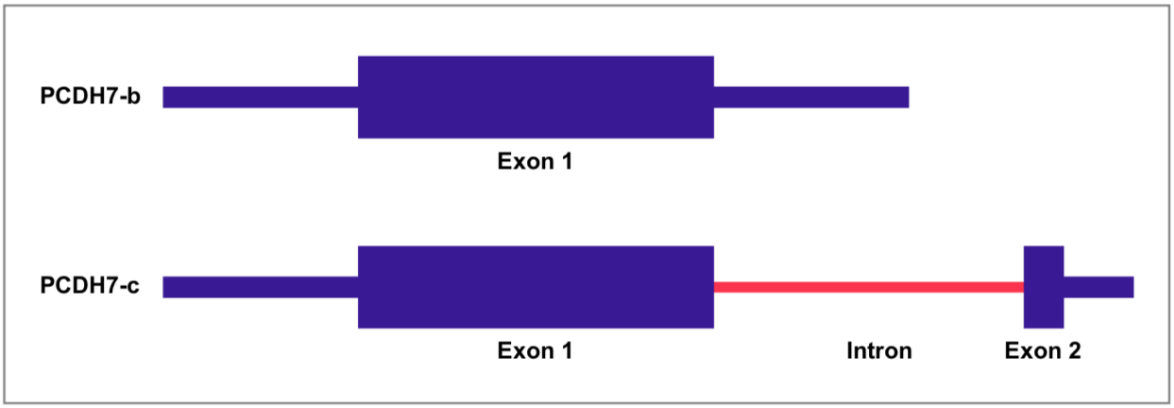

Figure B. 2: There are two isoforms of PCHD7 represented as PCDH7-b and PCDH7-c.

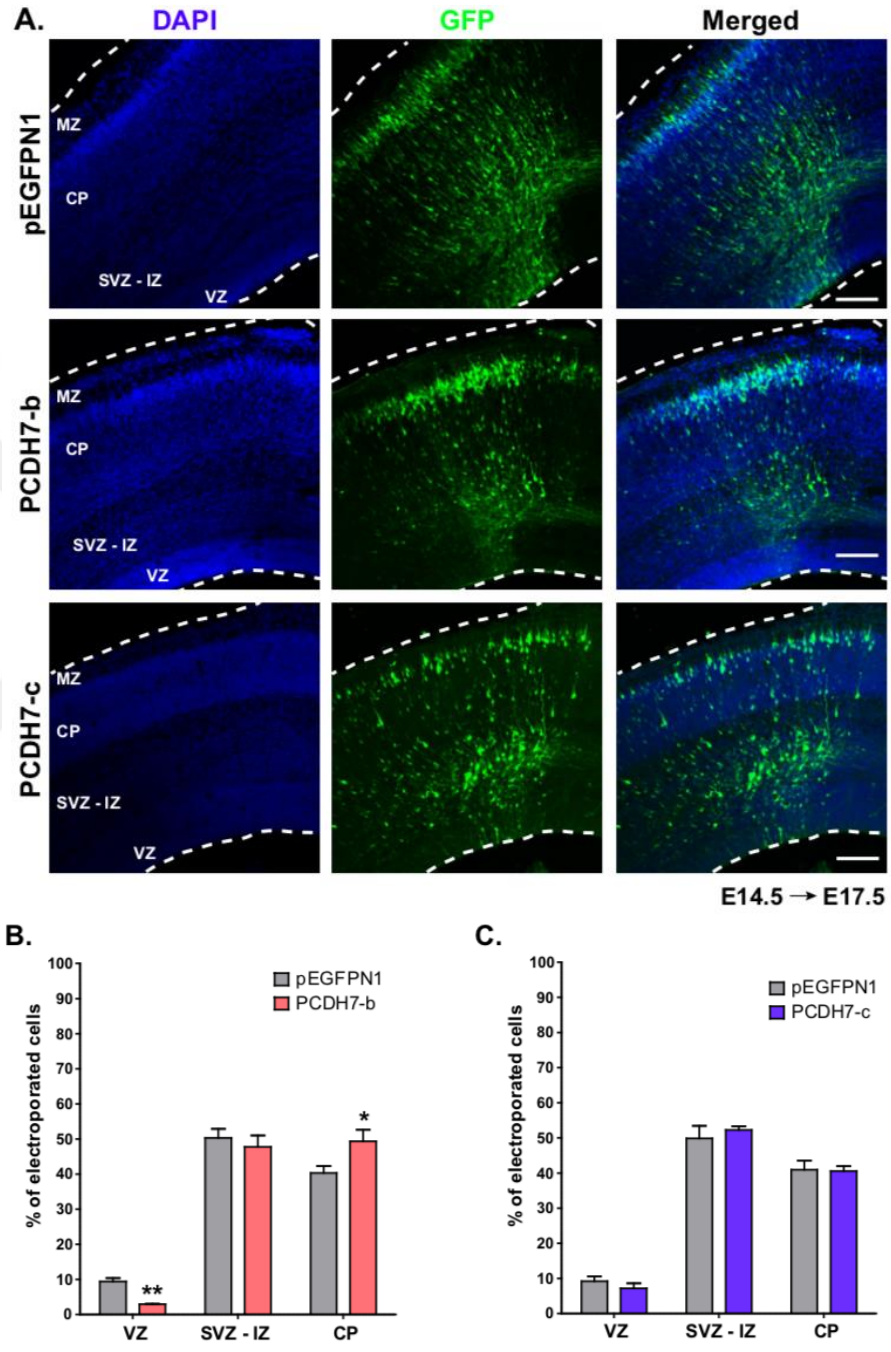
A.
DAPI
GFP
Merged
pEGFPN1
PCDH7-b
PCDH7-c
MZ
CP
SVZ - IZ
VZ
E14.5 → E17.5
B.
C.
% of electroporated cells
pEGFPN1
PCDH7-b
PCDH7-c
**
*
VZ
SVZ - IZ
CP

Figure B. 3: Role of different PCDH7 isoforms in cortical radial migration.

A. Immunofluorescence staining of E17.5 coronal sections *in utero* electroporated with pEFGPN1 (control) or either one of the PCDH7 isoforms (PCDH7-b or PCDH7-c) and pCAGGS_IRES_GFP at E14.5. Sections were stained with GFP to visualize the transfected neurons and DAPI was used to visualize nucleus. Scale bar, 100 μm. **B. and C.** Quantification of *in utero* electroporation experiment of PCDH7-b **(B)** and PCDH7-c **(C)**. Cortical sections were divided into zones. White dashed lines indicate boundaries of cortical sections. Percentages of GFP-positive neurons counted in individual zones are plotted. (For PCDH7-b a total of n=3373 for pEGFPN1, n=3316 from 2 biological replicates; for PCDH7-c a total of n=5929 for pEGFPN1, n=4519 from 3 biological replicates). Data is represented as bar graphs. Lines represent S.E.M. Unpaired two-tailed *t* test, p value: *p<0.05, **p<0.005.

Appendix C: Primer List

Primer Name	Primer Sequence
qPCR-Gapdh_F	5’-CGACTTCAACAGCAACTCCCATCTTCC-3’
qPCR-Gapdh_R	5’-TGGGTGGTCCAGGGTTTCTTACTCCTT-3’
qPCR-Kif2a.1_F	5’-CCAGGGTGAAAGAATTGACTG -3’
qPCR-Kif2a.1_R	5’-GCTTCATGGAAAGTGAACAGC-3’
qPCR-Kif2a.2_F	5’-GCAAATAGGGTGAAAGAATTGACTG-3’
qPCR-Kif2a.2_R	5’-TCTGGGAGACAGCTTCATGG-3’
qPCR-Kif2a.1_ex5-long_F	5’-CTCCTTCACGTAGAAAATCCAATT-3’
qPCR-Kif2a.1_ex5-long_R	5’-GTCTCTGATCATACACATAATTTCGT-3’
qPCR-Kif2a.3_ex5-short_F	5’-CAGAATGCACGTAGAAAATCCAA-3’
qPCR-Kif2a.3_ex5-short_R	5’-TCTGAAGTCTCTGATCATACACATA-3’
NS_F	5’-GATCCCCGCGCGATAGCGCTAATAATTTTTCA AGAGAAAATTATTAGCGCTATCGCGCTTTTTA-3’
NS_R	5’-AGTCTAAAAAGCGCGATAGCGCTAATAATTTT CTCTTGAAAAATTATTAGCGCTATCGCGCGGG-3’
shKif2a_F	5’-GATCCCCGGAATGGCATCCTGTGAAATTCAA GAGATTTCACAGGATGCCATTCCTTTTTA-3’
shKif2a_R	5’-AGCTAAAAAGGAATGGCATCCTGTGAAAT CTCTTGAATTTCACAGGATGCCATTCCGGG-3’
resKIF2A_F	5’-CCAGGAATGGCTTCGTGCGAAAATACTCT-3’
resKIF2A_R	5’-AGAGATTGTGGCAATCATGCAGGTACGAG-3’

Primer Name	Primer Sequence
Kif2a_c959G>A_F	5’-GCAGACTGGAAATGGGAAAACTCATACTATGG-3’
Kif2a_c961C>G_F	5’-GCAGACTGGAAGTGGGAAAACTGATACTATGG-3’
Kif2a_sdm_R	5’-CCATAAGCAAAGCACGTAGCCATGCCCCTTT-3’
pEGFPC1_Kif2a_F	5’-TTTAAGCTTGAATGGTAACATCTTTAAATGAAGAT AATGAAAGT-3’
pEGFPC1_Kif2a_R	5’-TTTGAATTCTTAGAGGGCTCGGGGCCTCTTGGGGTTA ATTTGC-3’
pc4A_Kif2a_F	5’-AAAGAATTCTATGGTAACATCTTTAAATGAAGAT-3’
pc4A_Kif2a_R	5’-AAAGGATCCGAGGGCTCGGGGCCTCTTGGGGTT-3’
BirAN_Kif2a_F	5’-AAACTCGAGATGGTAACATCTTTAAATGAAGAT-3’
BirAN_Kif2a_R	5’-AAAGAATTCTTAGAGGGCTGGGGCCTCTTGGG-3’